A COLLAPSE STUDY OF A LIGHTLY REINFORCED CONCRETE SHEAR WALL BUILDING DURING THE FEBRUARY 22, 2011 CHRISTCHURCH EARTHQUAKE

by

Alex Barnes

B.S., California Polytechnic State University, 2009

A THESIS SUBMITTED IN PARTIAL FULFILLMENT OF
THE REQUIREMENTS FOR THE DEGREE OF

MASTER OF SCIENCE

in

THE FACULTY OF GRADUATE AND POSTDOCTORAL STUDIES

(Civil Engineering)

THE UNIVERSITY OF BRITISH COLUMBIA

(Vancouver)

February 2014

Abstract

The Canterbury earthquake sequence in New Zealand started with the September 2010 earthquake, followed by large aftershock events throughout the following year. This sequence displayed the vulnerability of lightly reinforced concrete buildings built prior to 1980; specifically, the Pyne Gould Corporation (PGC) building, which collapsed during the February 22, 2011 event in Christchurch, New Zealand. PGC was a lightly reinforced concrete shear wall building with an exterior gravity frame built in 1964. A previous seismic study by Beca Carter Hollings and Ferner (Beca) of PGC was prepared for the Canterbury Earthquake Royal Commission and concluded flexural failure of the shear core governed the collapse. Failure initiated by rupture of the reinforcement in the west wall flange, followed by crushing of the east wall flange, leading to an increase in deformation demand on the building causing the exterior frame to lose its vertical-load-carrying capability.

A seismic performance study and collapse analysis was performed on PGC during the September and February earthquakes. The study focuses on the vulnerabilities of the shear core and the exterior gravity frame, as well as the torsion irregularity and how it may have contributed to the collapse. Two comprehensive nonlinear models, a fiber element model and a multiple-vertical-line-element model were used to simulate the September and February earthquakes within the computer software OpenSees. Non-linear time history analyses were performed to determine the primary cause of failure, how the gravity frame lost its vertical-load-carrying capacity and how the torsional irregularity affected the seismic response.

The analysis concluded failure of the core walls was likely initiated by shear failure in the highly perforated wall at the north end of the core. This conclusion is consistent with the observation of sizable diagonal cracks in the third story of the north wall, indicating possible shear failure. By comparing multiple configurations the analysis concluded the location of the core had minimal influence on the collapse. This is consistent with the post collapse photos of the floor slabs indicating minimal plan rotation. Post-processing indicated the exterior gravity frame was governed by joint shear failure causing the frame to fail in a sidesway mechanism.

Preface

This thesis is ultimately original, unpublished, independent work by the author, A. Barnes.

Table of Contents

List of Tables

List of Figures

Acknowledgements

Special thanks are owed to Sydney for always being there and all those who have supported me throughout my years of education.

Chapter 1 **Introduction**

On September 4th 2010, Christchurch, New Zealand (NZ) was struck at approximately 4:35 am by a major earthquake (Darfield Earthquake) registering a magnitude 7.1 on the Richter scale. It occurred 25 miles (40 km) east of the central business district (CBD) of Christchurch, near the town of Darfield, at a depth of 6.25 miles (10 km). This event resulted in zero casualties even though it was the most damaging earthquake since the 1931 Hawke's Bay earthquake (GeoNet 2013). Prior to this event Christchurch had only registered three moderate earthquakes (magnitude 4 to 5 on the Richter scale) in the past 40 years (GeoNet 2013). The Darfield event is thought to be the catalyst for the following events to come. Since that event, Christchurch has experienced approximately 417 earthquakes (now referred to as the Canterbury earthquake sequence) registering a magnitude of 4.0 or greater as indicated by the data organized by Nicholls (2013) of the University of Canterbury. The most notable event was the 22nd of February, 2011 earthquake occurring at 12:51 pm and registering a magnitude of 6.3 on the Richter scale. The event occurred at a depth of 3 miles (5 km) and a distance of about 6.25 miles (10 km) southeast of the CBD of Christchurch near the town of Lyttelton. Even though the magnitude was less than the Darfield event, due to the closer proximity and shallower depth, the February earthquake caused considerable damage to all of Christchurch, resulting in numerous injuries and 185 deaths (GeoNet 2013). The Canterbury region continues to be active today.

Majority of the structural damage was concentrated within the CBD, which is approximately 114 square blocks and contains roughly 200 concrete and 500-600 masonry buildings (EERI 2011). Two office buildings, the Pyne Gould Corporation building (PGC) and the Canterbury Television building (CTV) collapsed, accounting for 70% of all the casualties. Among the other severely damaged buildings were the Grand Chancellor Hotel and Forsyth Barr building. Nearly 50% of the building stock within the CBD was deemed unusable and was condemned to be either deconstructed or demolished, including hundreds of unreinforced masonry buildings, many of which holding historic significance to the city of Christchurch. The total cost of destruction was estimated over 20 billion New Zealand dollars (EERI 2011).

In April of 2011, following the February event a Royal Commission was created by the NZ government in conjunction with the Department of Building and Housing (DBH) with the purpose of investigating all aspects of earthquake resilience for Christchurch, as well as all of New Zealand. Technical reports were prepared by practicing professional engineers regarding the collapse investigation and seismic performance of PGC, Forsyth Barr, Grand Chancellor Hotel and CTV, through the DBH to the Royal Commission, for reference. Beca Carter Hollings & Ferner Ltd (Beca), Dunning Thornton Consultants, Compusoft Engineering, Hyland Consultants Ltd and StructureSmith Limited were among the companies consulted to provide these reports. The commission also called upon expert panels of engineers from all backgrounds and locations around the world, majority of which were structural engineers, from both academia and industry, to express their expert opinions to the commission. The discussions regarded the review of the technical reports on the collapse of the buildings, the effectiveness of the post-earthquake building assessment procedures and the state of the current building codes of New Zealand, among others. The Royal Commission also gathered testimonies from witnesses to the collapses, for review. The final reports compiled by the Royal Commission were released to the public in August 2012 (Royal Commission 2012a).

1.1 Objectives and Methodology

The focus of this thesis is the seismic performance of the Pyne Gould Corporation building during the September 2010 and February 2011 events, specifically targeting the vulnerabilities of the shear core and the exterior gravity frame, as well as the torsion irregularity and how each component contributed to the collapse.

In order to capture the response of the shear walls as accurately as possible, two comprehensive nonlinear computer models are calibrated using experimental tests by others, validated with simple analysis techniques, and used in nonlinear time history analyses to determine the governing failure type . The response of the exterior gravity frame is post processed given the performance of the shear walls and assessed using techniques from past research to determine the governing failure mechanism. The torsion irregularity effect on the seismic performance is obtained by incorporating two configurations into each model, one which represents the actual layout of walls as the Pyne Gould Corporation building and another, which considers the building to be symmetric, essentially removing the torsion irregularity.

1.2 Scope and Organization

The following work is intended to supplement the currently available information regarding the collapse and understanding of the seismic performance of the building. It is not the intent of this work to dismiss the findings by the Royal Commission and Beca regarding the performance of PGC, nor will it be determining the effectiveness of the New Zealand codes as they pertain to the post-earthquake assessment of existing buildings. Refer to the Beca (2011a) technical report or the Royal commission's final report (Royal Commission 2012a) for further information on the performance of PGC, how it was designed per the NZ building codes and the procedures regarding the post-earthquake assessment of existing buildings. Other severely damaged or collapsed buildings during any of the earthquakes in the Canterbury earthquake sequence will not be discussed nor will their subsequent reports be referenced.

The following provides a brief description of the chapters to follow.

Chapter 2 provides a more detailed background of the PGC building, considering the physical description, its location within Christchurch, a site analysis and a summarized history of past events, renovations and observations.

Chapter 3 summarizes the findings as reported by Beca, the expert panel discussions and the Royal Commission's final report regarding the collapse of PGC.

Chapter 4 shows the preliminary estimates that will be used in the following non-linear static and non-linear dynamic analyses, such as material properties as well as component capacities including the shear walls, exterior columns and joints.

Chapter 5 describes the analytical models used in the computer programs to represent the PGC structure as well as the calibration of the element models by past experimental tests and validation of the models through sectional analysis.

Chapter 6 uses response analysis results from ETABS and Opensees to further validate the element models, summarizes the different modeling approaches and compares non-linear static analysis results between model types and approaches, to gather information on expected performance of PGC.

Chapter 7 shows the results of the non-linear dynamic analysis and compares the appropriate data with the findings of Beca and the observations of the actual building, as well as discusses the findings of this analysis.

Chapter 8 summarizes the findings from the previous chapters and discloses opportunities for future research.

Chapter 2 **Background**

Figure 1: Pyne Gould Corporation Building (South East Face) (Stuff.co.nz 2012)

The Pyne Gould Corporation building was a 5-story reinforced concrete (RC) structure built in 1964 (Figure 1). The occupancy of the building was mixed use office space, with partition walls distributed throughout each level. The main lateral-force-resisting system was a set of 8-inch walls offset to the north end of the plan (Figure 2 and Figure 3). The core walls extend from the ground story to the roof, at an elevation of 68.7 feet above the ground level. The ground level columns and walls extend 5 feet below grade to typical RC shallow pad and strip footings, connected by a grid of grade beams (see structural drawings in Appendix A.1).

The gravity system was a 6-inch concrete slab supported by a grid of beams and columns along the perimeter spanning inward to the core walls. The ground level contains a more substantial amount of lateral resilience than the upper stories, due to the greater number of walls and the steel encased circular columns (Figure 2 and Figure 3). Timber, steel and concrete-masonry units (CMU) were among the other materials used in construction, mainly located at the roof top penthouse structure, used for the housing of mechanical equipment, but majority of the main structure was reinforced concrete.

The typical floor plans of the ground level and upper levels displaying the wall layouts, column locations, grid dimensions, and important wall opening sizes are shown below in Figure 2 and Figure 3. The building was laid out on an approximate 16 foot 6 inch grid, with a 4 foot 4 inch cantilever at level 1 (Figure 4). The plan was roughly symmetric about its north-south axis, but asymmetric about the east-west axis due to the eccentric nature of the core walls. For any information not shown in Figure 2 and Figure 3, refer to the full set of the original structural drawings from 1963 in Appendix A.1.

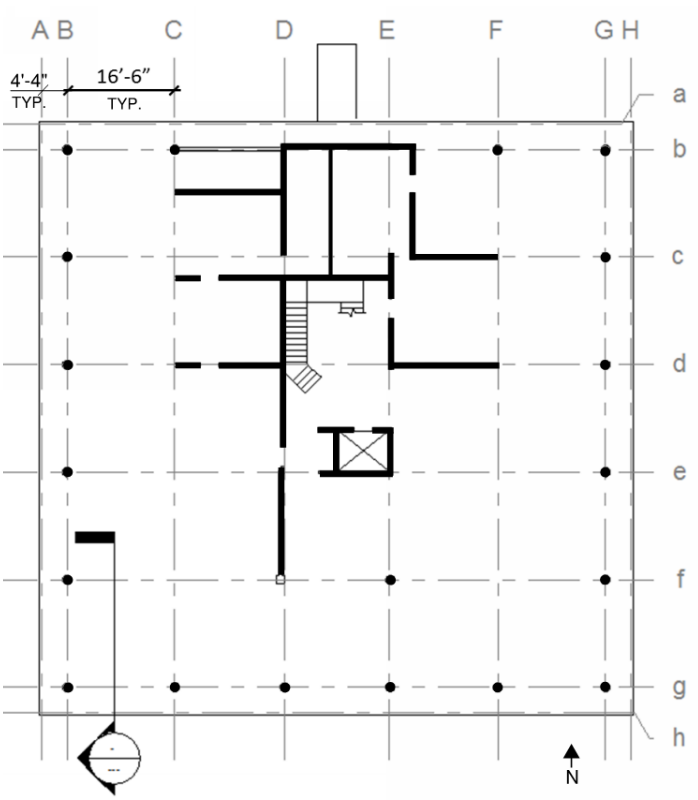

Figure 2: Ground floor plan (See Figure 19 for full height section) (based on original structural drawings provided by Beca 2011a, refer to Appendix A.1)

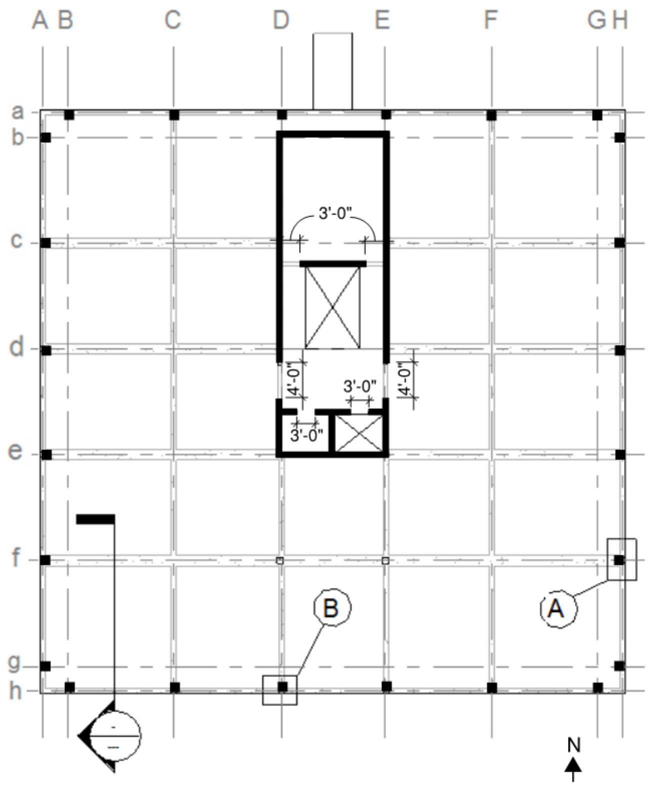

Figure 3: Typical upper level plan (level 1 similar) – see Figure 7 and Figure 8 for detail A and B, respectively (based on original structural drawings provided by Beca 2011a, refer to Appendix A.1)

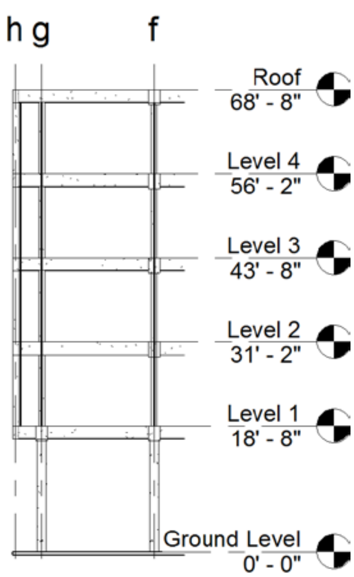

Figure 4: Full height section of the cantilevered exterior frame at level 1, as indicated in Figure 2 and Figure 3 (based on original structural drawings provided by Beca 2011a, refer to Appendix A.1)

2.1 Building Location

PGC is located at 233 Cambridge Terrace within the heart of the central business district (CBD) of Christchurch, New Zealand (Figure 5). The CBD was hit the hardest by the February event causing majority of its buildings to be red tagged, deconstructed or demolished. Figure 5 shows the progression of the CBD cordon area over the last 2 years. The red area was closed to the public for a month following the February event, the green area was closed for over a year following February 2011 and the area in yellow is the cordon area as of February 2013, as indicated by the Canterbury Earthquake Recovery Authority (CERA 2013).

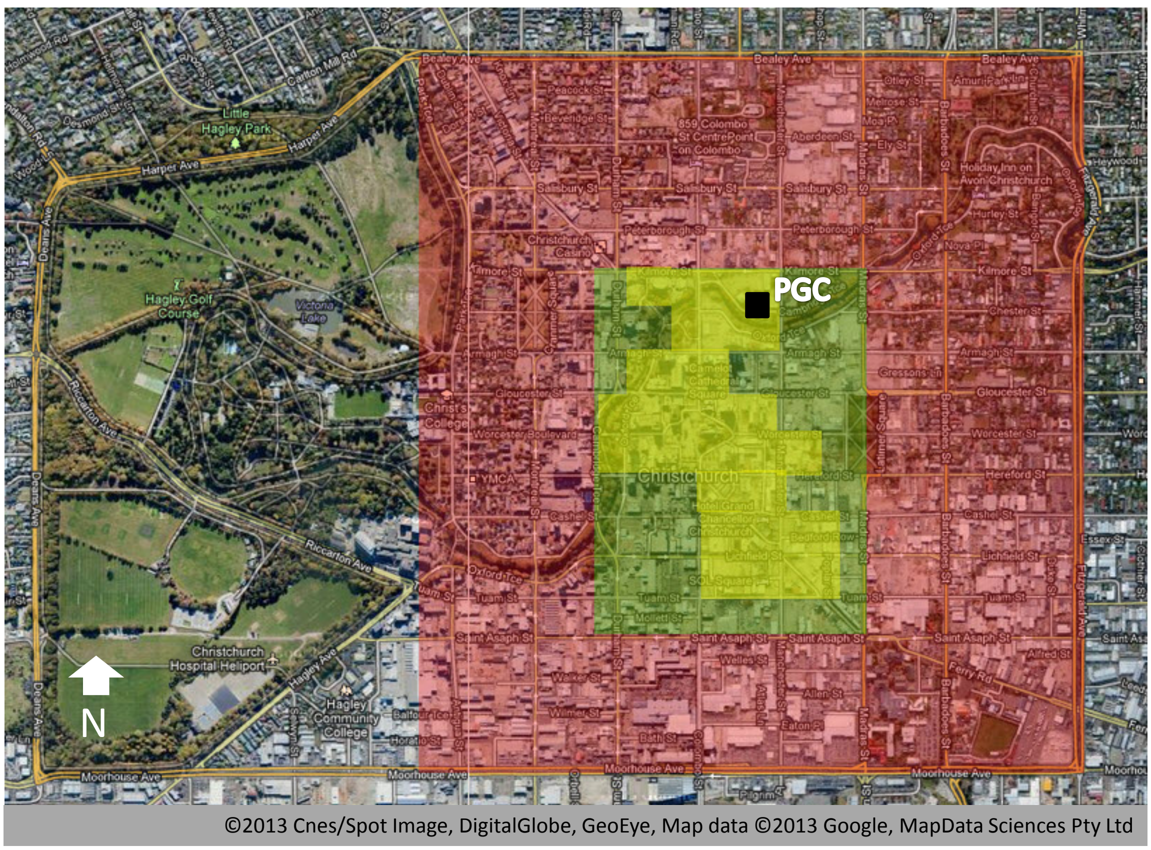

Figure 5: Central business district of Christchurch indicating the different cordon areas over time. Red: 1 month, Green: 1 year, Yellow: As of February 2013

The building site is 130 feet (40m) north of the Avon River, it is relatively flat with little topographical features. The building is oriented north to south as shown in Figure 5.

2.2 Site Analysis

The site conditions surrounding PGC are thought to contribute very little to the collapse. A team of engineers from Beca were at the site 2 months after the collapse to investigate the surrounding conditions. The city of Christchurch could not find any records of a full geotechnical report during the time of construction, therefore it is impossible to know what conditions the building was designed for and what they were expecting with the soil. Bore holes were drilled by Pro Drill Ltd, as part of the Beca's investigation of the site. The bores found medium-dense sand and gravelly soil, with traces of water. Liquefaction was a large issue in all of Christchurch, but after cone penetrometer tests were completed, it was deemed unlikely that liquefaction were to occur in the sandy gravels up to and greater than a peak ground acceleration of 0.8g. Liquefaction was assumed a non-factor in the collapse of the building. For more detailed information regarding the results of the machine boreholes and cone penetration tests refer to the geotechnical report in Beca (2011b).

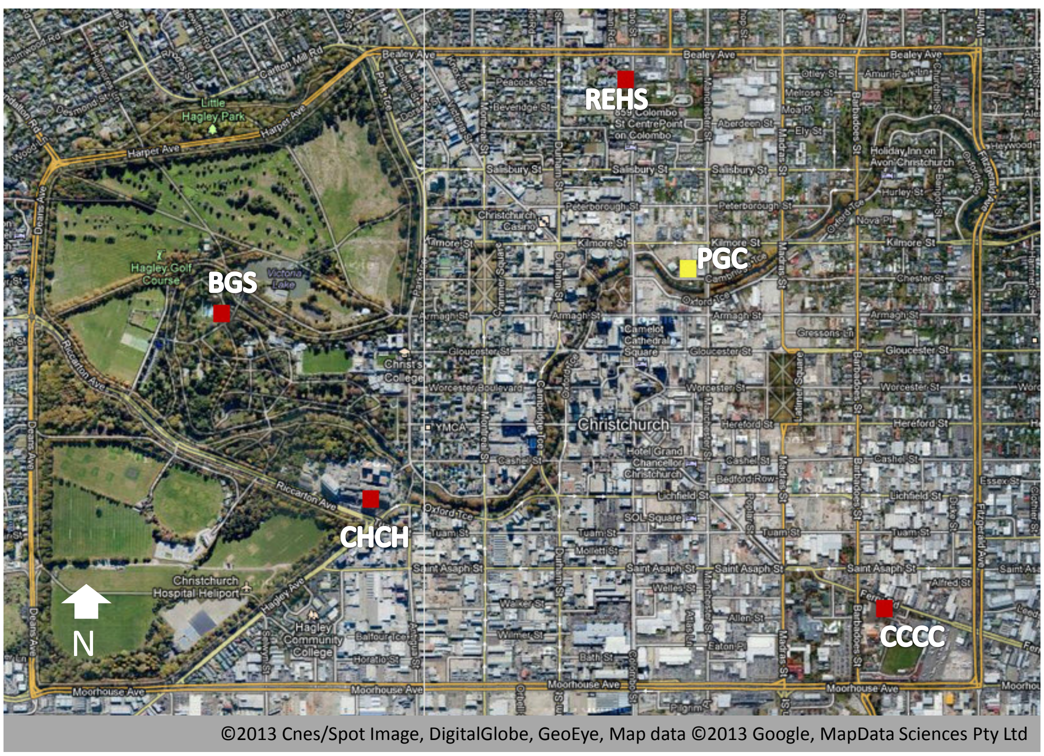

Figure 6: Central Christchurch indicating the locations of the four ground motion recording sites with respect to PGC

There were four locations taking strong motion readings using seismographs during the September and February events. All four sites were investigated by Beca in order to determine the site that most closely represented the PGC site. The closest site to PGC was Resthaven Rest Home (REHS), roughly 2200 feet (670m) north northwest. The other three sites Catholic Cathedral Collage (CCCC), Christchurch Hospital (CHCH) and the Botanical Gardens (BGS) as well as REHS are shown in Figure 6. Along with Beca, GNS Science also provided site analysis, summarized in Beca (2011a) for the four strong motion sites indicating that they all were very different than PGC. All four sites consisted mostly of clay type soils. These types of soils would alter the ground motion in a different way than the sandy gravels found at the PGC site. In conclusion to the reports provided by both Beca and GNS Science, the REHS site was considered the most similar (Beca 2011a). The PGC site was found to be stiffer than that of REHS, most likely causing the intensities and frequencies of the recorded motions to be greater than those felt by the structure. This would make choosing the records from REHS slightly conservative. The ground motions recorded from the REHS site will be used for the remaining analyses.

2.3 PGC History

PGC was designed in 1963 per a multitude of possible design codes. No design calculations or specifications were found from the original design therefore it is thought that any of the following could have been used: Part 4 of the NZSS 95, Chapter 8 of the NZSS 1900, British Concrete Code CP114 or the ACI 318-63 (Beca 2011a). As stated previously no further investigation into the New Zealand building codes will be completed, please refer to A.2 for a brief history of NZ concrete codes as they adapted and changed over the years.

2.3.1 Summarized Assessment and Renovation History

Since being designed, PGC has under gone minor and major, structural and non-structural upgrades that have altered the original plans. The most notable being the 1997 seismic assessment of PGC done by the owner’s engineer. This assessment resulted in a full seismic analysis of the building, indicating serious vulnerabilities in the lateral-force-resisting-system and the deformation capacity of the exterior columns. The following is a summarized list of architectural and structural upgrades occurring since 1964 as provided by Beca (2011a).

1997-1998

- The building was fully assessed by the owner's engineers and stripped to the bare structure where elements such as ceilings, partitions, glazing and an air conditioning system were added.

Based on the 1997 structural assessment the existing columns had deficient plastic rotation, which led to the installation of steel props directly behind the existing columns from level one to the roof (Figure 7 and Figure 8). Only one prop was installed behind the two corner columns at gridlines b and g and no props were installed behind the two columns adjacent to the north wall (gridline D/b and E/b). The steel props were installed to act as a secondary gravity support system following severe damage to the columns. The props are insufficient however if the failure is localized in the beam-column joints and would contribute very little to the overall deformation capacity of the frame.

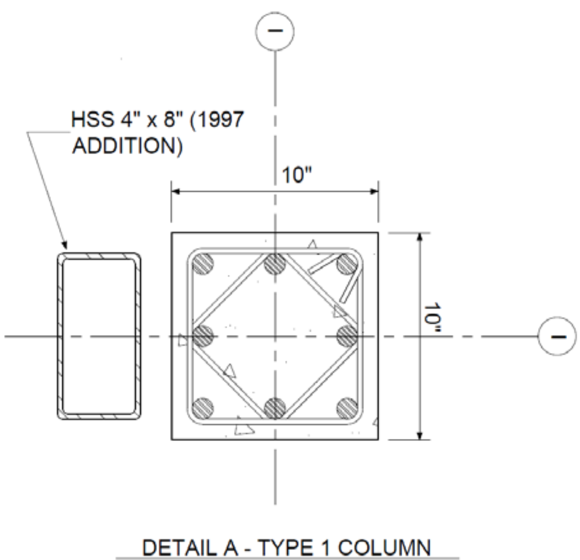

Figure 7: Detail A showing column type 1. Typical column located along gridline A and H (Figure 3) from level 1 to the roof (based on original structural drawings provided by Beca 2011a, refer to Appendix A.1)

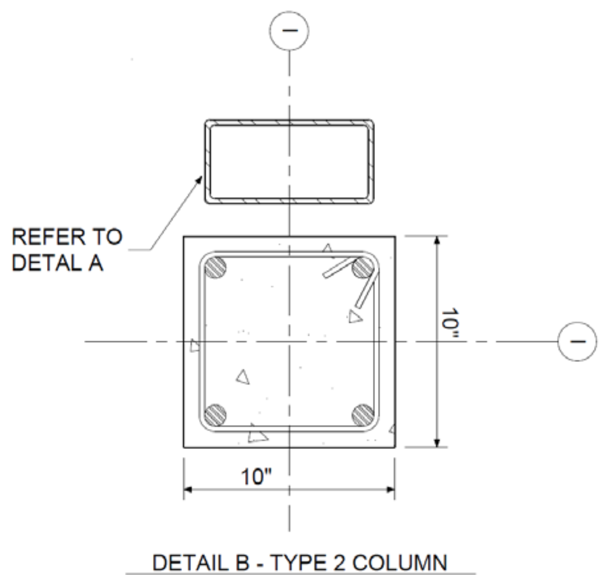

Figure 8: Detail B showing column type 2.Typical column located along gridline a and h (Figure 3) from level 1 to the roof (based on original structural drawings provided by Beca 2011a, refer to Appendix A.1)

- Door and window openings were added and removed to the main set of core walls along gridlines D and E. The most significant being the door opening along gridline D between d and e at all levels above the ground.
- The short 28” concrete perimeter components were removed, reference Sheet S.3 in A.1.
- The concrete umbrella structures shown in the drawing Sheet S.17 of A.1 were removed.
- The ground level stair location was moved and the alternate staircase that reached from the ground level to level one was completely removed.

2008

- A 40 foot (12 m) high cell-phone tower was added to the roof
- More door and window openings were added and filled in.

2009

- Repair to cracks due to corrosion in the concrete columns along the perimeter above level 1 was completed.

2010

- Site and structure assessment performed twice by the owner’s engineer and once by a third party engineer, following the September 4th Darfield earthquake.

2011

- Site and structure assessment following the December 26th 2010 earthquake.
- Following the collapse of PGC, during the February event, visual assessment of the site and structure from observers and the urban search and rescue (USAR).

A more detailed summary regarding major events in the buildings lifecycle can be found in Beca (2011a).

2.4 Observations: From Design to Collapse

Based on the original structural drawings and photos of the collapsed building following the February event, observations were made and compared to a list of critical deficiencies commonly seen in reinforced concrete buildings built prior to 1980 (Figure 9). According to the Applied Technology Council document 76-05 (ATC 76-5) (ATC 2010) these deficiencies have been linked to collapsed reinforced concrete buildings from past earthquakes. Figure 9 lists the ten most common critical deficiencies as determined from ATC (2010) with a brief description explaining each one.

Deficiency A: Shear-critical columns	**Deficiency F: Overall weak frames**
 Shear and axial failure of columns in a moment frame or gravity frame system.	 Overall deficient system strength and stiffness, leading to inadequacy of an otherwise reasonbably configured building.
Deficiency B: Unconfined beam-column Joints	**Deficiency G: Overturning mechanisms**
 Shear and axial failure of unconfined beam-column joints, particularly corner joints.	 Columns prone to crushing from overturning of discontinuous concrete or masonry infill wall.
Deficiency C: Slab-column connections	**Deficiency H: Severe plan irregularity**
 Punching of slab-column connections under imposed lateral drifts.	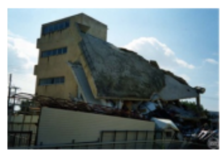 Conditions (including some corner buildings) leading to large torsional-induced demands.
Deficiency D: Splice and connectivity weakness	**Deficiency I: Severe vertical irregularity**
 Inadequate splices in plastic hinge regions and weak connectivity between members.	 Setbacks causing concentration of damage and collapse where stiffness and strength changes. Can also be caused by change in material or seismic-force-resisting-system.
Deficiency E: Weak-story mechanism	**Deficiency J: Pounding**
 Weak-column, strong-beam moment frame or similar system prone to story collapse from failure of weak columns subjected to large lateral deformation demands.	 Collapse caused by pounding of adjacent buildings with different story heights and non-coincident floors.

Figure 9: Critical Deficiencies observed in pre-1980 reinforced concrete buildings (ATC 2010)

Shear-critical columns (Critical Deficiency A), based on the photos following the collapse, very little damage can be seen in the columns (Figure 10). Majority of the damage is concentrated in the beam-column joints (Figure 10), refer to section 4.3.2 for more detailed information regarding the expected performance of the beam-column joints. It is unclear based on the observed damage if the columns were shear critical, since majority of the damage is sustained within the joints. The non-ductile exterior frame of PGC was constructed with minimal transverse reinforcement through the beam-column joints (critical deficiency B), resulting in very little deformation capacity. The lack of continuous transverse reinforcement in the joints is common practice for buildings built at this time. The exterior gravity frame failed in a sidesway mechanism, following the increase in displacement demand from the shear core, as it collapsed to the southeast, see Figure 10. The props installed from the 1997 assessment provided little assistance for this type of failure mechanism.

Figure 10: Typical joint damage (left) South elevation showing the collapse of exterior gravity frame (right) (photos courtesy of Ken Elwood)

Plan and vertical irregularities (critical deficiencies H and I) are both present and can be identified by looking at the plan drawings of Figure 2 and Figure 3. The plan irregularity is a result of the off center location of the lateral system, located to the north of the building plan. This can cause an increase in displacement demand to the exterior gravity frame along line h, as well as an increase in shear demand on the shear core. An observation made by an investigation (Beca 2011b) following the February collapse showed that the slabs were nearly stacked on top of one another, shifted towards the east, indicating very little plan rotation. This may have been the final state of the slabs relative locations, but it does not indicate whether the torsional irregularity caused an increase in shear demand, which could have contributed to the collapse. This issue will be discussed further, throughout the remaining sections. The vertical discontinuity is the result of the discontinuous wall along gridline E, between the ground level and level 1. Discontinuous walls can cause large demands in the transfer elements such as the slab at level 1. Following the February event the urban search and rescue team members did not observe any punching of the wall through the slab at level 1 along gridline E, therefore, this likely did not contribute to the collapse. The vertical discontinuity can also be attributed to the increase in strength and stiffness at the ground level, due to the additional 8-inch walls as well as the additional 16-inch circular, steel encased column grid at the perimeter (see the plan drawings, Figure 2 and Figure 3). The increase in strength at the ground level compared with the upper stories is the main reason why this level did not collapse, forcing large deformations and collapse of the core wall at Level 1 rather than the ground level.

Poor connectivity between elements, critical deficiency D, is a significant factor when considering the separation of the floor system (girders and slabs) from the shear core. From Figure 11, the red circles show the large openings where the floor beams used to be connected to the core. Minimal to no continuous reinforcement or hooks of any kind are shown in the drawings at the connection between the beam and the shear core, requiring the minimal slab reinforcement, which were spliced at this location to transfer majority of the load to the shear core.

Figure 11: Detached floor systems from shear core shown by large holes where the girder slab connection pulled away from the wall due to lack of continuous reinforcement (photo courtesy of Ken Elwood)

Only 2-#8 bars, embedded 4 inches into the core at the top and 4-#10 bars, embedded 4 inches at the bottom (with respect to the attached beam) are used at the connection. A quick calculation of bond strength for these two types of bars is shown in A.3, the 2 -#8 bars govern the bond slip ultimate capacity estimated at 5.3 kips. Looking closer at the picture in Figure 11, the embedded beam reinforcement had removed a portion of the wall during collapse (a concrete pull-out failure). Beyond the critical deficiencies that have been observed from existing buildings that may have caused collapse in past earthquakes, PGC is unique and more specific deficiencies can still be observed.

The shear core consists of 8-inch wall sections with a single layer of #5 bars spaced at 15 inches, each way, with no boundary elements or confinement. Due to the thin sections and poor detailing, the wall flanges along gridlines D and E are susceptible to bucking or crushing from high demand in the east-west direction. Also, the door openings in the core walls on gridlines D and E increase this critical vulnerability in the wall at this location. It is assumed the location of failure is just above level one, due to the previously described vertical discontinuity at this location and by inspection of Figure 12,where the wall at level 1 cannot be seen between the floor slabs of level 1 and 2.

Figure 12: North Elevation indicating loss of the level 1 wall along gridline E (photos courtesy of Ken Elwood)

By further observation of the post-earthquake photos, it appears that the failure of the walls at level 1 caused the entire shear core to lean towards the southeast (see Figure 13), which would be consistent to a crushing and buckling type failure at the wall opening along gridline E. Figure 13 indicates the core rotation based on the final positions of column at grid E-b.

Figure 13: North Elevation of the collapsed structure showing the end location of the core relative to its starting position (photo courtesy of Ken Elwood)

A final observation regarding the failure of the wall is the large diagonal cracks shown in Figure 14, located around the window opening of the north wall of the core at level 2. Considering the severity of the cracks shown at level 2 and the expected increase in demand from level 2 to level 1, it is possible a shear type failure mechanism controlled the failure of the wall at level 1. This type of perforated shear wall is susceptible to shear failures and considering the lack of confinement and thin wall sections of the core walls, this would only increase this susceptibility. These cracks do not definitively indicate shear failure occurred, but they do lead to the possibility that it could have influenced the collapse. The cracks, shown in Figure 14 span from the top right to the bottom left, which is consistent with a loading demand from the west to the east, which is the direction the entire structure failed. Shear failure of a concrete wall is essentially a compression or tension failure along a diagonally cracked plane. Following a shear failure of the north wall at level 1, the east flange of the core, considering the increase in demand could have still failed in compression, which would explain the previously stated observations regarding the final position of the shear core.

(a) (b)

Figure 14: Diagonal shear cracks at the window openings of the north wall at level 2 (a) and (b) (photos courtesy of Ken Elwood)

Shear failure at this location has been speculated by numerous academics and practicing engineers as summarized by the Royal Commission (2012a), but no analytical evidence has been shown. The 1997 structural assessment identified the walls as being vulnerable, stating that:

“The wall shear strains are also relatively high although cracking is confined to specific portions of the walls, mainly the coupling beams and around openings. The main effect of this cracking is to reduce the stiffness of the wall but as the cracks do not close there are potential serviceability problems. For walls which have been strained to the degrading portion of the curve there will be some loss of gravity load carrying capability. However, the consequences of this are not likely to be as severe as for columns as each wall portion supports a relatively small tributary area of floor” (Beca 2011b).

Since the expected damage to the walls around openings was expected to be minimal and not life threatening, no retrofit procedures were undertaken. Further supporting the possible shear failure, an engineer’s site report following the December earthquake stated:

“General diagonal cracking to all shear walls (Beca 2011a).”

In order to better determine which mechanism, whether it was flexure or shear, governed the failure of the core wall system during the February earthquake, a more detailed look into the performance of the walls is required. This type of in depth analysis is undertaken in the sections to follow where majority of these observed vulnerabilities are addressed from an analytical stand point.

Chapter 3 **Royal Commission Report**

Royal Commissions or Commissions of Inquiry are established following any significant event in New Zealand, as determined by the government, in order to investigate and gather valuable information as it pertains to the public. Following the Canterbury earthquake sequence a Royal Commission inquiry was established, according to the terms of reference (Royal Commission 2011), "…to report on the causes of building failures as a result of the earthquakes as wells as the legal and best-practice requirements for buildings in New Zealand Central Business Districts.". In the following sections a summary of the findings specific to the collapse of PGC will be discussed, for more information regarding the other buildings or a more detailed investigation report please refer to DBH (2013).

3.1 **Beca**

Beca Carter Hollings and Ferner (Beca) is a consulting engineering firm in New Zealand, who was contracted by the DBH, through the Royal Commission, to investigate the Pyne Gould Corporation building, following the collapse during the February event. The report was completed considering the seismic performance of PGC as compared to the current design codes and the existing building assessment procedures. Both the existing building assessment procedures and the new design codes of NZ are beyond the scope of this thesis and will not be discussed any further. All other information regarding PGC as compiled by Beca and summarized in Beca (2011a and b) such as site conditions, material tests, observations following major events, assessment history, static and dynamic analyses, and the concluding remarks and discussion are discussed and referenced throughout the remainder of this thesis.

Beca used two computer models to capture and investigate the performance of PGC during the September, December and February earthquakes (Beca 2011b). The first model used was a stick model or a single element model representing the shear core only, used for the purpose of calibration and validation of the second model, a full 3D, finite element model. The full 3D finite element model incorporated the entire building. Using material properties from their materials investigation (Hyland 2011) backbone responses for each element were incorporated into the full 3D model these properties are summarized in Chapter 4. Six analysis procedures were undertaken: sectional, static pushover, modal, response spectrum and nonlinear time-history. The sectional analysis produced a moment-curvature response for the wall elements above level 1, using the computer software Response-2000 (Bentz 2000). Based on this analysis the flange reinforcement ruptures at a curvature of 0.000254 rad/in (0.01 rad/m). It is unclear the assumptions Beca made to determine this moment-curvature response for the entire core above level 1, but this data will be compared with the findings of the current study in succeeding section 5.3.4. Modal analysis, static pushover and response spectrum analysis were used to calibrate an accurate stiffness and mass into the finite element model, validating its use in the non-linear time history analysis. Using the computer software Perform (Computers and Stuctures, Inc. (CSI) 2013) Beca completed three time-history analyses using the recorded ground motions from the September, December and February events. Following all three analyses, Beca concluded that PGC was not capable of sustaining the demand produced by the February event, resulting in collapse. Their results show the critical failure mechanism as being flexure within the shear core. Based on eye witness accounts and the findings from the analysis, a sequence of failure was estimated (Figure 15). At 5.3 seconds the west flange reinforcement fractured causing the building to sway to the east an unsustainable distance, causing the east flange to crush at 5.6 seconds. At 5.6 seconds into the earthquake the wall was expected to fail. The sequence after failure of the wall is unknown, but the remaining gravity components and connections, specifically the exterior frame and slab to wall connections, could not withstand the large displacement and rotational demands following failure of the shear core. As the building continued to displace under the earthquake excitation, the remaining structural components began to lose vertical–load-carrying-capacity, resulting in the pancaking effect of the floor slabs, as seen in the Figure 10.

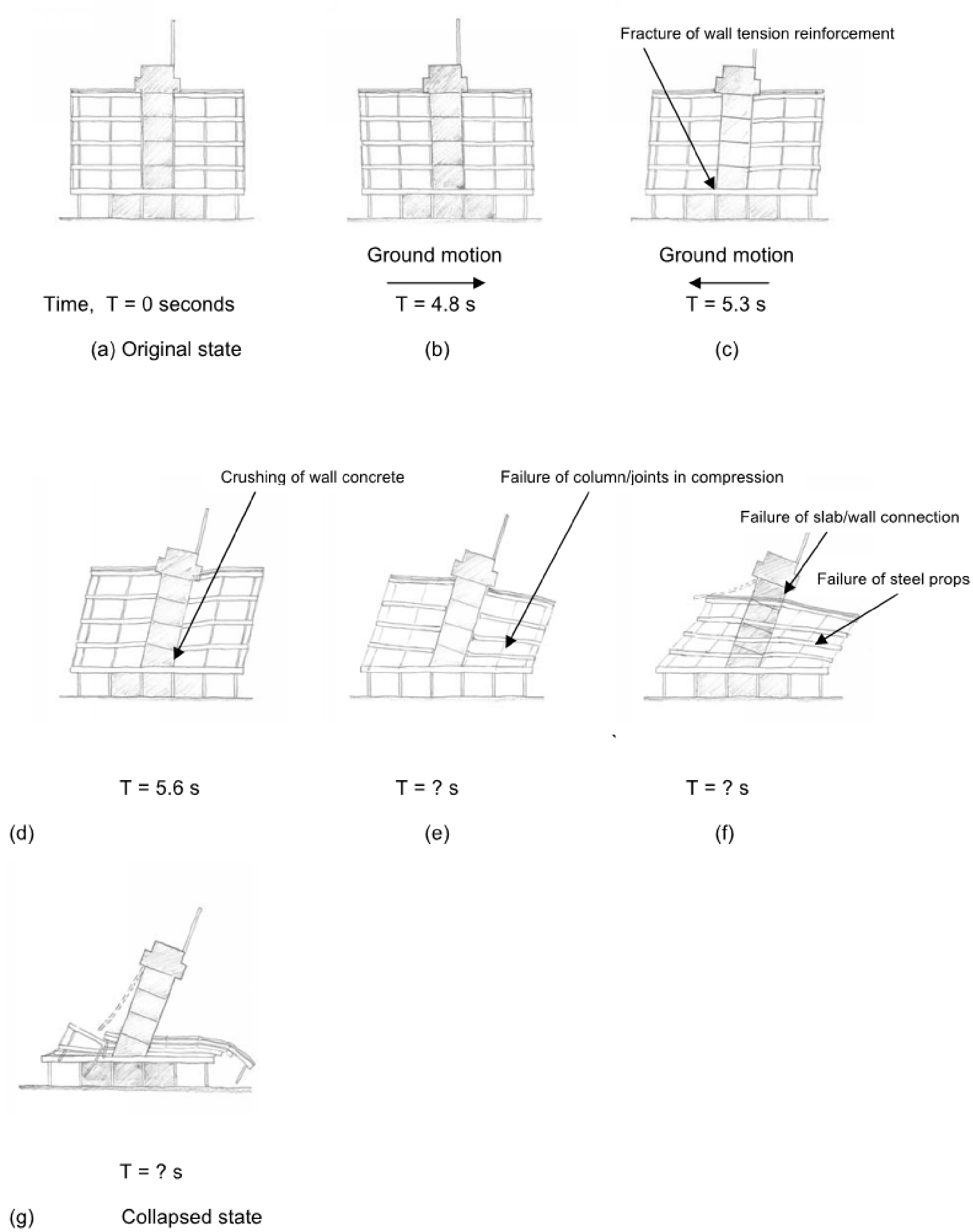

Figure 15: Estimated sequence of collapse as provided by Beca (2011a)

The provided findings from Beca indicated that plan twisting was present throughout the simulation, but dissipated as the shear core elements began to fail. This supports the post collapse photos which indicated very little plan rotation as the final position of the slabs was directly on top of one another (Beca 2011b). Beca concluded that torsion did not influence the collapse. This assessment will be considered in the remainder of this thesis, as it is possible that the torsional response may have influenced a shear-type failure mechanism in the north wall. Beca also concluded that failure would not have occurred within the exterior gravity frame joints without failure of the shear core occurring first. This is based on the findings that the columns did not develop extensive yielding until after the shear core had failed. The findings from Beca were thorough and will be used as a reference for comparing different modeling approaches as well as discussing alternative failure mechanisms in the succeeding chapters.

3.2 Hearings – expert opinions

As part of the inquiry, the Royal Commission held hearings and called upon academics and practicing engineers from many backgrounds to come forward and discuss their opinions regarding the submitted technical reports and the overall performance of the structures. The expert committee answered questions from the Royal Commission as a group and as individuals at different times regarding the technical report submitted by Beca, as well as presented their own material on their option regarding the issues. The discussion of most importance was regarding the possibility of shear failure in the perforated wall segment at the north of the core wall system. The possibility that the core may have failed in shear prior to failing in flexure brings insight into the vulnerability of other similar buildings in danger of performing similar to PGC. Other notable discussions regarding PGC was the influence of the vertical component of ground motion on the collapse, which was considerably larger in magnitude than similar past earthquakes, the discontinuous wall towards the north end of the core system at level 1 and the vertical stiffness irregularity due to the large amount of lateral resistance at the ground level versus the levels above. For more details regarding the expert opinion hearings refer to the royal commission website http://canterbury.royalcommission.govt.nz/, where the videos of the hearings are archived.

3.3 Final Report Summary

The final report published by the Royal Commission compiles all of their findings regarding the collapse of PGC as well as the collapse and performance many other buildings during the Canterbury earthquake sequence. The final conclusions are separated into two categories, critical weaknesses and collapse mechanisms, a summary of these categories are listed below (as concluded by Royal Commission (2012a).

Critical Weaknesses:

- Vertical discontinuity in load path from the shear walls above level one to the ground level.
- Low levels of flexural reinforcement in the plastic hinge region of the shear walls incapable of activating secondary cracks.
- Eccentric location of the shear core causing an increase in torsional response inherently weakening the building.
- The lack of proper anchorage of gravity beams into the shear core.
- The non-ductile detailing throughout the building.

Collapse Mechanisms:

- Bi-axial demand causing high stress regions at the corners of the shear walls where less effective compressive area is present, specifically the discontinuity of the east wall below level 1.
- The transverse walls containing an inadequate amount of horizontal reinforcement to resist the high shear demands leading to shear failure or flexure shear failure.
- Failure of the eastern wall from a local punching-type failure due to the high shear forces in the transverse walls following tension failure of the western wall reinforcement
- Compression failure of the eastern wall following tension rupture of the western wall.

The specific report regarding the collapse of PGC used the technical report submitted by Beca and the expert panel discussions and reports as the main supporting documents. The

PGC portion of the report did not give any new information which had not been discussed or reported on previously. The entire report is broken into seven different volumes and can be downloaded from the royal commission website at the above link.

Chapter 4 **Preliminary Estimates**

Following the collapse of PGC, Hyland Consultants, a fatigue and earthquake engineering company, partnered with Sai Global, a material testing facility, produced a materials report (Hyland 2011). The report included tests for both the concrete and the reinforcement of all major components within PGC, 3 types of beams, 3 types of columns, the slab and a portion of the shear core. Chemical analysis was also provided for the steel and concrete. This is not considered within the scope of this thesis. A summary of the material properties for the shear core, columns, beams and slab, as found from Hyland (2011), is shown in Table 1. It was determined from the materials investigation that some of the tested columns consisted of two different types of longitudinal reinforcement, USA standard #8 and D24 from Japan. As a result of this finding, the lowest value is used and if multiple test results were provided, the average of the tests is used. These material properties are used for the remainder of the analysis, unless noted otherwise.

Table 1: Material Properties (adapted from Hyland 2011)

<table>
<tr><th rowspan="2" colspan="2">Component</th><th colspan="4">Concrete[1]</th><th colspan="4">Steel[1,2]</th></tr>
<tr><th>Expected Concrete Strength, f'c</th><th colspan="2">Concrete Stress at failure, fcu</th><th>Strain at Failure, εcsu</th><th>Yield Stress, fy</th><th>Ultimate Stress, Fsu</th><th>Yield Strain, εsy</th><th>Ultimate Strain, εsu</th></tr>
<tr><td rowspan="2">Walls</td><td>Core</td><td rowspan="2">-3.5</td><td rowspan="2" colspan="2">-0.7</td><td rowspan="2">-0.004</td><td rowspan="2">45</td><td rowspan="2">65</td><td rowspan="2">0.00155</td><td rowspan="2">0.075</td></tr>
<tr><td>Non-Core</td></tr>
<tr><td rowspan="2">Columns</td><td>Type 1</td><td rowspan="2">-6.86</td><td rowspan="2" colspan="2">-1.4</td><td rowspan="2">-0.004</td><td>47.6</td><td rowspan="2">66.7</td><td rowspan="2">0.0016</td><td rowspan="2">0.075</td></tr>
<tr><td>Type 2</td><td>46.4</td></tr>
<tr><td>Beams</td><td>Typical At exterior</td><td>-5.903</td><td>-</td><td>-</td><td>-</td><td>47.6</td><td>-</td><td>-</td><td>-</td></tr>
</table>

1: All appropriate values in ksi

2: For both longitudinal and transverse steel in all components

Along with the properties from the material tests, failure strain limits for the concrete and steel of the shear core are assumed based on judgment and previous research. For the concrete, a maximum compressive strain of -0.004 will be used, this is recommended for walls of these types by the American Society of Civil Engineers: Standard for Existing Buildings (ASCE-41-06) (ASCE 2006). This is high compared with current research, which shows that lightly reinforced walls, with little to no transverse confinement in the boundary zone can crush at strains as low as -0.001 (Adebar and Lorzadeh 2012). The compressive stress, at the crushing strain, f_{cu} was determined as 20% of the compressive strength f_c' , this is recommended by a Pugh (2012) regarding the computer modeling of RC walls. Considering the age of the concrete and the history of past events the tensile strength within the shear core is considered negligible and will be assumed as 5% of the compressive strength.

The reinforcement within the walls was tested using standard 8 inch sections, removed from the core wall and pulled in tension until rupture. Four different specimens were tested, failing at an average elongation of 36%. Research shows that stress-strain relations under monotonic loading, similar to the standard test done by Hyland, differ greatly than those under cyclic loading, similar to a seismic event (Mander, Panthaki and Kasalanati 1994; Heo Kunnath and Xiao 2009). Mander et al. and Heo et al. show that ordinary grade reinforcing bars under both monotonic and cyclic loading vary greatly in their tension strain limits. Under the monotonic loading, the strain limits reached a maximum of 15%, but the same specimen under cyclic loading showed failures ranging from 3-8%, depending on the rate of stain and other loading characteristics. Since the bars within PGC are ordinary deformed bars, used in construction in the 1960s, the failure strain provided by Hyland is too high. Therefore a strain limit of 7.5% is used, which is consistent with past research.

4.1 Design Details

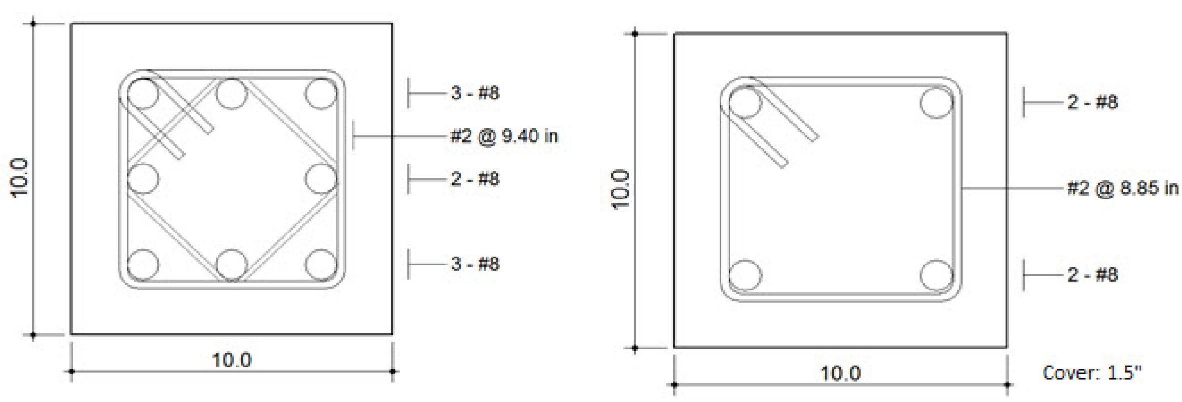

Figure 16: Typical gravity column type 1 (left) type 2 (right)

Two typical 10-inch by 10-inch gravity columns were used in the construction of PGC to support the slab and beam system above level 1, indicated in Figure 16 as type 1 and type 2. Both types of columns are supported on the first story by cantilevered beams and rise vertically through four stories to the roof by a story height of 12-feet 6-inches. Type 1and type 2 are located at the perimeter along gridlines A and H and a and h, respectively (Figure 18). Section cuts at level 1for both columns (Figure 16) show the typical reinforcement sizes and spacing, as well as important dimensions, which will be used in the capacity assessments in the sections to follow. The reinforcement ratio for column type one is very high at 6.28%, this is reduced at level 3 becoming similar to column type 2 (3.14%). The issue becomes at the splice locations (level 2), which would yield a reinforcement ratio of well over 8%, the limit for any section cut through a column (ACI 2008).

Table 2: Specimen Design Properties (adapted from Hyland 2011)

<table>
<tr><th colspan="2">Component</th><th>P/Agf'c</th><th>ρl (%)</th><th>ρt (%)</th><th>a/d*</th><th>s/d**</th></tr>
<tr><td rowspan="2">Columns</td><td>Type 1</td><td>0.29</td><td>6.28</td><td>0.18</td><td>7.5</td><td>1.11</td></tr>
<tr><td>Type 2</td><td>0.29</td><td>3.14</td><td>0.11</td><td>7.5</td><td>1.04</td></tr>
<tr><td rowspan="3">Walls</td><td>Core</td><td rowspan="2">-</td><td rowspan="2">0.002583</td><td rowspan="2">0.002583</td><td rowspan="2">-</td><td rowspan="2">-</td></tr>
<tr><td>Non-Core</td></tr>
<tr><td>CWN Web Pier</td><td>0.08</td><td>0.00323</td><td>0.00258</td><td>-</td><td>-</td></tr>
</table>

*a/d = shear span-to-depth ratio

**s/d = transverse reinforcement spacin-to-depth ratio

The shear walls contain minimal reinforcement as seen from the reinforcement ratios in Table 2. Based on the original structural drawings (Appendix A.1) all the walls are 8 inches thick and contain the same reinforcement in both directions, #5 at 15 inches oc each way within the web portion of the walls and 2-#5 at the boundary conditions, as shown in Figure 17.

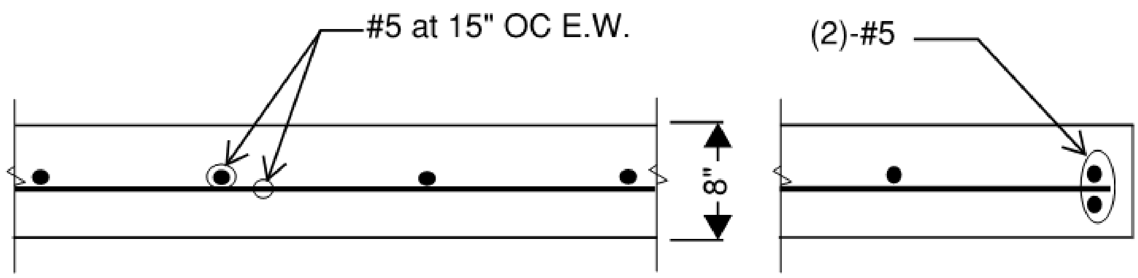

Figure 17: Typical web and boundary wall reinforcement for all walls (adapted from the original structural drawaings provided by Beca, 2011b)

Figure 18 displays the walls which will be used in the analytical modeling. For modeling purposes any vertical discontinuities at level 1 were ignored. All of the walls being modeled are separated into two groups, either core walls (CW) or non-core walls (NCW). The CW group is then again separated into three main wall assemblages (Figure 18). The three main wall assemblages are core wall north (CWN) , core wall center (CWC) and core wall south (CWS), both CWN and CWS have east and west flanges and web segments and will be denoted as such in the remainder of this thesis. Three full height elevations are shown in Figure 19, as indicated in Figure 18 showing typical wall openings. The elevation of CWN, Figure 19 (a), shows the expected location of the critical pier at level 1 (Figure 20) below the observed diagonal cracks following the collapse. The design details of the CW assemblages, non-core walls and the critical wall pier are summarized in Table 2.

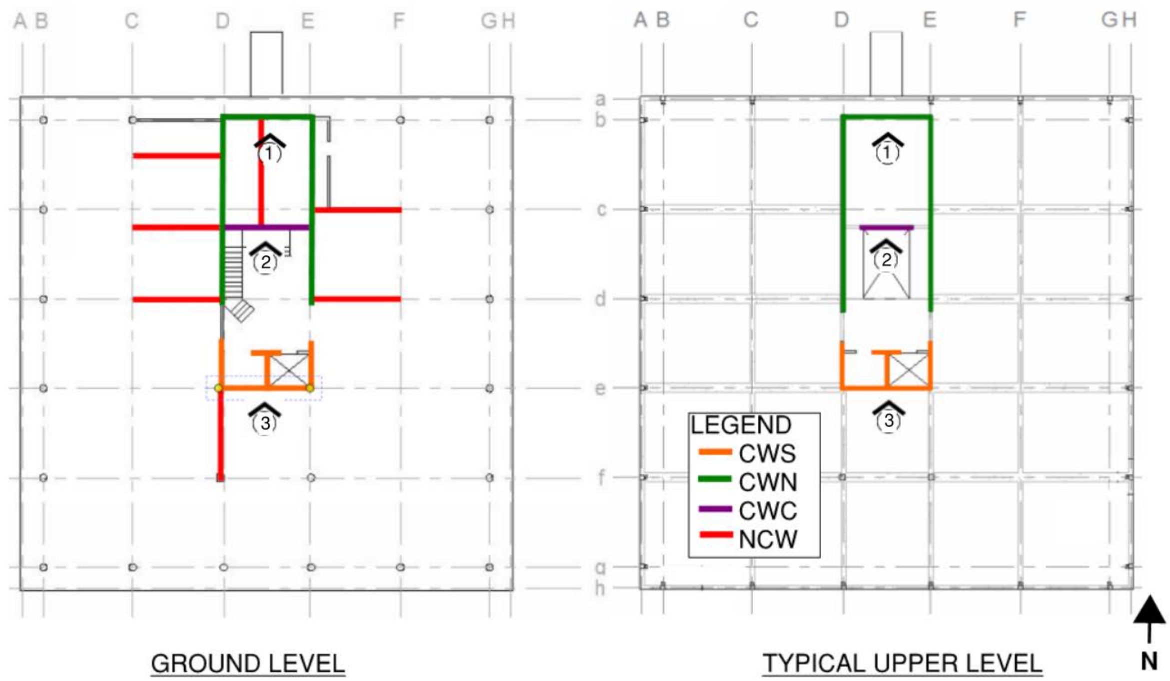

Figure 18: Wall notation diagrams (adapted from the original structural drawings provided by Beca 2011b)

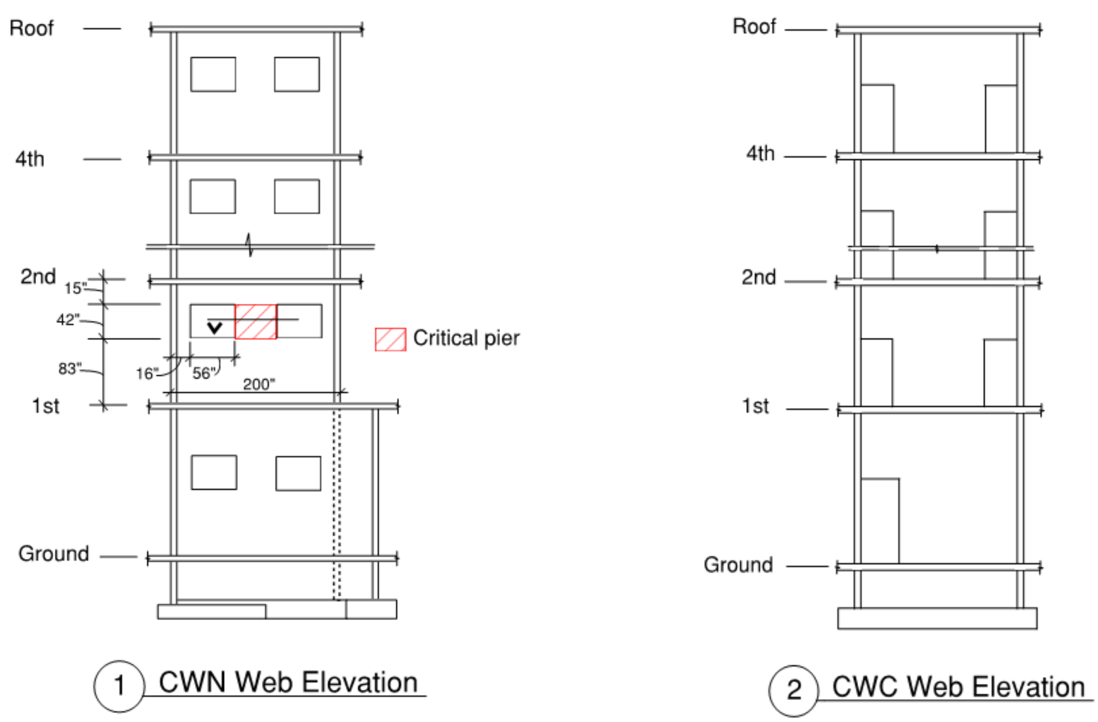

(a) (b)

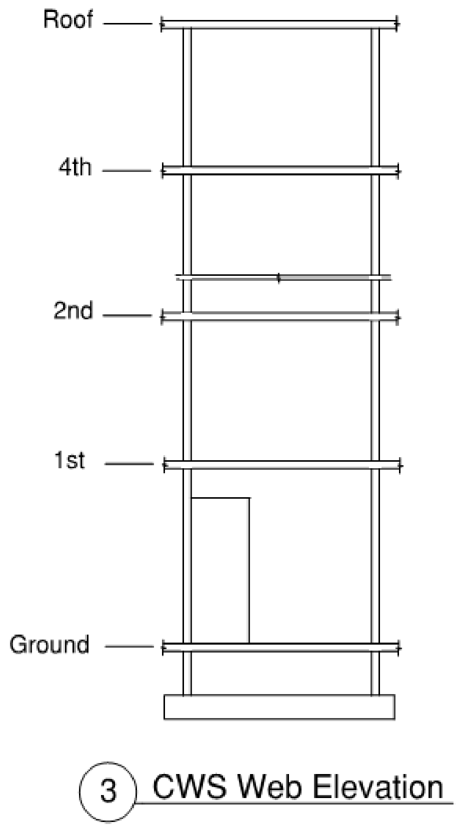

(c)

Figure 19: Elevation view (a), (b) and (c), as indicated on plan in Figure 18 (adapted from the original structural drawings provided by Beca 2011b)

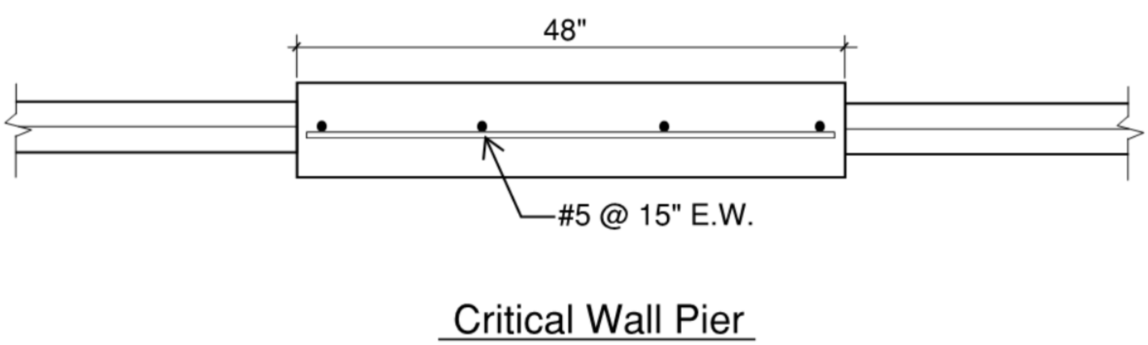

Figure 20: Plan view of the critical wall pier as indicated in Figure 19 displaying reinforcement

4.2 Component Capacities

A simple capacity analysis is completed in order to determine whether the columns, under maximum loading, will fail in shear, flexure-shear, or pure flexure. The purpose of this assessment is to estimate the failure mechanism of the two types of typical gravity columns (Figure 16) and to grasp how these columns will respond under seismic loading. Assuming a fixed-fixed condition, a comparison between the maximum shear strength of the column, V_n versus the shear at the plastic moment capacity, V_p is made. The determination of the type of failure for different outcomes is displayed in Table 3.

Table 3: Failure Conditions (adapted from ASCE 2007)

i = Vp/Vn	Failure Type
i ≥ 1.0	Shear Failure
1.0 > i > 0.7	Flexural - Shear Failure (Flexural yield prior to shear failure)
i ≤ 0.7	Flexural Failure

Using the shear model developed by Sezen (2002), the shear strength, V_n (equation (1), of these gravity columns can be obtained as follows.

$$V_n = k(V_c + V_s) = k\left(6\,\frac{\sqrt{f'_c}}{\frac{a}{d}}\sqrt{1+\frac{P}{6\sqrt{f'_c}\,A_g}}\,0.8A_g\right) + k\left(\frac{A_{ST}df_{yt}}{s}\right) \quad \textbf{(1)}$$

Equation (1) shown above breaks the shear into two parts, V_c, the shear strength provided by the concrete and V_s, the shear strength provided by the transverse reinforcement, assuming a 45° truss model. The factor k is a degradation factor related to ductility, k decreases with increasing ductility demand. For the purposes of this assessment the factor k will be taken as one, which assumes a ductility of less than 2, according to the model presented by Sezen (2002). All the other variables are obtained through geometric and material properties (Table 1) of the specimen, where f'_c is the compressive strength of the concrete (psi), a is the shear span, d is the depth to the center of the tension reinforcement, P is the axial load on the column, Ag is the gross cross sectional area, Ast is the area of the transverse reinforcement, f_{yt} is the yield strength of the transverse reinforcement and s is the longitudinal spacing of the transverse reinforcement. The nominal shear strength, V_n for column type 1 and 2, using equation (1 is shown below in Table 4 and Table 5, respectively.

The applied gravity load was determined based on the worst case tributary area of each column type. This was then used to determine the amount of load transferred to each column from the slab and beam system, including the self-weight. A 75 psf dead load was also added to account for miscellaneous items. Due to the repetitious nature of the floors above level 1, the axial load per story is 50 kips. The final gravity load applied to the column sections, is 200 kips, an axial load ratio ($\frac{P}{f'cAg}$) of roughly 0.3. Sectional analysis was performed for both column types, using the engineering software Response-2000 (Bentz 2000) and an approximated tri-linear moment-curvature approach, in order to obtain an estimate of the plastic moment capacity, M_p. These plots are located in Figure 21 and Figure 22, respectively. The shear at plastic capacity V_p is obtained using statics, shown in equation 2, where L is the clear height of the column.

$$V_p = \frac{2M_p}{L} \tag{2}$$

According to ASCE-41 section 6.4.2.3.1, maximum usable strain for a concrete member in complete compression with confinement is -0.005. Since these sections have little confining reinforcement it was assumed that the maximum compressive strain of concrete, ϵ_{cu} would be -0.004 (Table 1).

Table 4: Shear Capacity Column Type 1

Mp	1426	kip-in	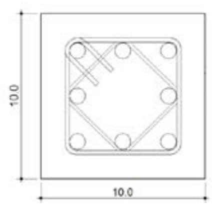
Vp	22.45	kips	
Vn	20.59	kips	
Vp/Vn	1.09	kips	
Failure Type	Shear Failure		

Table 5: Shear Capacity Column Type 2

Mp	1027.64	kip-in	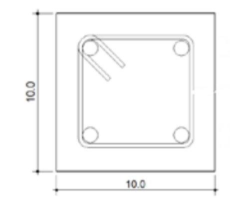
Vp	13.7	kips	
Vn	13.5	kips	
Vp/Vn	1.01	kips	
Failure Type	Shear Failure		

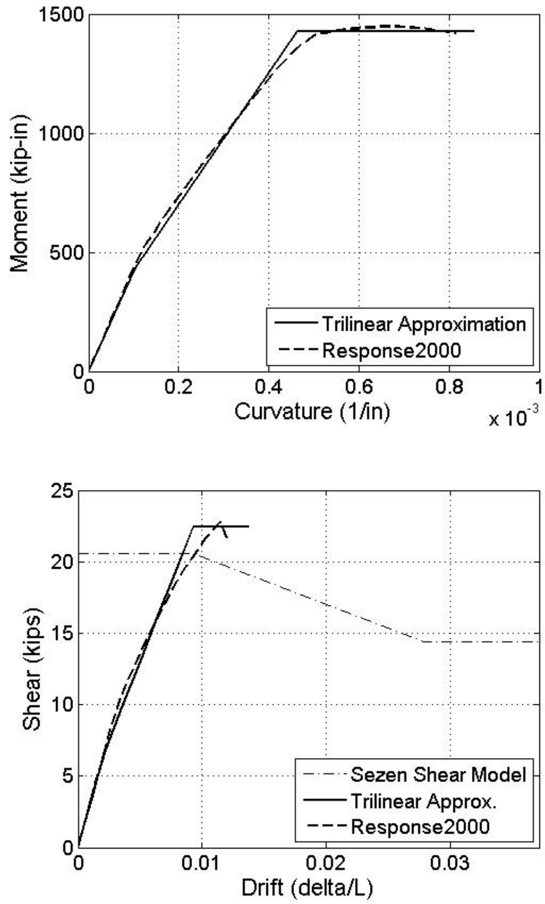

Figure 21: Column Type 1: Moment-curvature response (top) Shear capacity Model (bottom)

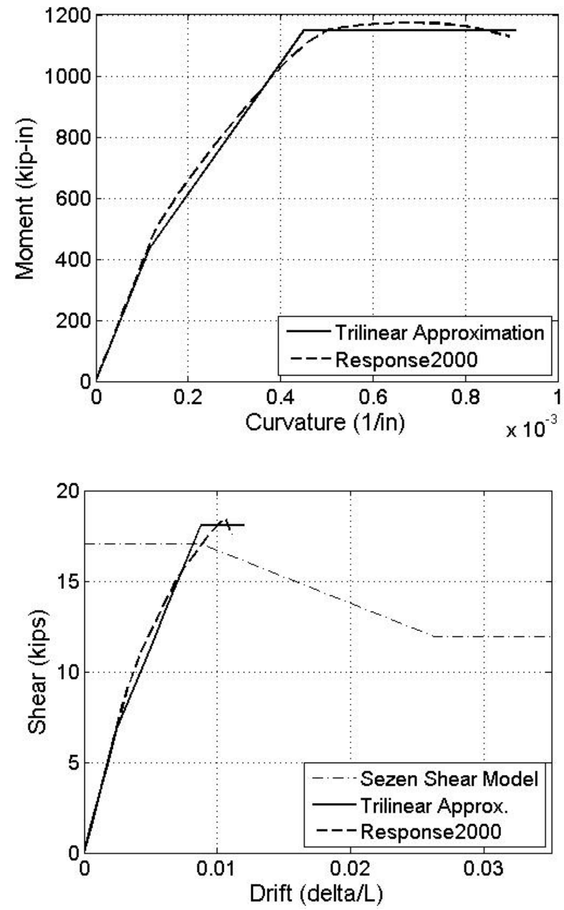

Figure 22: Column Type 2: Moment-curvature Response (top) Shear capacity model (bottom)

Sezen's shear model is visually shown in the bottom two plots. The curve is obtained by using equation (1 with a k of either 1 or 0.7 for selected ductility values of 0 to 2 and greater than 6, respectively, while allowing a linear regression for ductility values between 2 and 6. The shear-drift plot for each column type is obtained by Response-2000 as well as estimated by summing the displacements due to flexure, shear and slip of the reinforcement. This approach is based on past research, assuming that the column is fixed from rotating at each end and has a linear curvature distribution (Elwood, Eberhard 2006). Both results are very comparable. The capacity analysis results are summarized in Table 4 and Table 5. This information is reiterated in Figure 23 and Figure 24 with interaction diagrams of both columns type 1 and type 2. The column's axial load, 200 kips is denoted with a star in Figure 23 and Figure 24, indicating the relative location of the columns within the interaction diagrams.

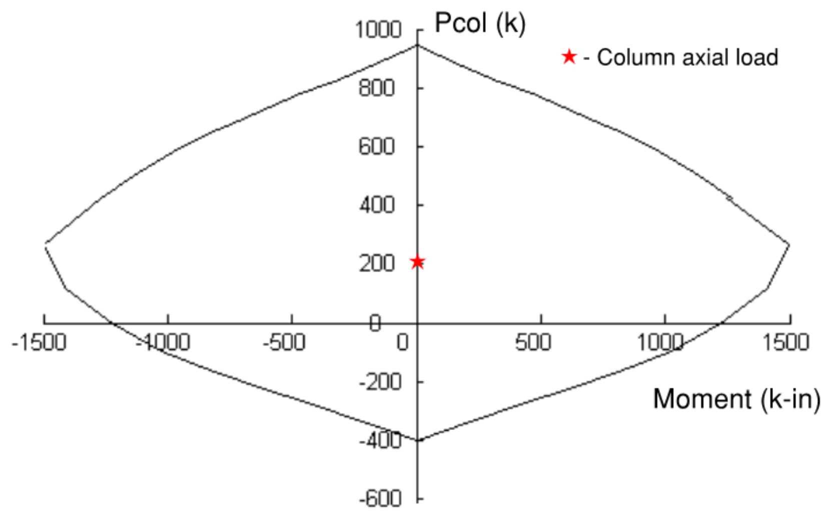

Figure 23: Interaction diagram - column type 1

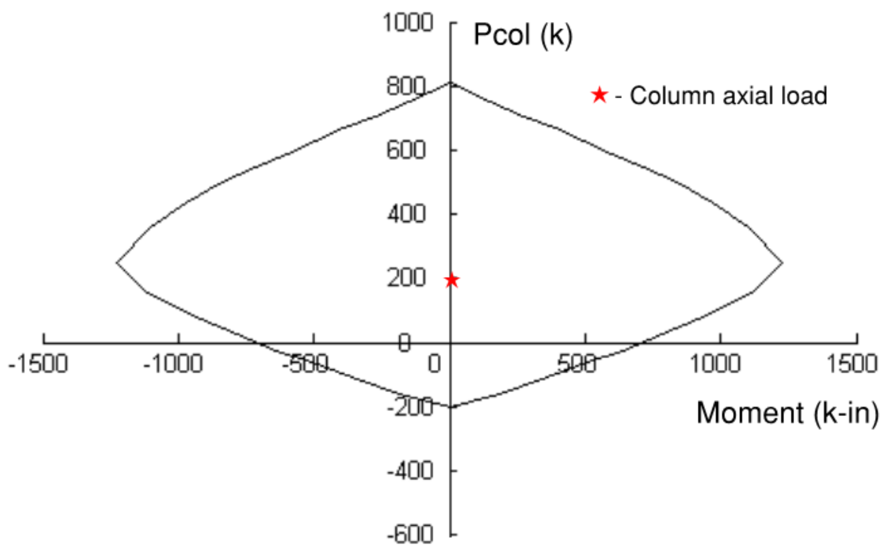

Figure 24: Interaction diagram - column type 2

The results show that for both columns, the ratio of V_p/V_n is larger than one, indicating a shear dominant failure mechanism. This is an undesirable mechanism because of its brittle nature as well as it can lead to loss of vertical load carrying capability and possible collapse. Since the ratios of plastic shear, to shear strength are so close to one, further investigation into determining whether this is shear failure or flexure-shear failure is necessary. According to Figure 25, as presented by (Zhu, Elwood & Haukaas, 2007), the ratio of Vp/Vn is not a definitive parameter when determining failure type and thus more information is needed. Figure 25 is a scatter of 125 column specimens consisting of a typical range of properties. Besides the longitudinal reinforcement ratio of 6.2% for column type 1, all the other properties for both column types are within range of the 125 specimens shown in Figure 25.

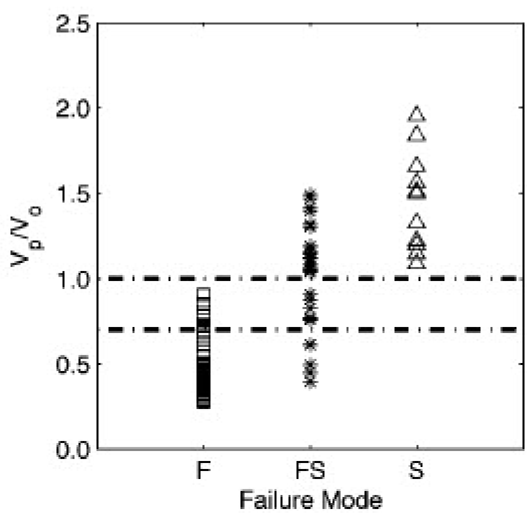

Figure 25: Experimental failure types related to the calculated Vp/Vn ratio (Zhu et al., 2007)

It is recommended, by Zhu et al. (2007) to follow a two-zone column classification method, which takes into account not only the V_p/V_n ratio as well as the transverse reinforcement ratio (ρt) and shear span to depth ratio (a/d). The procedures for this method state if ρt < 0.002, which it is for both column types then the column is categorized under shear type failure. The oddity of these columns is the large a/d ratio, in most cases where a column has an a/d > 4 it is assumed to be controlled by flexure, but since it has such a high longitudinal reinforcement ratio (outside the range of the test specimens) the reinforcement nearly reaches yield before failure occurs in shear. By following the procedures in the two-zone column classification method both columns are still categorized under shear type failure due to d, depth of the section.

4.2.1 Beam-Column Joints

The columns are only one component of the entire gravity frame system. Investigations into typical 1960s frames show, due to the lack of continuous transverse reinforcement throughout the joint, that the joints are likely to be the most vulnerable to failure (Hassan 2011). Even though shear failure is expected in the columns it is possible that the joints would fail first even before reaching the necessary demand to fail the columns.

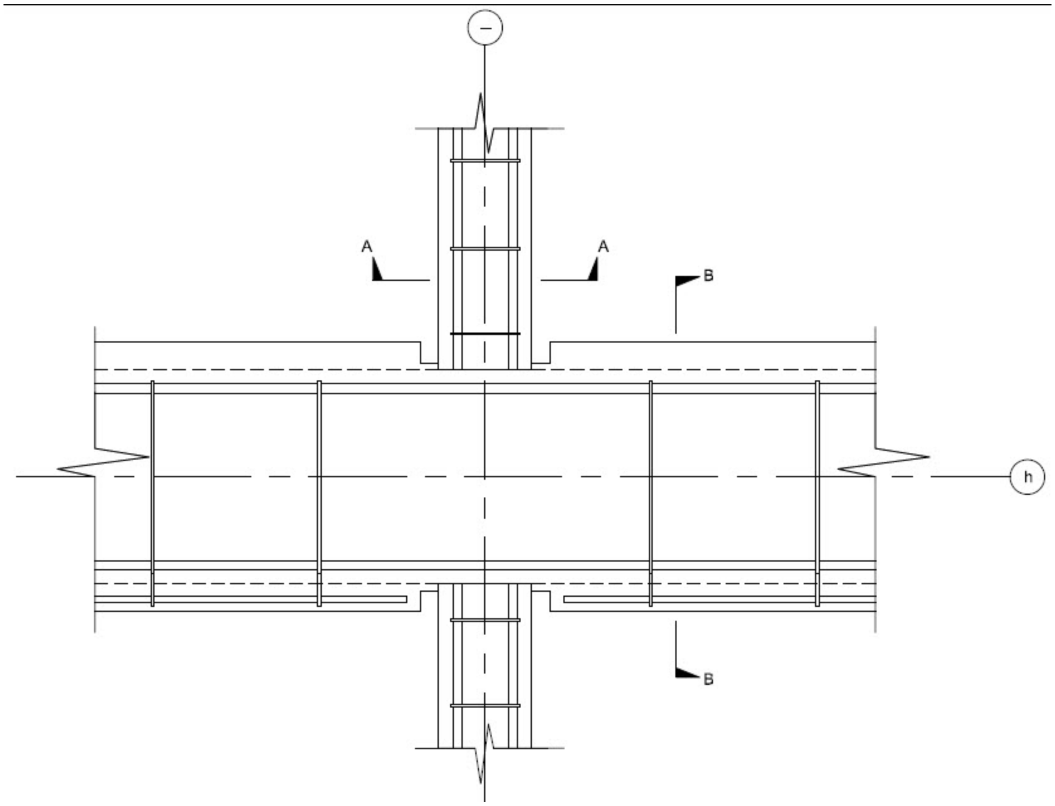

Figure 26: Typical interior joint of gravity frame along gridline h (gridline a similar)

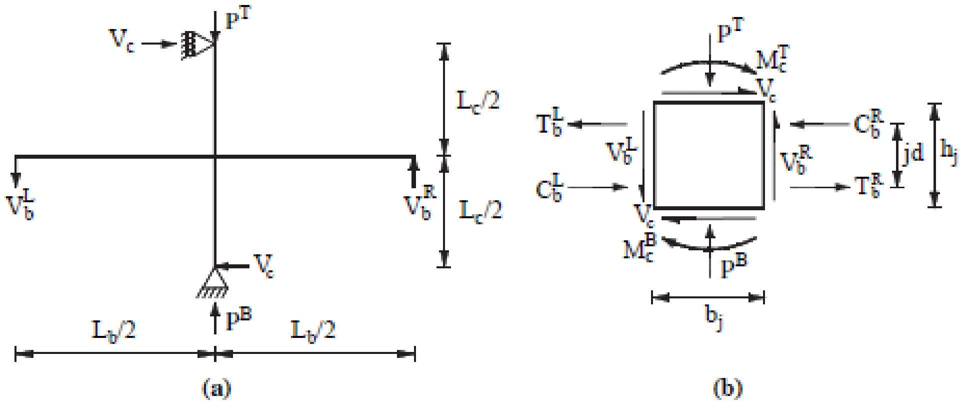

Figure 27: (a) Free-body diagram of the typical joint at column type 2 (b) Forces acting on the joint (Celik and Ellingwood, 2008)

Only column type 2 was used in the following procedure because it is considered the worst case for demand in the E-W direction. The demand on the joint is calculated using simple statics based on the free-body diagram in Figure 27. This is a simplistic procedure that provides an adequate estimate of horizontal joint shear demand as seen in research by Celik and Ellingwood (2008). Using the column shear at shear failure V_n, denoted as V_c, the beam shear V_b and the beam moment M_b were determined. The results are summarized in Table 6. Assumptions such as each framed beam is of equal stiffness, beam axial loads are equal to zero and inflection points are located at half the beam span, L_b of 200 inches were used when determining the beam forces.

Table 6: Beam Properties and Forces

<table>
<tr><td colspan="4">Section A - A</td></tr>
<tr><td colspan="4">See Figure 1 and Table 4- Column Type 2</td></tr>
<tr><td colspan="4">Section B - B</td></tr>
<tr><td rowspan="8">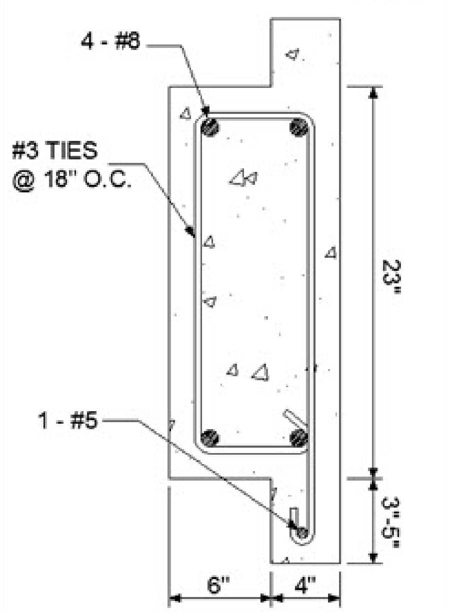
</td><td colspan="3">Material Properties</td></tr>
<tr><td>f'c *=</td><td>5.903</td><td>ksi</td></tr>
<tr><td>fy =</td><td>47.6</td><td>ksi</td></tr>
<tr><td colspan="3">Beam Forces</td></tr>
<tr><td>Vb =</td><td>10.52</td><td>kips</td></tr>
<tr><td>Mb =</td><td>1052</td><td>kip - in</td></tr>
<tr><td>Tb** =</td><td>53.2</td><td>kips</td></tr>
<tr><td colspan="3">Notes:
*Based on material testing performed by Hyland, 2011
**The single #5 bar was ignored while determining the coupled tesile force</td></tr>
</table>

The moment within the beam, M_b is well below the yield moment of 1660 kip-in yet above the cracking moment, this is expected as this is clearly a strong-beam weak-column mechanism. M_b is broken up into the coupled compression and tension forces, as shown in Figure 27. Since the beam on the left and right are the same, $T_b^L = T_b^R = T_b$ from Table 6. By summing the forces in the horizontal direction, the joint shear demand V_{jh} is determined from Equation 3 and produces a shear demand of 92.9 kips.

$$V_{jh} = T_b^L + T_b^R - V_c \tag{3}$$

In order to determine the hierarchy of strength between the joint and the column, joint shear strength V_{jn} was calculated using an approach from ACI 369 working document (2013), shown below in equation 4.

$$V_{jn} = \lambda \Upsilon \sqrt{f'_c} A_j \ (psi\ units) \tag{4}$$

Where λ is 1.0 for normal weight concrete, A_j is the effective horizontal joint area as defined by the column depth, h times the effective beam width, b and the geometric factor ϒ is defined below in Table 7. For this case the geometric factor ϒ will be somewhere between cases 1 and 2 since there are only three adjoining beams. Case 1 will be used as an upper bound and case 2 will be a lower bound when comparing with the joint shear demand.

Table 7: Geometry Factors (ACI 369 Working Document 2013)

Geometry	Geometry Factor, ϒ	Comments
1 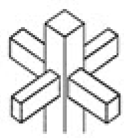	$\Upsilon = 16.8\kappa\alpha_j^{-0.5}$	Interior joints with transverse beams
2 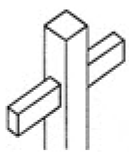	$\Upsilon = 14\kappa\alpha_j^{-0.5}$	Interior Joints without transverse beams

Axial load and joint aspect ratio are considered through factors κ and α_j, respectively as shown in equations 5 and 6 below.

$$\kappa = 1 + (0.86 - 0.3\alpha_j)\left[\frac{P}{f_c' A_j} - 0.15\right] \qquad 1 \le \kappa \le 1.35 - 0.1\alpha_j \tag{5}$$

$$\alpha_j = \frac{h_b}{h_c} \tag{6}$$

The typical gravity frame beam-column joint is unable to withstand the shear demand at shear failure of the adjoining columns. The upper bound estimate of the joint shear strength V_{jnu}, as calculated by the above procedure, using a joint area of 100 square inches, is 87.8 kips, which is less than the demand, V_{jh} of 92.9 kips. For reference, the lower bound shear strength is 73.2 kips. Since it is understood that the estimated joint shear strength would be lower than the case 1 upper bound of 87.8 kips, it is reasonable to state from these calculations that the joints within the gravity frame are the most critical. These calculations are estimates and serve as starting points when determining the cause of collapse under dynamic earthquake loading. Further analysis will be provided in subsequent sections regarding the possible failure mechanism of the gravity system.

4.2.2 Walls

Estimates of flexural strength for the entire core and the wall assemblage CWN are determined using simplified methods. The critical wall pier within the web of CWN is also assessed. A preliminary shear strength estimate for the web wall segments of CWN and CWS and the flexural strength of the full shear core is determined (Figure 18). Since this is a specific case, where the ground level is known to not have collapsed, all values of strength will be determined at level one.

4.2.2.1 Flexural Strength

An idealized I-section is used for simplicity, as shown in Figure 28, to represent the core since this is a flexural strength estimate and shear is not a factor. The central walls are assumed to account for negligible flexural strength due to the poor detailing of the coupling beams and are ignored for this strength estimate.

Following an approach used in many texts and noted in the NEHRP Seismic Design of Cast-in-Place Concrete Special Structural Walls and Coupling Beams: (Moehle et al. 2011), the rectangle core was idealized, using an effective flange width. Shown in Figure 29, is a pictorial representation of the core with the effective flange widths denoted. Since openings occur closer to CWS the effective flange width is less than that on the right. Assuming a cantilever displaced shape and following the procedures discussed in Moehle et al.(2011), effective flange widths (Figure 29) for both the tension and compression flanges of 150 inches for CWN and 130 for CWS, for a total shear wall core flange width of 280 inches at both gridlines D and E. The effective width is used due to shear lag, which causes a higher concentration of stress at the point of connection between the web and the flanges and diminishes as it moves further from that point (Figure 28).

A gravity load take-off using the existing material properties and self-weight of the known materials was undertaken to capture an accurate vertical load of each of the wall sections individually and the core as a whole. The Total gravity load tributary to the entire core at Level 1 is 1580 kips. The three core wall assemblages have gravity forces of 1020 kips, 79 kips and 481 kips for CWN, CWC and CWS, respectively. As expected, CWN attracts majority (about 60%) of the gravity load.

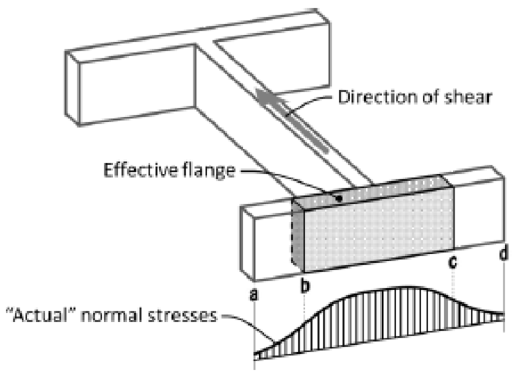

Figure 28: Stress profile as a result of shear lag (Moehle et al. 2011)

The flexural strength of the idealized wall section is determined assuming a criterion for failure as either rupture of the steel or crushing of the concrete. Using the maximum assumed strain value, -0.004 for concrete and 0.075 for steel (Table 1), both possibilities are checked and the lower of the two governs. The rupturing of the steel governed the flexural strength and curvature capacity, due to the lightly reinforced flanges. The reinforcement within the flange is assumed to carry uniform stress over the effective width (Figure 29). Since it is the steel that governed the capacity, the determination of an effective flange width is very important as not to overestimate the amount of steel being utilized. In order to accurately predict the flexural strength of the core, the distance from the extreme fiber to the neutral axis, c, must be obtained. . An accurate estimate of both flexural strength and curvature capacity is determined using the assumed linear strain profile governed by the ultimate strain of the steel and an equivalent stress block for the concrete.

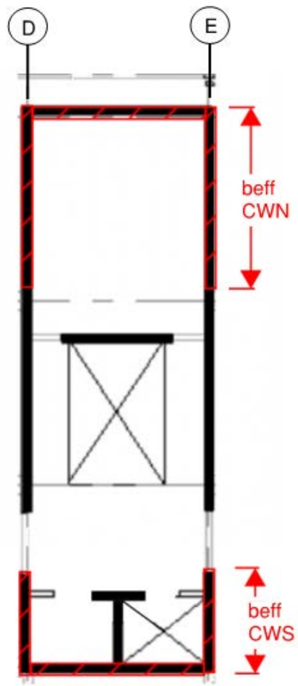

Figure 29: Idealized core representation at level one

Following the same process as described above for the core flexural strength at level 1, the flexural strength of CWN at level one is also determined. The flexural and curvature capacities of the core as well as CWN are validated by sectional analysis, response spectrum analysis and static pushover analyses in sections 6.1, 6.2 and 6.3, respectively. Below is a summary of the strength estimates of both the idealized core and CWN.

Table 8: Wall Capacity Estimates

Type	CWN	Core
Moment above level 1 (kip-in)	229008	366177

4.2.2.2 Shear Strength

The web wall segments for both the CWN and CWS (Figure 18) are assumed to be the most critical. They both contain large openings from windows and doors as seen in the elevation views in Figure 19. This assessment will focus on the web segment of CWN as it is assumed to be the most critical considering the post collapse photos (section 2.5) showing the large diagonal cracks in the wall pier between levels 2 and 3. The 48 inch wide pier shown in Figure 20 only contains a single layer of #5 rebar at 15 inches both ways, resulting in a transverse reinforcement ratio of 0.00285. The two 16 inch piers on either end of the web segment are assumed to contribute negligible shear stiffness to the overall section and therefore the central web pier will be assumed to provide all the shear resistance.

The shear strength, V_n of the critical wall pier is determined by three different approaches, ASCE-41, CSA A23.3 (Canadian Standards Association 2004) and Response-2000. Equation 7shows the shear strength as determined by ASCE-41, which references section 21.9.4 of the ACI 318 code (ACI 2008). It is based on the shear area of the concrete A_{cv}, transverse reinforcement ratio ρ_t, rebar yield strength f_y, and the concrete compressive strength f'_c.

$$V_n = A_{cv}(\propto \lambda\sqrt{f'_c} + \rho_t f_y) < 8A_{cv}\sqrt{f'_c}\ (psi\ units) \tag{7}$$

The aspect ratio factor, α, and the normal concrete weight factor λ are 3.0 and 1.0, respectively. The aspect ratio is based on the height to length of the wall pier which is about 1.0, yielding α = 3.0. The height to width ratio of the pier is used because it is assumed that the pier will resist all shear demand due to the minimal flexural reinforcement in the small piers on either ends of the window openings, see Figure 19.

Equation 8 shows the shear resistance as determined in CSA A23.3, which is determined by the concrete compressive strength, f'_c, the width of the section, b_v, the depth from the extreme compression fiber to the tension reinforcement, d_v, the area of the transverse reinforcement, A_v within a given spacing, s, θ, the angle of inclination of the expected crack pattern and the yield strength of the steel, f_y. The β factor accounts for shear resistance of cracked concrete, shown below in equation 9.

$$V_n = \lambda\beta\sqrt{f'_c}b_v d_v + (f_y A_v d_v \cot\theta)/s\ \ (MPa\ units) \tag{8}$$

$$\beta = 230/(1000 + d_v) \tag{9}$$

The third approach used the computer software Response-2000, which is based on the modified compression field theory (Bentz 2000).

Using all material properties as referenced in section 4.1, the shear strength at level 1 for the critical web of CWN, CWC and CWS as determined by ACI, CSA and Response-2000 shown below in Table 9.

Table 9: Shear Capacities

Wall	ACI 318		CSA A23.3		Response-2000	
	v (psi)	v/√f'c	v (psi)	v/√f'c	v (psi)	v/√f'c
CWN	294	4.97	297	5.02	320	5.41
CWC	235	3.97	235	3.98	165	2.80
CWS	235	3.97	236	3.98	241	4.07

The shear demand produced from the static pushover and the dynamic analysis in the succeeding sections will be compared with the capacities to determine if a shear failure mechanism governed the failure of PGC.

Chapter 5 **Analytical Models**

The computer software program OpenSees (open source earthquake engineering system) (PEER 2013a) is used to analyze the seismic response of PGC. The following line element models, multiple-vertical-line-element models (MVLEM) and fiber element models have been implemented into the framework of OpenSees and are used to model the response of the walls of PGC. The models are discussed, calibrated and validated, in the following sections. Refer to section A4 of the Appendix for a clear representation of all the modeling assumptions.

5.1 Background: Multiple-Vertical-Line-Element Models (MVLEM)

MVLEMs are a specific type of macroscopic fiber model, which utilize the simplicity of springs to accurately capture the interaction of the concrete and steel under axial, flexure and shear, within a reinforced concrete wall. More of these models are being implemented into OpenSees. The flexure-shear interaction beam-column element for planar walls (PEER 2013) is a version of an MVLEM, which captures the interaction of not only axial and flexure, but shear as well. This model is only available for 2-dimensional analysis and therefore, not appropriate for this case. These types of macro-multiple spring models continue to evolve, becoming more practical and more efficient to use. The MVLEM, specifically used in the following analysis is known as the modified MVLEM, introduced by Fischinger et al. (1990). To understand more about the evolution of MVLEM reference Orakcal, Massone and Wallace (2007).

The modified MVLEM uses a distribution of springs along the length of the wall, bounded by a rigid top and bottom plate (Figure 30), to capture the axial-flexure interaction, seen in concrete walls. The distribution of springs is determined based on the location of the reinforcement, as shown in Figure 31. This is very different than a mesh discretization, as used with a fiber model, because the accuracy is dependent on the number of springs, unlike the fiber model, which is based on the density of the specific mesh, among other parameters. The details of a fiber mesh will be discussed further in the fiber element section 5.2. MVLEMs can be used for 2-dimensional or 3-dimensional analysis, see Figure 30 for a representation of a typical 2D and 3D element. Figure 31 shows how a simple planar wall is discretized into sections (similar to how a fiber model is meshed), followed by a vertical spring representation of each of these sections.

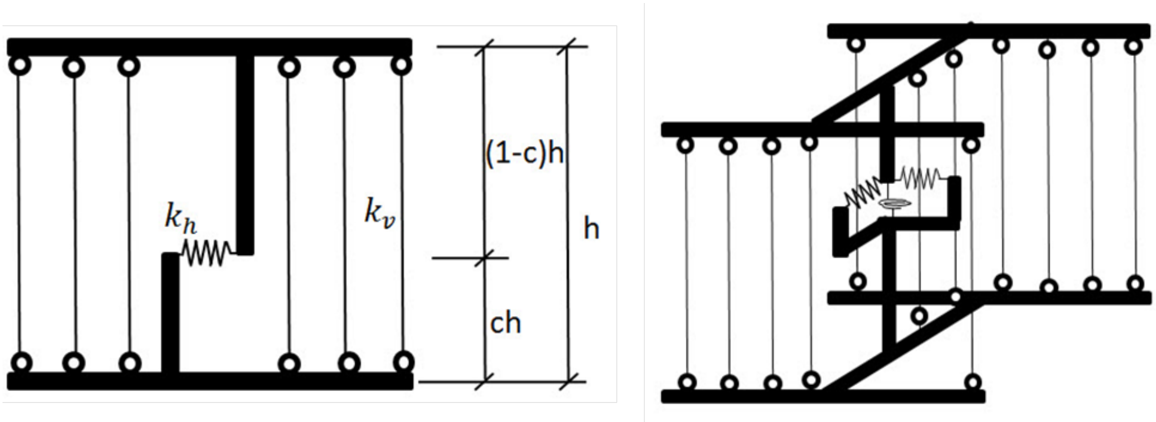

Figure 30: MVLEM typical 2-D and 3-D elements respectively (adapted from Ficshinger, 1992)

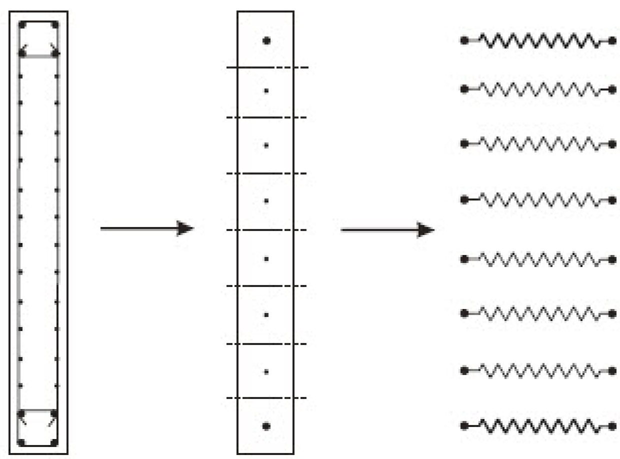

Figure 31: Diagram of a typical wall being represented by vertical springs (Ficshinger, 1992)

Each spring represents the composite response of the concrete and steel reinforcement within a section. The spring's stiffness, both in compression and tension, is determined from the material properties of both the concrete and steel, then, using compatibility, an axial force-displacement response for each spring can be determined (Figure 32). VerticalSpring1 and VerticalSpring2 (Figure 32) are the displayed hysteretic axial force-displacement responses of a single spring, called uniaxial material models. The main difference between the two is the degradation of the curve in compression beyond the strength of the concrete. VerticalSpring1 stays constant at the max compressive strength, Fc and VerticalSpring2 degrades to a contraction limit, Δ_{cu}, ultimate spring contraction (based on the concrete strain at crushing) and a strength at failure, F_{cu} (20% of the compressive strength, F_{c}). The material parameters (F_{c}, F_{y}, F_{cu}, etc.) in Figure 32 are based on the properties of the concrete and steel, which are provided in Table 1.

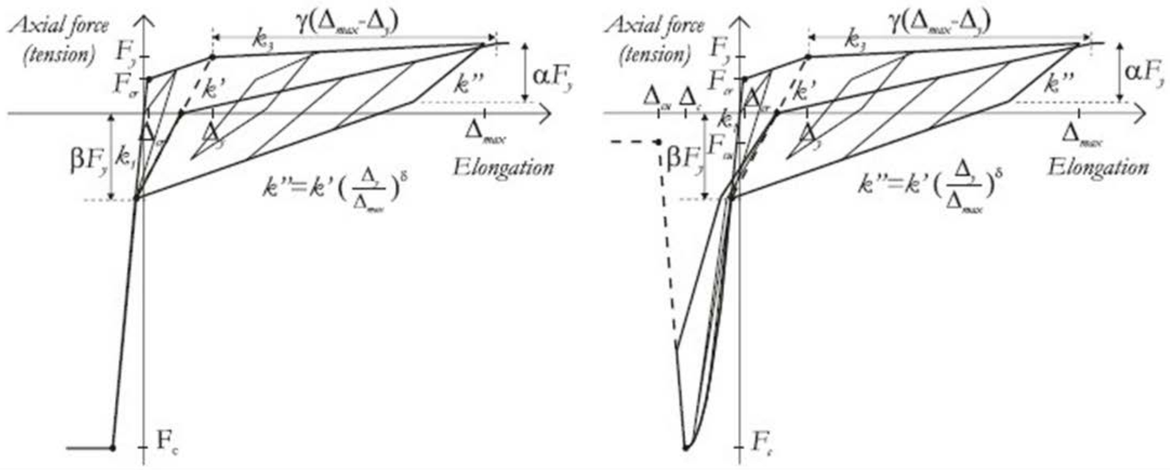

(a) (b)

Figure 32: Hysteretic response of uniaxial materials (a) VerticalSpring1 (b) VerticalSpring2 (Fischinger, 1992)

A major difference between the MVLEM and fiber model is the use of displacement-based elements (DBE) or force-based elements (FBE). The modified MVLEM uses DBE. The DBE use an approximate displaced shape assumption, leading to a linear curvature distribution over the height of the element (Terzic 2011). Therefore, in order to accurately represent the non-linear distribution of curvature and to minimize the variation in moment, these types of models require many elements over the height. It is especially important to include more elements in critical locations where inelastic deformations are expected to be great, such as the base of walls or expected failure locations (Orakcal et al. 2007). The differences between the FBE and DBE are further discussed in section 5.2.

In addition to the vertical springs, which account for the axial-flexure interaction, horizontal springs and a rotational spring (for 3-D models) are also included to incorporate shear deformations and rotations due to torsion within the wall. Unlike the flexure-shear interaction beam-column element, described previously, the modified MVLEM does not consider the coupled response of axial-flexure and shear. Shear deformation is included through superposition, see Figure 33.

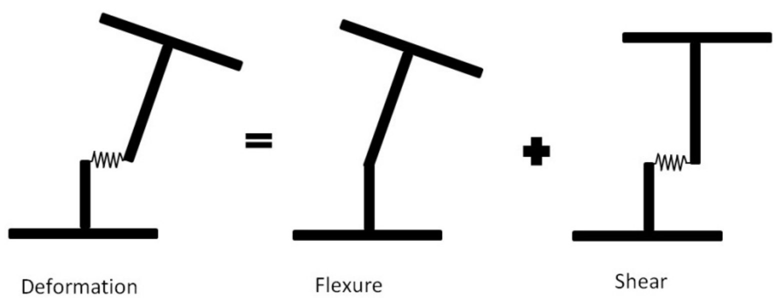

Figure 33: Uncoupled flexure and shear deformation (adapted from Fischinger, 1992)

Two uniaxial material options, for modeling the horizontal shear springs are provided; linear elastic or non-linear shear slip (essentially a bilinear response curve). The uniaxial material for the rotational spring only has the capabilities of being linear elastic. The horizontal and rotational springs are located at a specific length along each element, c*h, where h is the length of the element and c, defines the location of the relative rotation between the top and bottom portions of the MVLEM (Figure 30). The parameter c is meant to account for the distribution of curvature over the height of the element. If the curvature was uniform over the height of the element, a c value of 0.5 would result in a perfect representation of the curvature. Since this is not the case, it is recommended to use a smaller value. According to experimental tests done by Orakcal, Wallace and Conte (2004), a c value of 0.4 should be used. The value of c, along with the four hysteretic parameters, α, β, γ and δ (Figure 32) must be determined based on experimental tests or engineering judgment. Calibration will be used to determine the parameters because basing them off judgment is very difficult. In the following two sections, two calibrations are completed for the MVLEM to determine the four hysteretic parameters and the parameter c that will be used for the PGC model.

5.1.1 MVLEM Calibration: McGill University Experimental Tests

The first of the experimental tests used in calibration were performed at McGill University in Montreal, Quebec (Layssi, Cook, Mitchell 2012). Layssi et al. tested four specimens, two, non-ductile, lightly reinforced wall segments (W1 and W2), both with slightly different reinforcement arrangements. Specimens W3 and W4, were the same as W1 and W2, but were wrapped at the base with CFRP. Specimen W1 was used for the following calibration because it closely resembled the wall segments found in the PGC shear core.

Specimen W1 (Figure 34) was constructed consistent with 1963 ACI-318 code practice, most likely similar to the construction of the core walls of the PGC building.

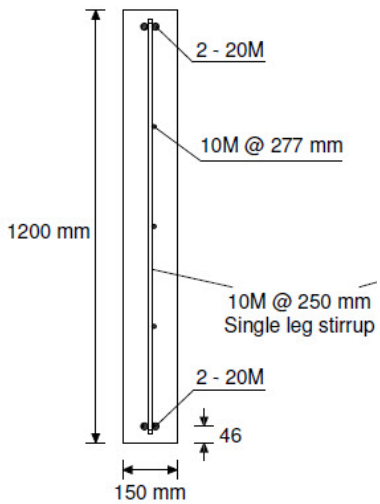

Figure 34: McGill University Test Speciman, W1 (Layssi et al. 2012)

The tested section is 47 inches (1200mm) by 6 inches (150mm) and the following reinforcement ratios of the tested specimen, as compared with a typical PGC section and the minimum requirements of the 1963 ACI code (ACI 1963) are shown below, in Table 10. The boundary elements, which are noted as 2 – 20M bars, are not true boundary elements as they are designed today, but will be considered boundary elements for consistency with Layssi et al. (2012). Similar to PGC, there is no confinement present throughout the section. This is a key characteristic to have similarity, since confinement can greatly alter the hysteretic response.

Table 10: Reinforcement Summary (adapted from Layssi et al. 2012)

Specimen	Boundary Element	Web	
	ρl	ρl	ρt
W1	0.0033	0.0016	0.0026
PGC (typical)	0.0027	0.0027	0.0025
1963 ACI minimum	-	0.0015	0.0025

Using nothing but the material properties and the section geometry, a modified MVLEM was created in OpenSees to calibrate the four hysteretic parameters, α, β, γ and δ. Also included in this model, is the use of the non-linear shear slip uniaxial material model for the shear spring, which will be used in the PGC model.

The test setup for this particular specimen was unique in that the walls were tested on their sides as if they were cantilevered beams, thus resulting in an axial load of zero on the specimen. The OpenSees model assumed zero self-weight for this particular test. It is assumed that this will not alter the hysteretic parameters when axial load is added, because it will be considered within the vertical spring uniaxial materials. The specimen was loaded through three cycles before increasing to the next load level. This was repeated until failure occurred in the wall.

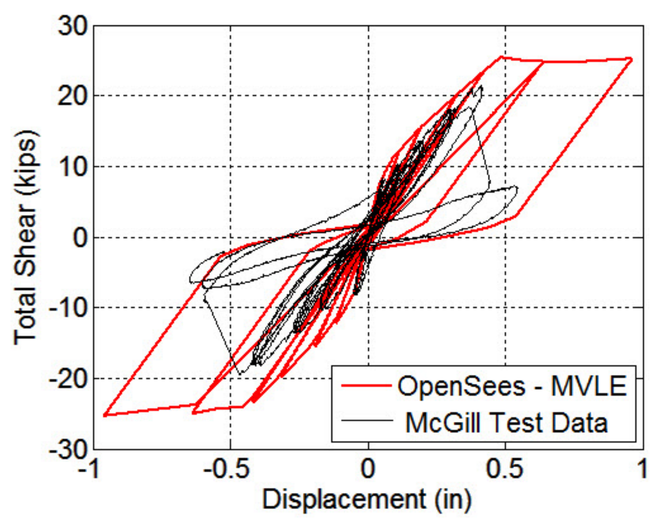

Figure 35: Force Displacement Hysteresis Calibrating MVLEM (adapted from Layssi et al. 2012)

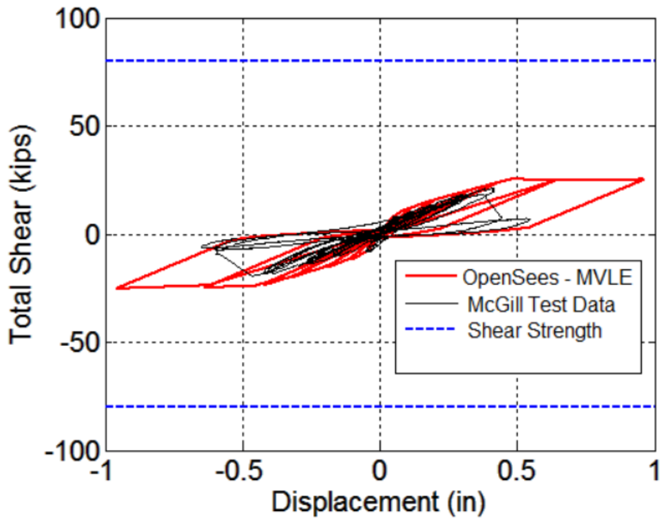

Figure 36: Force Displacement Hysteresis Calibrating MVLEM indicating shear strength of the wall specimen (adapted from Layssi et al. 2012)

According to Layssi et al. (2012), the failure mechanism of specimen W1 was due to slip at the lap splice location of the 2-20M bars at the base of the wall. This type of slip failure is brittle in nature, thus the quick drop in capacity prior to the plateau of the OpenSees model. The MVLEM used did not take into consideration slip failure and thus did not capture the loss in capacity prior to yielding, which is evident from the plot in Figure 36. The slip failure occurred at a shear stress of 72 psi. The calculated shear strength of the specimen is 82 kips and is noted by the dotted line in Figure 36. The shear strength is well above the flexural yielding captured by the analysis. Therefore the specimen is not expected to fail in shear as in the PGC model. To further validate the MVLEM, the model's calculated flexural strengths were checked with capacities from Layssi et al. (2012). The MVLEM produced maximum moment strength of 3,182 k-in, compared to the calculated strength by Layssi et al. (2012) of 3,416 k-in, indicating a slight underestimate of the strength.

The hysteretic parameters α, β, γ and δ were iterated until an acceptable fit was produced and are summarized in Table 11 along with the geometric parameter c. These parameters will be discussed further and compared with the second calibration test in succeeding sections.

5.1.2 MVLEM Calibration: Oesterle et al. Experimental Tests

The experimental tests provided by Oesterle, Fiorato, Johal, Carpenter, Russell and Corely (1976) were used for the calibration of the parameter *c*, and the four hysteretic parameters of the MVLEM. The specimen used is identified as R1, a 4-inch by 75-inch planar wall constructed at 1/3 scale. The reinforcement arrangement consisted of confined boundary elements with transverse hoops spaced at 4 inches vertically, accompanied by a double layer of both longitudinal and transverse steel throughout the section, see Figure 37. Specimen R1 is not similar to the typical section of PGC, considering it contains confined boundary elements and considerably more longitudinal steel in the boundary elements, a vertical reinforcement ratio of 0.011 compared to only 0.0027 in the walls of PGC.

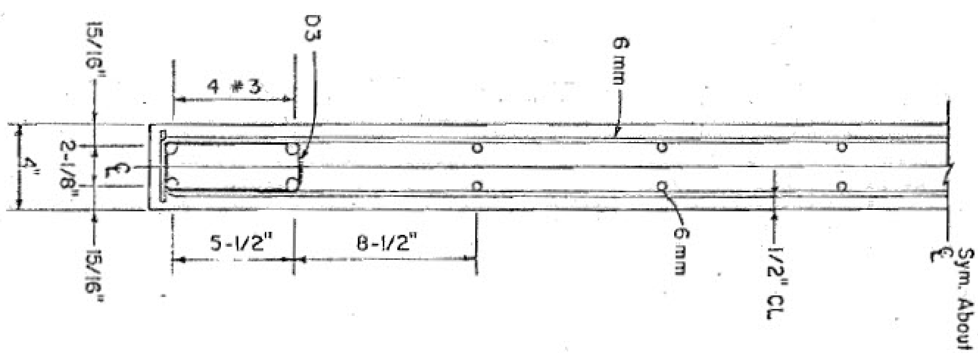

Figure 37: Oestral et al. (1976) experimental test specimen R1 (Oestral et al. 1976)

The longitudinal and transverse reinforcement ratios of specimen R1 are very similar to that of the walls of PGC, roughly 0.003. According to Oesterle et al. (1976), the construction of all the test specimens was in accordance with the 1971 ACI 318. It is easy to see the changes in minimum design requirements in 1963, when PGC was constructed, to 1971.

The loading scheme for specimen R1 was displacement controlled. The specimen was loaded through three cycles to a specific displacement before being increased to the next, until failure. Based on the observations, the specimen underwent 29 cycles before failing in flexure. The MVLEM is capable of predicting the strength and global response very well, as seen in the plot overlay of Figure 38. The hysteretic parameters were iterated to find the best fit and are summarized in Table 11, along with the parameter c. The maximum shear stress observed in the specimen was 93 psi, well below the calculated shear strength of 305 psi. Therefore this specimen is not expected to fail in shear which is evident from the ductile behavior shown in Figure 38. This is similar to the results from Layssi et al. (2012).

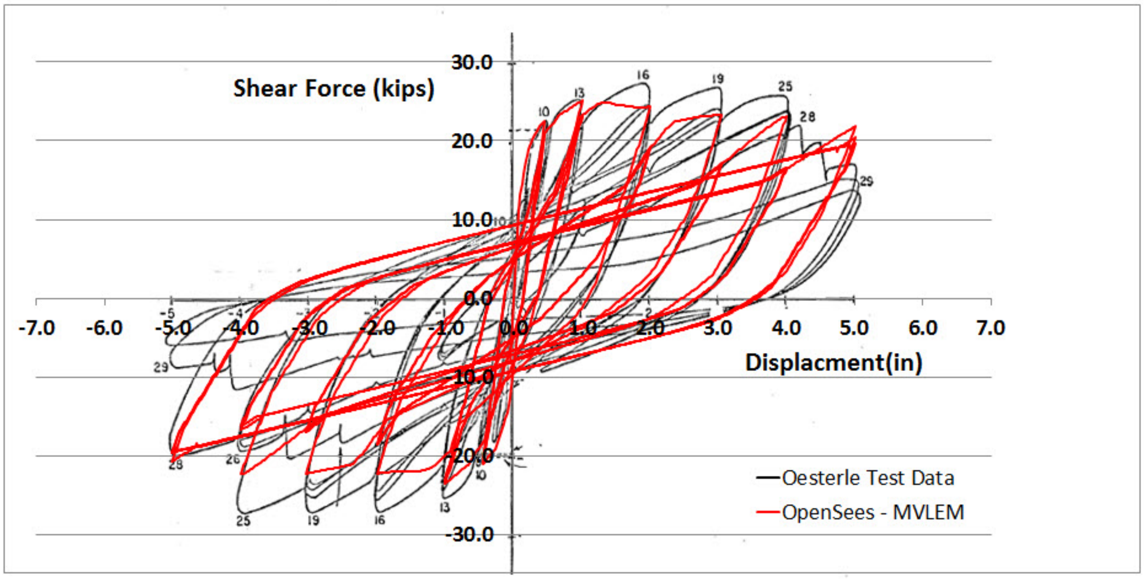

Figure 38: Force displacement hysteresis comparing the MVLEM and Oesterle et al. (1976) test data (adapted from Oesterle et al. 1976)

5.1.3 MVLEM: Hysteretic Parameters

The determination of c is important for areas expecting highly nonlinear curvature distribution (i.e. locations of expected failure). A c value of 0.3 or 0.4 is suggested by past research (Orakcal et al. 2007), but this did not yield the best results. For both calibration tests, c ranged from 0.1 to 0.15 for Layssi et al. (2012) and Oesterle et al., respectively. Sensitivity studies, regarding the influence of c on the hysteretic behavior, show that the more elements used (finer vertical discretization) along the height of the wall, the less important the determination of c becomes (Orakcal et al. 2007). Therefore, the number of elements at level 1 for PGC will be increased such that the parameter c has little impact. A c value of 0.1, as found from Layssi et al. (2012) calibration tests will be used for all wall sections for the remainder of the analysis.

Table 11: Hysteretic Parameters Summary

Hysteretic Parameter	Layssi et al. (2012)	Oesterle et al. (2007)
α	1	1.15
β	0.1	1.05
γ	1.02	1.5
δ	0.01	0.00001
c	0.1	0.15

Regarding the four hysteretic parameters both calibrations resulted in a wide range of values, which are summarized in Table 11. This wide range indicates how sensitive these parameters are to slight model differences. The wall specimen from Layssi et al. (2012) on a sectional level is the most similar to the walls of PGC andthe values of α, β, γ and δ are based on the performance of the specimen prior to splice failure thus being a good fit to capture the performance of the walls of PGC. These parameters will be used for all the remaining analysis, when appropriate.

5.2 Background: Fiber Model

The fiber element model is the most widely used within OpenSees for representing the modeling of reinforced concrete (RC) shear walls. There have been countless research institutes providing documents that explain how to appropriately use the tools provided by OpenSees to accurately obtain the response of the shear wall, particularly the document published by the University of Washington (Pugh 2012). This report is designated for the modeling of newly designed RC shear walls, but the same principles can be applied to existing walls. These guidelines are referenced for determining an appropriate fiber element model that accurately represents the core walls of PGC. Below is a summary of the most pertinent aspects to the fiber element model as they pertain to the walls of PGC. For a more general description regarding the use of fiber models for RC walls, refer to Pugh, 2012.

An appropriate mesh or horizontal discretization of fibers is the first of many important parameters to determine. The mesh represents the area of concrete and reinforcement throughout a given section. It is important to come up with a specific grid that will give the analyst accurate results without significantly slowing the computational process down. Judgment must be used to determine this grid as it varies greatly based on the wall type and geometry, but recommendations and guidance are available (Pugh 2012). Studies summarized by Pugh (2012), resulted in less than a 1% error in flexural strength using a single fiber mesh of planar walls under monotonic loading, but for cyclic loading a much finer mesh was necessary to produce the same results. Based on these studies a mesh using 32/β fibers for the entire wall section is recommended to accurately capture the flexural response (Pugh 2012), where β is the ratio of boundary element length to total length of the wall. Similar to older wall sections, the walls within the core of PGC do not contain boundary elements and therefore this recommendation is not applicable. A moment-curvature analysis study, discussing the mesh sensitivity and its impact on flexural strength of a typical section of PGC (no boundary elements), is shown in Figure 40.

Similar to a horizontal discretization (mesh), a vertical discretization is needed for better accuracy of the distribution of curvature over the height of each element, as discussed with the MVLEM in the section 5.1. Fiber models have the ability to be defined as either DBE or FBE. Both types of element models are distributed plasticity models, allowing for yielding to occur at any point along the element. FBE models, unlike the DBE models can capture the non-linear curvature distribution over the height of the element by enforcing both external and internal deformations to be in equilibrium (an exact solution). This can slow down the analysis process and is known to cause convergence issues in complex systems (Terzic 2011).

Determining the best vertical discretization for any given model is unique to each case. As in PGC's case, it is known that failure is occurring at level 1. Therefore, when using DBE many elements would be needed at level 1 to accurately capture the expected non-linear curvature distributions rather than increasing the number of integration points. As for FBE it is less important to discretize vertically and it is more important to increase the number of integration points along the height of the element. Sensitivity studies regarding the number of integration points versus number of elements for FBE and DBE on the accuracy of deformation capacities support this. To summarize these findings DBE required 16 elements to produce an error in curvature of 3%, whereas force-based elements required two elements with five integration points to produce an error less than 2% (Terzic 2011). This approach will be applied when it comes to determining the appropriate number of elements and integration points for the MVLEM and fiber element models used in the following analyses.

The most involved of all the parameters needed for creating an accurate fiber model of a RC shear wall is accounting for strain localization. Past research provided by Coleman and Spacone (2001) shows that typical fiber models do not accurately capture the full response shown in experimental tests due to strain localization. As one fiber fails it regains equilibrium by degrading along its specified post-peak slope, but as the wall continues to deform, the surrounding fibers also degrade, and since they have not reached their peak strength, they degrade elastically, causing an increase in inelastic deformation localized at the failed fiber (Pugh 2012). Research has shown that by adding more stations only causes more focused inelastic deformations due to the decrease in the length of the fiber element, this causes brittle response, which was not seen in experimental testing (Coleman and Spacone 2001).

The recommended approach to account for strain localization is based on the theory of constant fracture energy utilized in material regularization. Fracture energy, G_f is a material property defined as the area under the post-peak slope in the plot of stress versus deformation. The methodology recommends altering the ultimate deformation of each material to ensure constant fracture energy, G_f for all fibers throughout the section. When implemented within both the concrete and steel material models, similar responses can be obtained as compared with experimental wall tests (Coleman and Spacone 2001).

The sudden loss of flexural capacity, seen in wall tests provided by Lowes et al (2011) has been implemented in OpenSees through a minimum-maximum material model. The material model investigates the strain in the fibers at each step of analysis until one fiber reaches a specified limitation, such as the crushing strain of concrete or the rupture strain of reinforcing steel. Once the model indicates the fiber has crossed the threshold, it returns a zero tangential stiffness and stress, causing a sudden loss of capacity.

The final step in creating an accurate fiber model is the implementation of shear. This can be done by either aggregating the shear to the original response using the section aggregate tool implemented in OpenSees, or by use of zero-length springs at respective floor levels with an appropriate shear material model. Both options result in an uncoupled flexure- shear response. For three dimensional analyses, a torsional stiffness must be specified. This can be incorporated three different ways: by adding the torsional constant term, J within the input parameters of the element type, either FBE or DBE, by using the section aggregation tool, or lastly by using zero-length springs at the appropriate locations. The characteristics of both the fiber and MVLEMs being used for the analysis of the core walls of PGC is described in the subsequent sections.

5.3 Shear Wall Models for PGC

The following models are used for the three core wall assemblages, CWN, CWS and CWC (Figure 18). The non-core walls (NCW) (Figure 18) are modeled using a simplified force-based fiber model for better continuity with the core walls. The NCW span from the ground level to level 1 and since the ground level is known to not have collapsed, it is appropriate to use more simplified models and assumptions for better computational efficiency. For more details regarding the modeling of the NCW, refer to section A.4 of the Appendix

5.3.1 MVLEM

As described previously in this chapter the modified MVLEM will be used to represent the core walls of PGC. Since this model type uses displacement-based elements, a vertical discretization is necessary. Five elements are used between ground level and level 1, while 4 elements are used between level 1 and 2, resulting in an average element length of 40 inches for ground level and level 1. It is important to have many elements at level, since this is the expected failure location. The remaining story levels are represented by a single element. The uniaxial material used for all vertical springs is VertialSpring2, which contains degradation beyond peak strength, see Figure 32. The number of springs in each wall depends on the reinforcement layout. The springs are spaced at the same spacing as the reinforcement for each wall assemblage, 15 inches on center with a 4 inch concrete cover at the edges. For further information regarding the vertical springs, including hysteretic responses of a typical spring, see Appendix section A.5.

The non-linear shear slip model was adopted for the shear backbone. It was used to keep both the fiber and MVLEMs as similar as possible. The response is bilinear, following an initial stiffness of $0.4E_c$, where $E_c$is the modulus of elasticity of the concrete, up to a cracking shear stress,v_{cr}(Figure 39). Beyond cracking, the backbone follows a secondary stiffness of $0.01E_c$, this is recommended by NIST GCR 10-917-8 (NIST 2010). The cracking stress is calculated based on recommendations from Wallace (2013) as $3\sqrt{f'_c}$. This model does not contain any post-peak degradation and therefore post-processing will be necessary in order to determine if shear failure has occurred within the section.

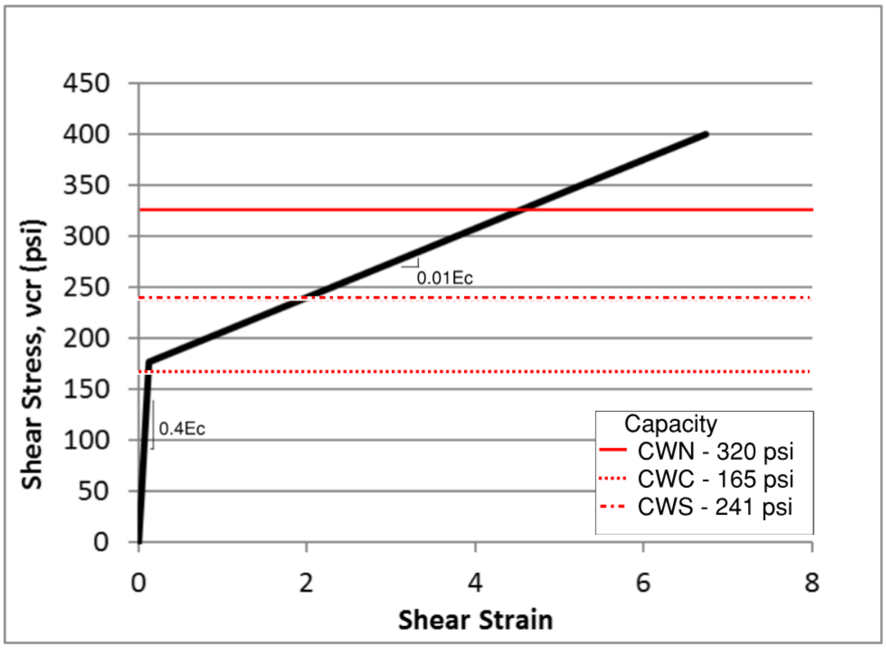

Figure 39: Typical shear backbone

Rotational stiffness is accounted for by a rotational spring built into the MVLEM and located at c*h along the height of each element. This imbedded rotational spring resulted in problems when determining the correct torsional stiffness of the entire core system, as well as it was limited to only an elastic material model. Based on these findings, zero-length rotational springs were added to the wall model at each of the story levels, containing elastic cracked stiffness based on experimental tests shown in Peng and Wong (2010). The elastic cracked stiffness used is 0.2JG, where J is the torsional constant of the section and G is the shear modulus (0.4Ec) (Figure 41). Torsional stiffness is usually ignored in majority of analyses because it is assumed to not influence the response and very few experimental tests of walls take it into consideration, therefore it is difficult to determine an appropriate value for effective stiffness. The location of the rotational spring (torsional stiffness of the section) in plan is another poorly discussed topic. A short torsion study regarding this issue of where to model the rotational stiffness is summarized in section 5.3.3.

5.3.2 Fiber Model

The PGC core walls will also be modeled using a typical fiber model following the same techniques described in 5.2. The three wall assemblages (CWN, CWS and CWC) will be modeled using two forced-based elements per story level, along with using five integration points for each element. This should provide a very accurate representation of the distribution of curvature. The uniaxial material models, Concrete02 and Steel02 (PEER 2013) were used for the concrete and reinforcement, respectively, as recommended by Pugh (2012). Typical hysteretic responses for each of the material models are shown in section A.5 of the Appendix.

Fiber mesh recommendations for modeling shear walls are typically for planar walls with boundary elements, as discussed before. Therefore three sectional analyses are produced to determine the sensitivity of the mesh size for the wall assemblage CWN (Figure 40). The course mesh of 8-inches by100-inches took the least amount of time, but did not capture a similar response compared with the two finer mesh plots (Figure 40). The mesh of 1-inch by 1-inch took considerably more time than the 4-inchby 4-inch mesh, but both show similar results. Therefore a mesh of 4-inches by 4-inches is used for all the walls.

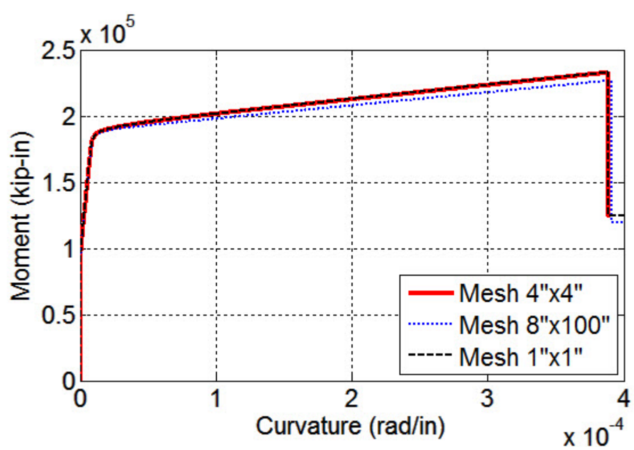

Figure 40: Moment-curvature plot of CWN showing mesh sensitivity

The material regularization technique, as described in section 5.2 is implemented for both the concrete and steel materials in order to alleviate strain localization. Although, this approach is not critical since the walls of PGC are lightly reinforced and unconfined it is expected that as soon as the concrete begins to descend down the post-peak slope failure ensues and localization of deformations will take place in the real walls. Use of the min-max material is also implemented in this model to capture brittle strength loss after material failure. The thresholds used for the min-max material models are based on the assumed strain limits for the reinforcement and concrete. These strain limits have been discussed previously under wall material properties (Table 1). The methodology for the implementation of the material regularization technique is described in detail as it pertains to this analysis in section A.5 of the Appendix.

Both shear and torsional stiffness are accounted for by aggregating them with the fiber element. Each length of fiber has a given shear and torsional resistance. The hysteretic material model implemented in OpenSees (PEER 2013) is utilized for shear. See Figure 39 for the typical shear backbone. The procedures used to determine the values of cracking stress and post cracking slope are identical to that explained in the MVLEM section 5.3.1. The aggregated rotational stiffness is calculated using the torsional constant J, as determined from geometric properties and the shear modulus, G. Current research of planar reinforced concrete walls subjected to pure torsion (Peng and Wong 2010) produce an idealized torque-rotation plot labeled as typical backbone in Figure 41. Based on this idealized backbone an effective elastic cracked stiffness of 0.2JG will be used for all analyses, shown in Figure 41.

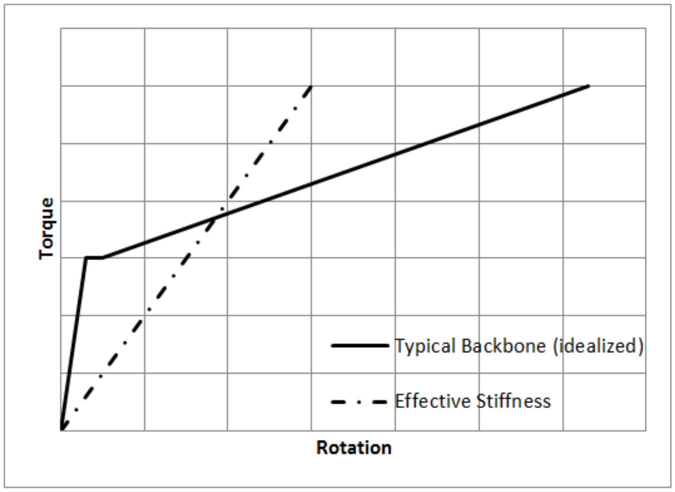

Figure 41: Effective torsional stiffness

Based on this plot, a more appropriate rotational spring material model would be a bilinear approach, similar to how shear is modeled, but with the lack of experimental tests showing how walls behave under pure torsion makes this difficult to quantify.

5.3.3 Shear Center vs. Geometric Center (Torsion Study)

When modeling asymmetric wall sections (c-shapes, L-shapes, etc.), where the geometric centroid (GC) is not in-line with the shear center (SC), the torque, which results from this eccentric distance e, is not accounted for (Figure 42). Where the GC is calculated based on a weighted average of surface area and the SC is the location where zero torque results from an applied load. The most common element models for representing shear walls within OpenSees (PEER 2013) are fiber element models and MVLEM. When using these models to construct asymmetric wall sections, such as c-shapes, the element's relative stiffness (axial, flexure, shear and torsion) are all located at the GC. The GC is the correct location for accurate modeling of the axial-flexure interaction, but is the incorrect location for modeling torsional resistance.

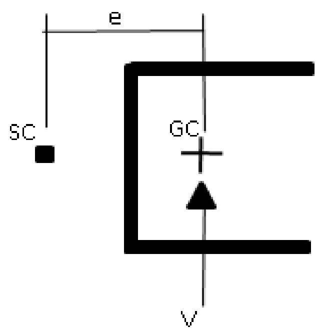

Figure 42: Typical c-shape section

Consider modeling the simple c-shaped wall (Figure 42) with a horizontal load, V, applied at the GC. Since the element and the applied load are both located at the GC, the wall will undergo zero rotation and thus result in zero torque. This is incorrect, because with an applied load at the geometric center, the wall should rotate about the shear center, causing a torque of V times the distance e.

The following study shows the error that results, when modeling the torsional stiffness at the GC, instead of the SC, is minimal and does not greatly affect the accuracy of the overall analysis. This study is specific to the parameters of PGC, the core location and the rigid diaphragm constraint. Three types of material models were used and for each type, two subsequent configurations were compared (Table 12). The material properties are the same or similar to that of PGC, as specified in section 4.1 for each type and configuration. Type 1 uses elastic beam-column elements with equivalent properties to that of type 2 and 3, which are similar to the layout of the core walls within PGC. Configuration 1, for all types, uses the rigid diaphragm assumption, therefore, translations in the X and Y and rotations about Z are constrained together for elements 1 and 2. Refer to Table 12 for the reference axis (type 1 configuration 2) and notation for each type and configuration. Configuration 2, for all types, is modeled as single element (element 3) at the CR of the system, but represents the same, two-element core system, as in configuration 1 (Table 12). In configuration 2, the eccentric center of mass (CM) is accounted for by attaching a rigid element spanning from the CR to the CM to capture the torque, since the rigid diaphragm constraint cannot be used in a single element system.

Table 12: Configuration Summary

Type		Configuration	
1	Elastic - Beam Column	1	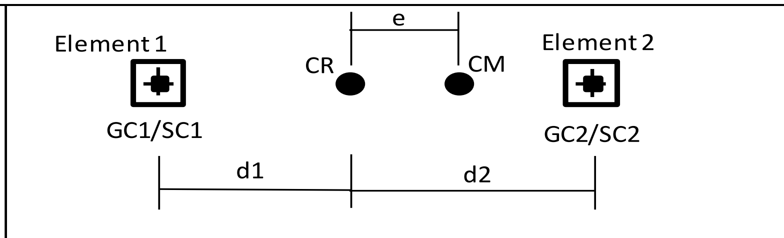
		2	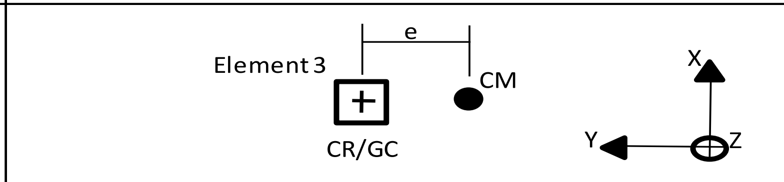
2	Fiber	1	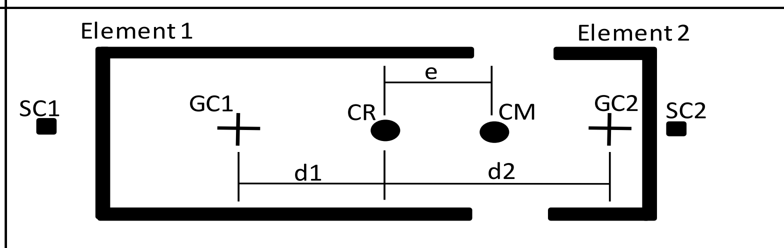
		2	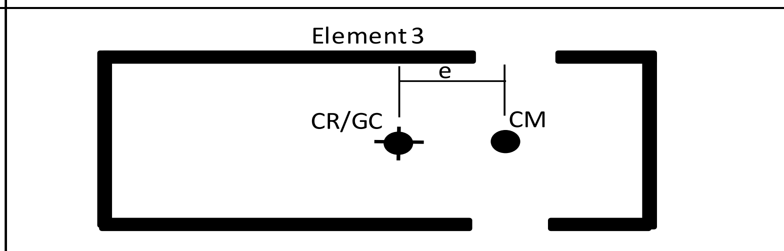
3	MVLE	1	same as the Fiber
		2	same as the Fiber

Key:

The location of the element at the GC of the section.

The location of the center of mass or center of rigidity for the sysemt of elements.

SC: The location of an applied horizontal force where zero rotation results within the element

CR: The location of an applied horizontal force where zero rotation results within the system of elements

A lateral point force is applied to all types and configurations at the location of the CM, which was chosen to be a distance, e, from the CR (enforcing a torque). For configuration 2, of all types, the torsional moment can be calculated by multiplying the applied load by the distance e, since it is a statically determinant problem. The torsional moment determined with configuration 2 is considered the control for this study since, it is known that the GC and CR overlay, resulting in zero error in the calculated torque. The torque versus plan rotation of configuration 2 will be compared with the calculated torque from configuration 1for all three types (Figure 43, Figure 44 and Figure 45).

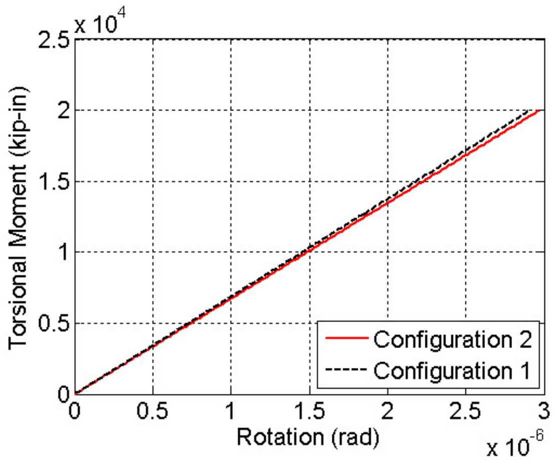

Figure 43: Type 1 - Elastic beam-column elements

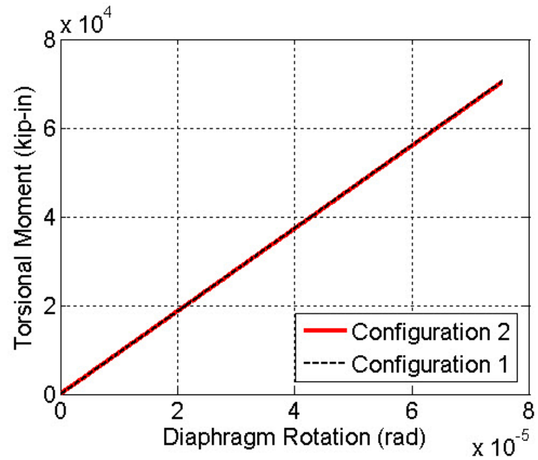

Figure 44: Type 2 - Fiber elements

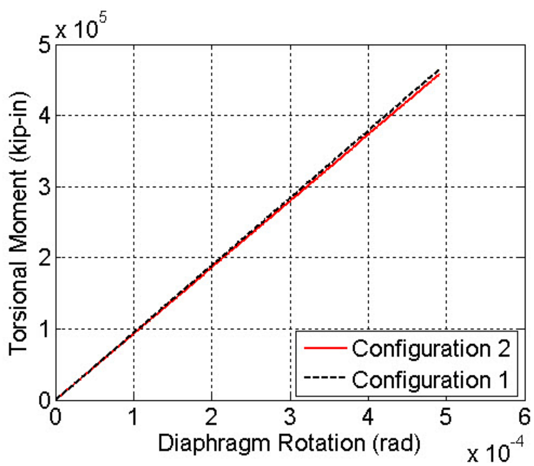

Figure 45: Type 3 - Multiple-Vertical-Line-Elements

For every element model, the torsional moment from configuration 1 is similar to that of configuration 2 thus proving that little error results when modeling the torsional stiffness at the GC, as in configurations 1 rather than the CR (or SC) as in configurations 2. These results are specific to this analysis, as the configurations and material properties are specific to that of PGC. It should be considered that by altering the distance e, element properties, applied load, etc. may cause the error between configurations to increase to an unacceptable level. Also, the applied load did not exceed a yielding force; therefore, all the elements remained elastic, which allowed for the CR to remain in the same location. Realistically, as the demand would increase and the elements begin to yield, the CR would move either further away or closer to the CM, depending on the rate and timing of element softening. Sample calculations of the different properties, the coupled force due to rotation and other procedures used in the findings of this study are shown in section A.6 of the Appendix.

5.3.4 Validation - Sectional Analysis

Confidence in the models being used is largely attributed to validation. In this section, as well as the following chapter, commercial software, hand calculations, sectional analysis and simple modal analysis will be used to validate both the fiber element models and MVLEM.

A moment-curvature response of both the fiber element models and MVLEM, as described in the previous sections, is used to validate the models capability to accurately represent the flexural performance of the walls. CWN was used to validate the model with multiple procedures; CWS is also shown for completeness using the OpenSees fiber element model only. This is the largest of the three wall sections used to make up the core of PGC, as seen in Figure 18. The section used in the following calculations is taken at level 1 and follows the same assumptions as the capacity calculations of section 4.3.3. In conjunction with the OpenSees models (Fiber and MVLEM), commercial software Response-2000 (Bentz 2000) and a hand calculation check were used as comparison, see Figure 46. As this is a flexural capacity, shear and torque are assumed rigid within both OpenSees models. This is not an option within Reponse-2000, thus resulting in a softer elastic response, which can be seen in Figure 46 (right), the zoomed in linear portion of the moment-curvature response. Even with the softer linear elastic response all three cases show a very good comparison of yield strength, roughly 90,000 kip-in. All of the responses show very comparable moment-curvatures throughout the total response. The maximum curvature determined from Response-2000 supports the findings from the fiber model, MVLEM and the hand calculation (indicated with a black diamond in Figure 46), with failures occurring at curvatures of 0.000368, 0.000389, 0.0003923 and 0.000386, respectively. Rupture of the steel governed the flexural response over crushing of the concrete for the fiber model, MVLEM, the hand calculation and Response-2000.

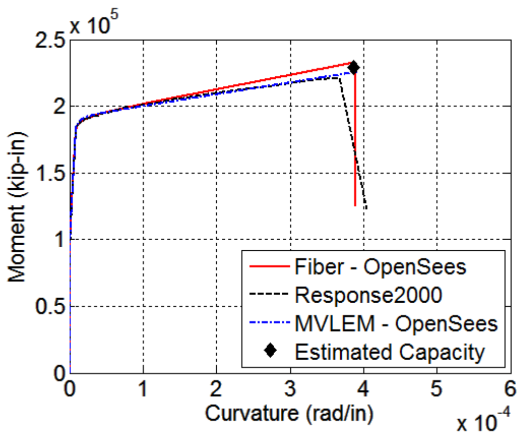

(a)

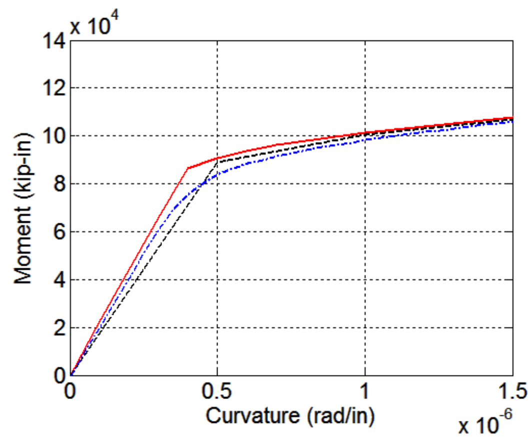

(b)

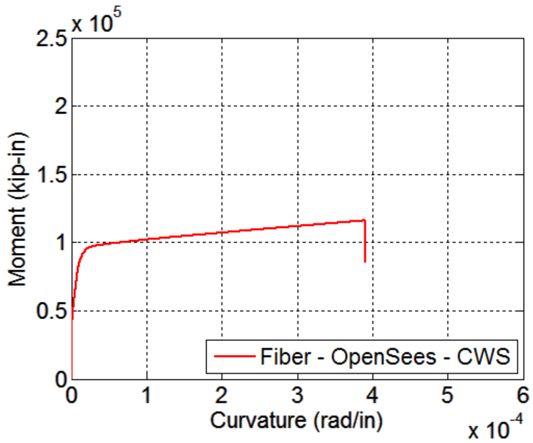

Figure 46: (a) Moment-curvature full response (b) Moment-curvature linear segment (c) Moment-curvature full response – CWS (Fiber element only)

The fiber model, with the addition of the min-max material model indicates failure once a single fiber, whether the material is steel or concrete, reaches the specified strain limit. The MVLEM does not have the capabilities to incorporate the min-max material, as in the fiber model, thus post-processing is necessary to determine where and when failure occurred. Once a spring reaches a specific strain, which is over the material limit, 0.075 for steel and -0.004 for concrete, failure is assumed to have occurred. This is similar to the methodology behind the min-max material model implemented in OpenSees thus the similar results. Once this limit is reached, in either a single fiber or spring, the model is assumed to have failed in total, as seen by the abrupt drop in capacity in the moment-curvature response. This is assumed since the accuracy of the model cannot be verified beyond failure of a single fiber or spring. Given the differences of each of the models and the different assumptions built into

Response-2000 and OpenSees, the results are very comparable. The use of the fiber and MVLEMs to accurately represent the flexural response of the walls, which make up the core of PGC, is validated by the summarized flexural response data in Figure 46.

Chapter 6 **Global Modeling and Expected Performance**

Two global modeling approaches are taken with the goals of determining how the walls failed during the February event and understanding how the location of the shear core of PGC affected its seismic performance. The first approach is based on the assumption that the walls, both core and non-core, account for majority of the lateral stiffness of the entire structure. This approach was utilized by considering only the walls in the models within OpenSees, referred to as shear core models. The second is an investigation regarding the location of the shear core and how it affects the overall response. Two configurations, A and B, are used for this investigation. Configuration A is the exact layout of PGC, where the walls are offset to the north of the plan causing the center of rigidity to be located away from the center of mass resulting in an eccentricity. In configuration B, the shear core is centered within the plan, essentially removing the induced eccentricity. Both approaches are validated by comparing data from the Beca technical report (Beca 2011a) and from models constructed in ETABS (CSI 2013). A table explaining the different models and configurations used in ETABS and OpenSees, as well as used by Beca are shown below.

Table 13: Model Summary

Source	Configuration	Element Type	ID	Mass Allocation
OpenSees	A	Forced-Based Fiber Element	Shear Core A	Lumped and rotational
		MVLE		
	B	Forced-Based Fiber Element	Shear Core B	Lumped
		MVLE		
ETABS	A	Shell/ Line	Full 3D	Distributed
	B	Shell	Shear Core	Lumped
Beca	A	Displacement-Based Fiber	Full 3D	Lumped
		Single Line	Stick	Lumped

For 3-dimensional graphical representation of the ETABS and OpenSees models used in the following analyses refer to section A.7 of Appendix A

6.1 Eigen Analysis

Eigen analysis is used to support and validate the use of the global modeling approaches discussed above. Comparison of modes and periods of vibration were made between the different models from ETABS, OpenSees and Beca. In order to construct the OpenSees shear core model accurately, the mass had to be allocated correctly. Using the full 3D model constructed in ETABS, a center of mass (CM) location for each level is found based on an accurate distribution of mass. These locations are used for the shear core A and B models within OpenSees. This is not enough to accurately represent the mass from the full 3D model. Since the mass is going to be lumped at the CM for each level, a rotational mass component is added in order to account for the inertial forces seen by the distributed mass structural model. The approach set forth in Chopra (2001) provides guidance for the determination of this rotational mass by calculating a term, Io for multistory asymmetric plan buildings. Io is the mass moment of inertia of the entire distributed mass across each floor diaphragm about the vertical axis passing through the center of mass for that respective floor level. This procedure assumes that the mass is distributed equally throughout the floor diaphragm, which is not the case for PGC. In order to be sure about this assumption, in ETABS, a uniformly smeared mass and a distributed mass model were compared to see how the location of the CM and rotation of the diaphragm differed. The assumption of using uniformly distributed mass, when determining the rotational mass, is acceptable based on the findings. This is reiterated in Table 14, which show the periods of vibration for the different models. There is little difference between the dominant torsional modes of the ETABS full 3D model, which directly captures the non-uniform mass distribution, and the OpenSees shear core model, which uses a lumped mass with rotational mass component. This validates the use of the shear core models to accurately represent the full response of the structure.

Table 14: Modal Analysis Summary (Configuration A) (adapted from Beca 2011a)

Mode	BECA	ETABS	OpenSees	
	Full 3D	Full 3D	Fiber	MVLE
1 (Tor.)	0.87	0.86	0.86	0.92
2	0.57	0.48	0.47	0.51
3	0.41	0.36	0.34	0.41
4	0.29	0.28	0.27	0.30
5	0.19	0.16	0.15	0.18
6	0.16	0.15	0.13	0.15
7	0.14	0.12	0.11	0.13
8	0.13	0.12	0.09	-
9	0.12	0.09	0.09	-
10	0.10	0.09	0.07	-

Table 15: Modal Analysis Summary (No Torsion) (adapted from Beca 2011a)

Mode	Dir.	BECA*		ETABS - Shear Core	OpenSees			
					Shear Core A		Shear Core B	
		Stick	Full		Fiber	MVLE	Fiber	MVLE
1	E-W	0.65	0.62	0.594	0.630	0.588	0.534	0.527
2	N-S	-	-	0.379	0.338	0.406	0.338	0.345
3	E-W	0.17	0.16	0.173	0.172	0.165	0.140	0.129
4	N-S	-	-	0.125	0.092	0.128	0.092	0.098
5	E-W	0.09	0.09	0.096	0.091	0.094	0.078	0.068
6	N-S	-	-	0.072	0.062	0.073	0.058	0.051

* BECA only provided data for the E-W direction

Table 14 and Table 15 summarize the periods of vibration for all the models listed in Table 13. The periods for both the fiber element model and MVLEM are essentially identical for both configurations respectively. This further validates the use of those models within these analyses. The models using configuration A, for all sources (Beca, ETABS and OpenSees) show a torsion dominant first mode response. This is not pure torsion though, it is a combination of east-west translation and rotation, as determined by the mode shapes. This was expected based on the observed torsional irregularity. A comparison of the dominant mode shapes for the ETABS and OpenSees models is shown in A.8.

The periods of configuration B, as those of configuration A, show great similarity, given the complexities that go into each of the model types. Beca uses the stick model to calibrate their full 3D model and by doing so, they provided modal analysis data, in which torsion was excluded. Configuration B periods from OpenSees as well as the Beca models excluding torsion are summarized in Table 15. The configuration B periods are shorter than configuration A, this is expected since configuration B removes the eccentricity between the center of rigidity and the center of mass. Ten modes were used to reach 90% mass participation for the configuration A models, as detailed in the Beca report (Beca 2011a). The ETABS models at the 10^{th} mode reach 88% mass participation, which is considered acceptable for this analysis. OpenSees does not have the capabilities to acquire the mass participation; therefore it is assumed that 10 modes are necessary in order to reach 90%. Six modes were enough to reach well over 90% mass participation for the configuration B models in Table 15. The models used in ETABS and OpenSees, as well as within the Beca report, produce similar mode shapes and periods, all based on different assumptions and using different computer software, therefore validating the use of the shear core models within OpenSees to accurately capture the response of PGC.

6.2 Response Spectrum Analysis

The REHS spectrum from Figure 47 is created from the recorded ground motion from the REHS site, for different fundamental periods, assuming 5% damping, for both the September and February events. Three components of motion were recorded, two horizontal and one vertical. The influence of vertical ground motion on the response of PGC is beyond the scope of this study. The two horizontal components, shown in Figure 47 are denoted by their bearings, South 88 degrees East (S88E) and North 2 degrees East (N02E). For reference, the 2500 year and 500 year design earthquake spectrums for Christchurch are also shown (Figure 47). Also included in the plot are the calculated first and second modes periods. The first mode period is dominated by torsion at 0.87 seconds whereas the second mode period at 0.6 seconds is in the east-west direction.

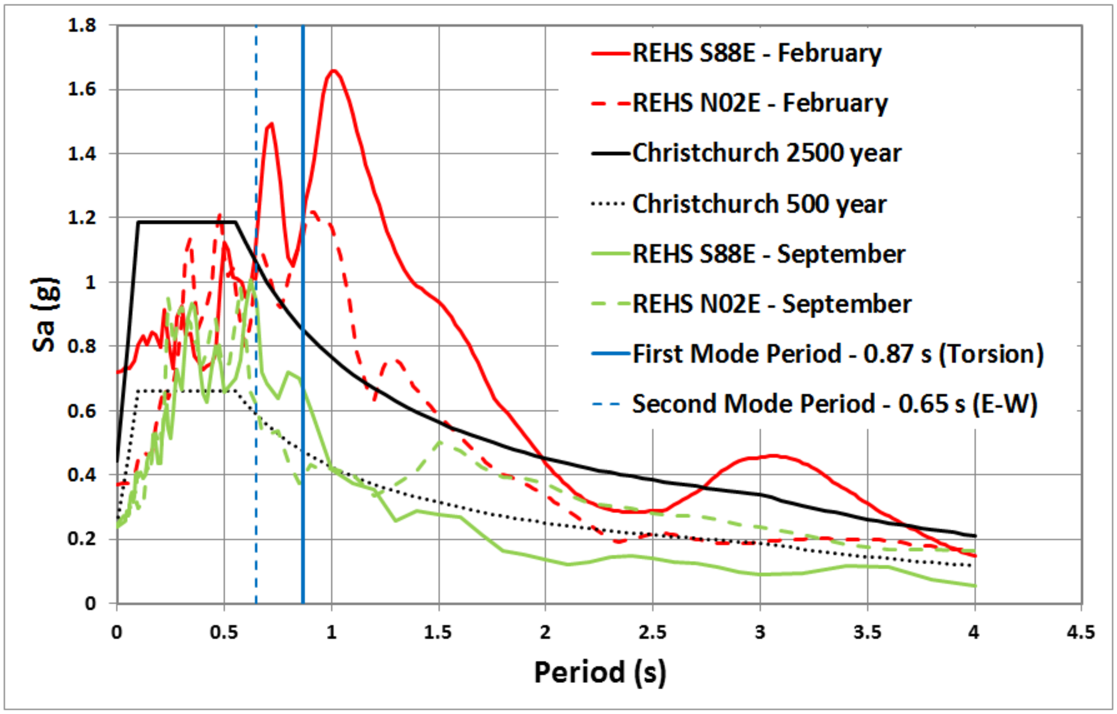

Figure 47: REHS response spectrums

Looking at the REHS S88E February spectrum, using the dominant east-west mode period of 0.6 seconds (Table 15) yields an acceleration demand of approximately 1.2 g. Again, for a east-west mode period of 0.6 seconds, the 500-year design spectrum for Christchurch would yield an acceleration demand of approximately 0.7 g and the 2500-year, which is the maximum considered event for this area, would yield an acceleration of just below 1.2 g. This shows for a building such as PGC under a first mode response, that the February event was equivalent to that of the maximum considered earthquake for that area, a 2% chance in 50 years of occurrence, a very significant event, even for today's building code standards. For the 2500-year design spectrum, PGC, at a period of 0.6 seconds is located on the descending portion of the curve. This would indicate that during period elongation (as the building begins to yield and experience damage) the expected acceleration would decrease reducing the demands, but for the February response spectrum the building is on the ascending portion of the curve indicating the acceleration would in fact intensify, increasing the demands on the building and greatly increasing the probability of collapse given the low levels of ductility within the structure. Another notable observation from Figure 47 is the highest intensity shaking from the September ground motions is occurring at a period of 0.6

seconds, the same dominant east-west mode period of PGC. PGC was not observed to sustain substantial damage during the September earthquake, yet it experienced the highest acceleration demand for the September earthquake at a period of 0.6 seconds.

Using both spectrums from Figure 47, a response spectrum analysis is performed using ETABS for both the shear core and full 3D models with the findings summarized in Table 16. There is little difference between the loads at level 1 and the loads at the ground level indicating the high relative stiffness of the ground story versus above. This is concurrent with the post-collapse photos indicating the ground level had not collapsed. These values represent the estimated demand on the structure for the February and September earthquakes and will be compared with the expected capacities of the pushover analysis in section 6.3.3. The demands for September are roughly 50% less than those for February for the Full 3D model. This is expected since at a first most period of 0.87 seconds the acceleration demand for September (0.65 seconds) is roughly 50% less than February (1.2 seconds).

Table 16: ETABS Response Spectrum Analysis Results

Response Type and Location	February		September	
	Full 3D	Shear Core	Full 3D	Shear Core
Moment at level 1 (kip-ft)	297294	350267	193495	241385
Moment at Ground (kip-ft)	326137	383605	211973	264241
Shear at level 1 (kips)	5862	6760	3729	4609
Shear at Ground (kips)	5899	6788	3778	4625
Roof Drift (%) (E-W dir. At CM)	0.63	0.55	0.37	0.34

6.3 Non-Linear Static Analysis

A non-linear static analysis, or pushover, is utilized for a better understanding of the performance of the fiber element model and MVLEM, as well as the global modeling approaches and response of the shear core. All models described in Table 13, except the

Beca models, are subject to a pushover analysis and described below. Insufficient information regarding the pushover response of the Beca models provided in the report, and hence will not be addressed. The direction of the pushover is west to east, since that is considered the most critical, due to the observed failure. The distribution of applied load, most commonly used, is based on a first mode shape, but since the first mode is a torsion dominant mode, it is inappropriate to use that approach, therefore a triangular load distribution is used. The force factors allocated to each story is based on a weighted average of the story heights.

The ETABS models, both full 3D and shear core are subjected to pushover analyses, using the same triangular load distribution as described above. The results are used to compare initial stiffness of the pushover curves for the OpenSees shear core A and B models. The initial stiffness of configuration B is stiffer than that of configuration A. This is expected, since the center of rigidity coincides with the center of mass in configuration B. An example of the ETABS full 3D model pushover, comparing its initial stiffness to the pushover profile of shear core A, is shown below in Figure 48.

6.3.1 Configuration A – PGC Layout (Torsional Irregularity)

Shear core A for both the fiber element model and MVLEM are compared in multiple figures below. The responses seen from each of the element models show great consistency in determining ultimate strength and displacement capacity as seen in the sectional analysis section 5.3.4.The MVLEM does not indicate flexural failure with a sudden drop in capacity, such as the fiber element model does. Compression failure (concrete crushing) is triggered within the MVLEM when the compression spring displacement is reached or exceeded, but no indication is displayed if failure occurs in tension. Therefore, post processing is necessary to determine whether flexural failure has occurred in the MVLEM. Shear failure is also not indicated within either element models and therefore will also be post-processed. Figure 48 displays the pushover response for both the fiber element model and the MVLEM referenced from the ground level. In order to compare the elastic stiffness of both the fiber model and the MVLEM with the ETABS full 3D model, the total response was required. This is the only plot to reference the full response of the shear core; all following plots will be referenced from level 1.

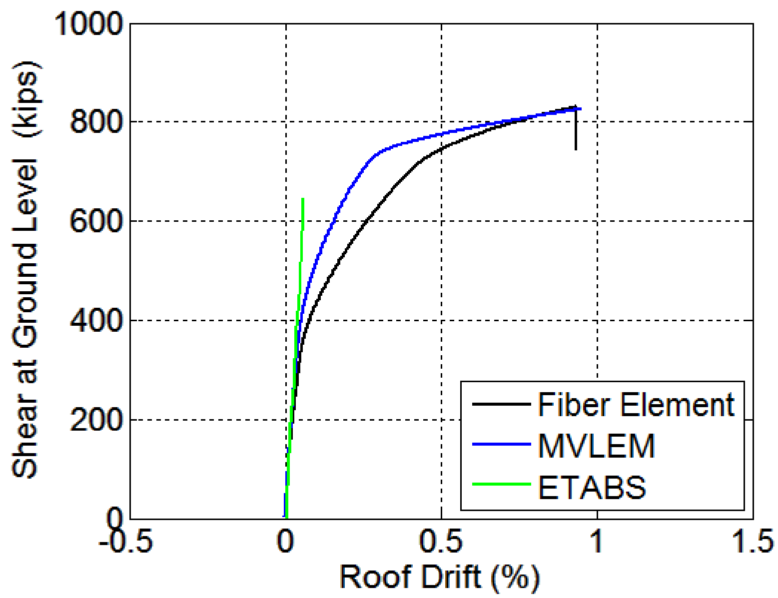

Figure 48: Pushover profile referenced to the ground level (base of the core)

The shear capacity of each wall assemblage, including the critical pier of CWN, as determined in section 4.3.3.2 and summarized in Table 9 are displayed below in Figure 49 and Figure 50 for the fiber element and MVLEM, respectively. Both the MVLEM and the fiber element model show similar results for each of the wall assemblages. The most observable difference is the relative strength between CWN and CWS which appears to be greater in the MVLEM than with the fiber element model. The overall response of the systems however is very similar as seen in Figure 48, the difference is likely due to the interactions with the rigid diaphragm constraints which may differ for fiber elements versus MVLEMs. The pier of CWN is the most critical case as the capacity is exceeded well prior to any yielding of the flexural reinforcement. Based on these findings the pier within CWN is considered shear critical. Since the other two walls of the core system do not exceed their shear capacity limits, it is expected that the shear loss from the pier of CWN would then be resolved within the other core walls (CWS and CWC), but further analysis would be required to support this. The full response of the core system appears to be a more desirable flexure-shear response, where the flexural reinforcement of the walls will yield prior to failing in shear. Wallace (2013) suggests reducing shear capacity based on flexural ductility demand, but since these walls have very little flexural ductility and are expected to fail quickly this type of reduction will not be necessary.

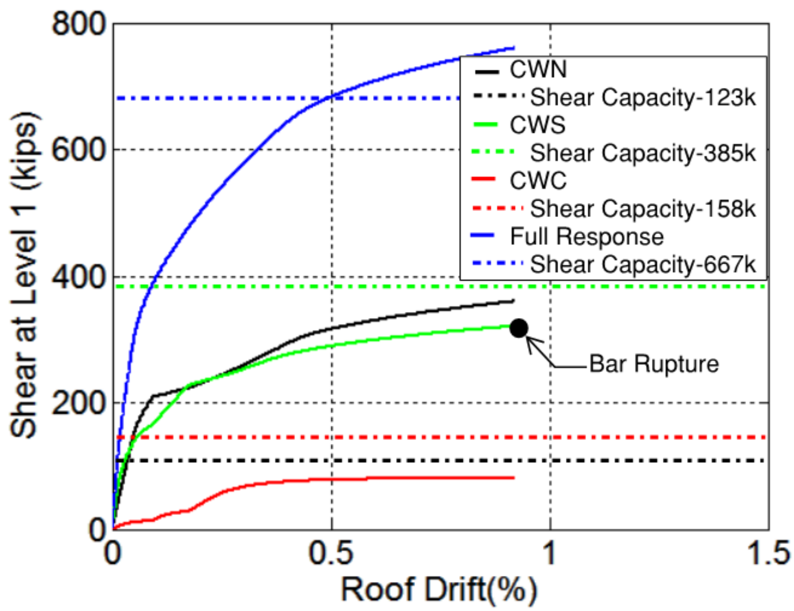

Figure 49: Fiber element - Shear response for each wall assemblage up to bar rupture with shear capacities for each wall indicated.

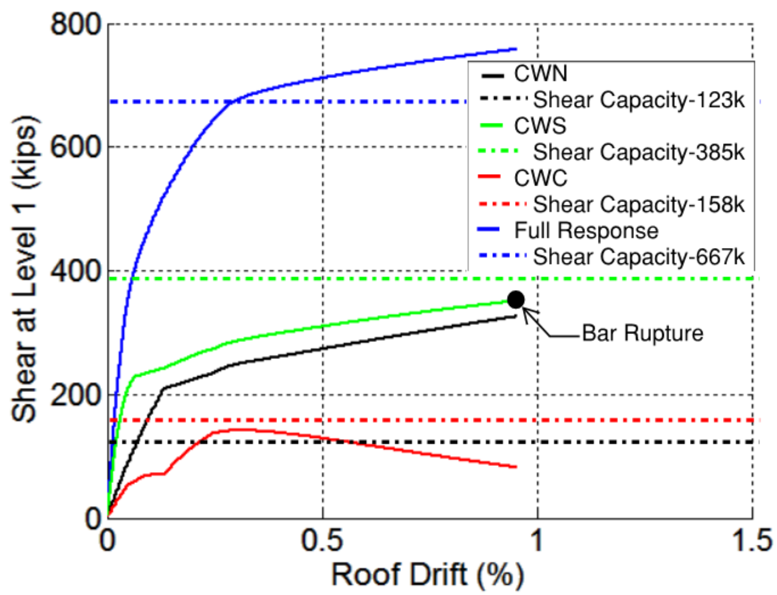

Figure 50: MVLEM - Shear response for each wall assemblage up to bar rupture with shear capacities for each wall indicated.

Figure 49 and Figure 50 indicate flexural failure by bar rupture occurring in CWN and CWS for the fiber element model and MVLEM respectively, but not until after shear failure has already occurred. Therefore, considering only the flexural response of configuration A as if the walls were not shear critical, as shown previously, produces results consistent with the finding from Beca's technical report (Beca 2011a). For all pushover analyses, the flexural failure occurred by rupture of the steel at an elongation of 7.5%. Figure 51 shows the full pushover response referenced at level 1 for both the fiber element model and the MVLEM. The results from both models are very similar indicating bar rupture at total roof drifts of 0.95% and 0.94 % for the MVLEM and fiber element model, respectively.

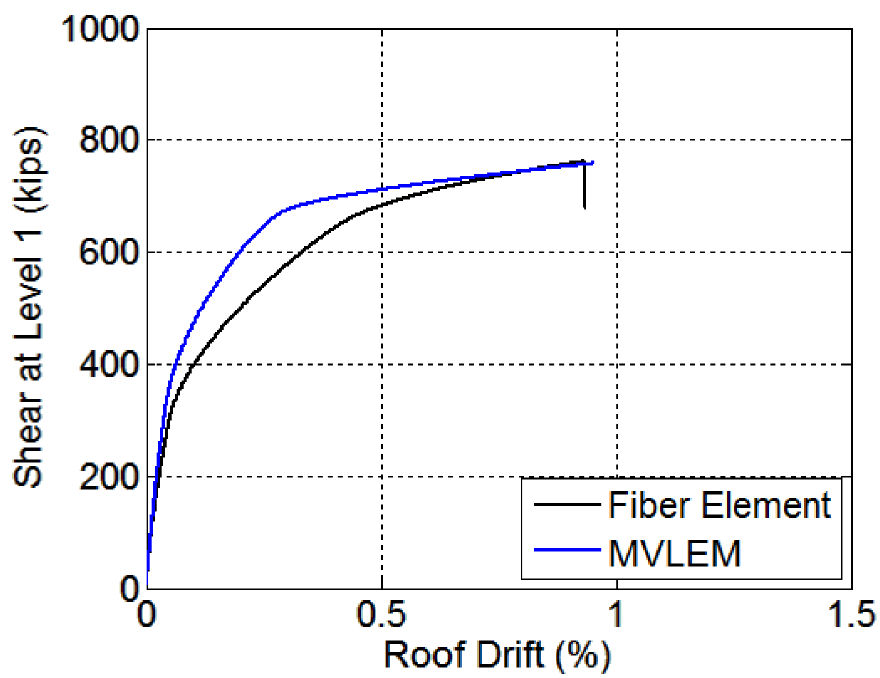

Figure 51: Pushover profile referenced at level

Level 1 is the most critical of all the levels, as seen in Figure 52, which displays a large concentration of curvature at level 1supporting the post collapse photos in which the ground level does not collapse. The curvature displayed is taken at the step in which bar rupture was indicated, at roof drifts of 0.95% and 0.94% for the MVLEM and fiber element model respectively. Based on the sectional analysis, provided in section 5.3.4 an expected curvature capacity for both walls is 0.0004 (1/in). Both models indicated the flange reinforcement of CWS ruptured prior to CWN. Since MVLEM does not indicate flexural failure with the min-max material model, the post processing indicated failure once the curvature within either wall reached the estimated failure point 0.0004, this is why the flexural capacity of CWS is exactly 0.0004 (1/in) in the MVLEM. As for the fiber model, which indicates flexural failure using the min- max material model and incorporates strain regularization does not indicate failure in CWS until a curvature of 0.0005 (1/in). The regularization technique utilized in the fiber model alters the maximum strain limit for each fiber based on the fiber length to control localization, explaining the slight variation.

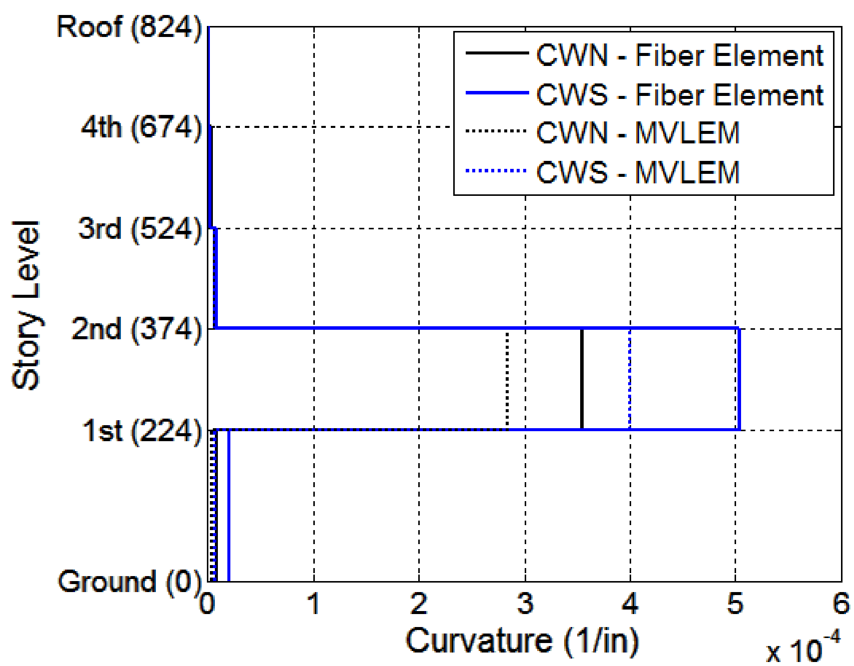

Figure 52: Curvature distribution over the height the walls, CWN and CWS for both fiber and MVLEM shear core models

The fiber element model and MVLEM continue to provide similar estimates for shear capacity, displacement capacity and now flexural strength. This is reiterated in the sectional analysis validation (section 5.3.4) and again, it is seen below in Figure 53, displaying the total moment distribution of the shear core over the height of the building at flexural capacity. The moment capacity at level one for the fiber element model is 28,358 kip-ft, and 30,025 kip-ft for the MVLEM. For comparison, a moment capacity of 30,515 kip-ft was estimated by hand calculations (Table 8) and Beca estimated a capacity of 39,609 kip-ft. A simple comparison of the estimated demand and the expected flexural capacity of PGC, based on a response spectrum analysis performed in ETABS is discussed in section 6.3.3.

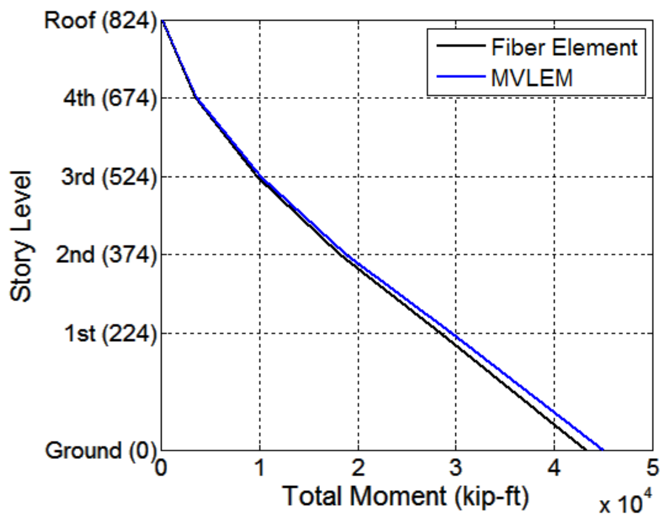

Figure 53: Total moment distribution over height of the shear core for both fiber and MVLEMs

6.3.2 Configuration B – Centralized Shear Core (No Torsion)

It was considered unnecessary to compare both element models for both configurations, as the similarities and differences between the fiber element model and MVLEM are shown in the configuration A plots above. Therefore, only the fiber element model is used for comparison of the response between shear core models A and B. The plots from configuration B are similar to that of configuration A, refer to the pushover profiles, curvature and moment distributions from the previous section for reference. The two plots below, Figure 54 and Figure 55 show three pushover profiles, one for the north most frame line a, the south most frame line h and the center of mass. All three of the profiles are taken at the roof and display the relative rotation of the roof diaphragm. The offset nature of the pushover profiles indicates that plan rotation is present. This is as expected as observations indicated a plan torsional irregularity for configuration A. As compared to Figure 55, configuration B shows all three profiles overlaying one another, this indicates that very little to no plan rotation is present. These figures are created assuming rigid diaphragm characteristics in order to project the displacement recorded from the center of mass, to frame lines a and h, at the exterior of the building plan.

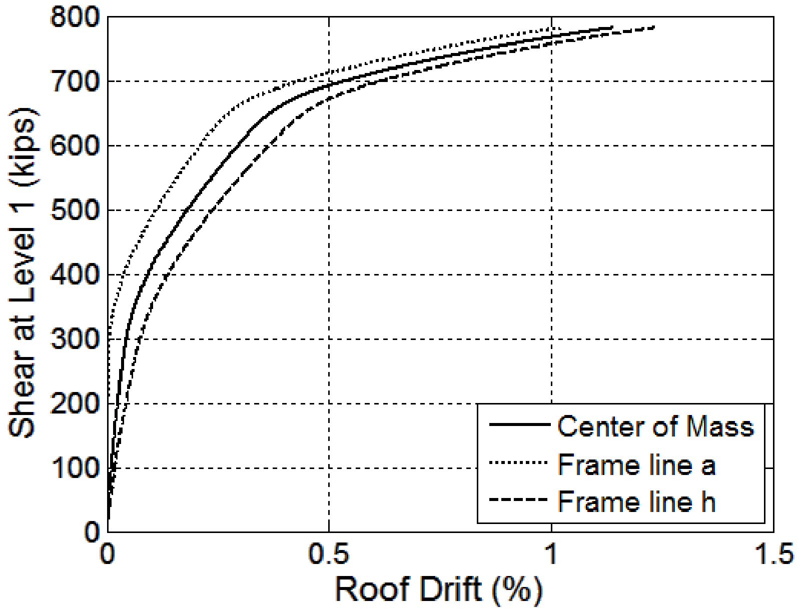

Figure 54: Pushover distribution profile of the roof diaphragm (configuration A)

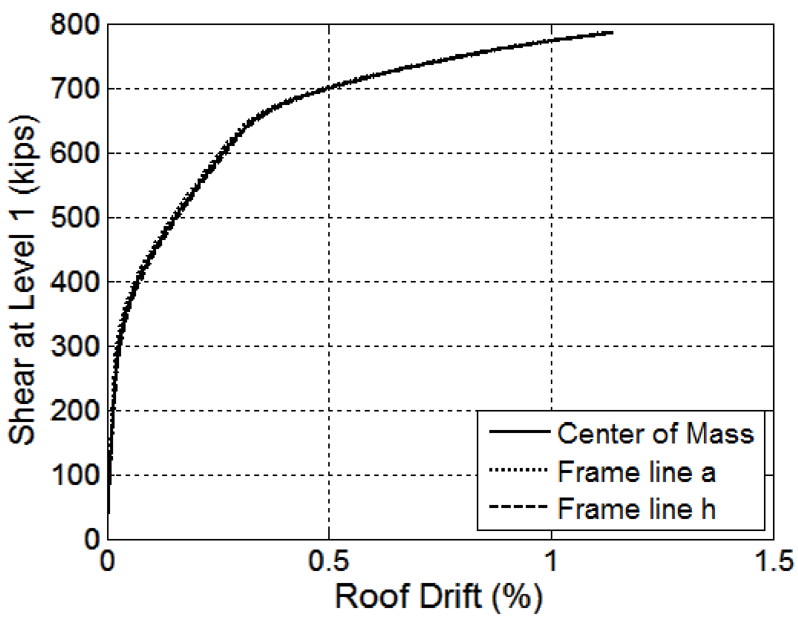

Figure 55: Pushover displacement profile of the roof diaphragm (configuration B)

The strength properties of the models of configuration B are exactly the same as configuration A and therefore the pushover profile figures, from a strength perspective do not differ greatly. This can be seen in the figures above, which show both configurations reaching maximum strength just below 800 kips. Configuration B will be utilized further in the non-linear time history analysis of Chapter 7 for determining if the location of the core influenced the collapse.

6.3.3 Discussion

As determined in section 6.3.1, with Figure 49 and Figure 50 the core of PGC is expected to be governed by shear. Specifically the critical web of CWN is expected to fail in shear prior to any flexural yielding of the flange reinforcement. CWS and CWC however did not reach shear capacity prior to flexural failure and therefore the total response of the shear core is expected to reach a more desirable flexure-shear failure mechanism. To further understand the governing failure mechanism during the February event a non-linear time history analysis is performed and discussed in the following Chapter. Refer to Figure 49 for shear capacities. Assuming shear failure does not govern the response, flexural failure is indicated at drifts of 0.95% and 0.94% for the MVLEM and fiber element model, respectively, as summarized in Table 17. Flexural failure is consistent with the findings of Beca (2011a) as explained in section 3.1. The elastic displacement demands from both February and September based on the ETABS response spectrum analysis summarized in Table 16 does not exceed the estimated roof drift capacity as determined from the pushover analysis, shown in Figure 51.. This would indicate that PGC is not expected to reach this drift capacity assuming the equal displacement theory, although it collapsed in the February earthquake. However, Priestley et al. (2007) indicates that the equal displacement theory is known to be conservative for short period structures which PGC, at a period of 0.6 is considered within range of short period structures. The general magnitude of these drifts is low for flexural capacity. Yet as a pre-1980s RC concrete building, this type of response is common as little displacement ductility is available for that type of construction (Liel 2008).

Table 17: Configuration A - Expected Capacities Based on the Pushover Analysis

Force Type and Location	Shear Core A	
	Fiber Element	MVLE
Moment at level 1 (kip-ft)	28358.3	30025.0
Roof Drift (%) (E-W dir.)	0.94	0.95

The expected flexural capacity at level 1 for configuration A is summarized in Table 17. The configuration B results were similar to those of configuration A and for the purpose of this discussion they will not be displayed. Based on the estimated flexural demands from both February and September response analyses at level 1 and the provided flexural capacities, in Table 17 the shear core is expected to yield at level 1. The large difference between the estimated demand and expected capacities does not indicate that the building would inevitably collapse, as there are many other factors that go into the probability of collapse other than strength.

The purpose of looking into an alternate configuration of the shear core within the plan of PGC was to determine how the torsional irregularity affected the performance. Based only on the non-linear static analysis findings it would appear both configurations produce similar results, indicating the torsional irregularity caused either very little effect on the strength and displacement capacity of the structure or that the vulnerabilities and critical weaknesses of the shear core far outweigh the torsional irregularity issues. Both configuration A and B will be further discussed in the succeeding sections. As for the continuing the comparisons between the fiber element model and the MVLEM, which show great consistency in representing the performance of PGC, only the fiber element model will be used for any further analysis.

Chapter 7 **Non-Linear Time History Analysis**

Two ground motions are used in the non-linear time history (NLTH) analysis, September 2010 and February 2011 as recorded by the REHS strong motion recording site in Christchurch. The relative proximity of the accelerometer to PGC's location is shown in Figure 6. Only the east-west ground motion component is used in the unidirectional time history analysis. This is the critical direction considering the vulnerabilities of PGC and the observed direction of collapse. Each ground motion is applied separately, therefore any damage sustained from previous earthquakes is not considered. Multidirectional effects are also are not considered. Figure 56 and Figure 57 display the acceleration time histories from the September and February earthquakes, respectively. The September ground motion has peak ground acceleration (PGA) of 0.24 g at 31.2 seconds as compared with the February ground motion with a PGA of 0.71 g at 17.18 seconds (GeoNet 2013). The strong shaking duration of the February earthquake is considerably shorter compared with September, but February has a pulse of more than twice the magnitude.

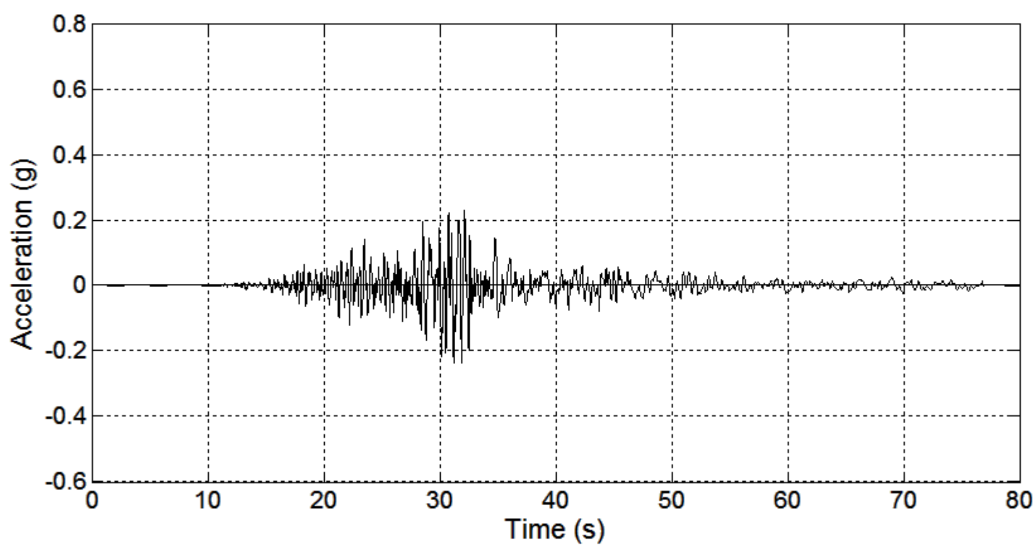

Figure 56: September acceleration time history (REHS – east -west component)

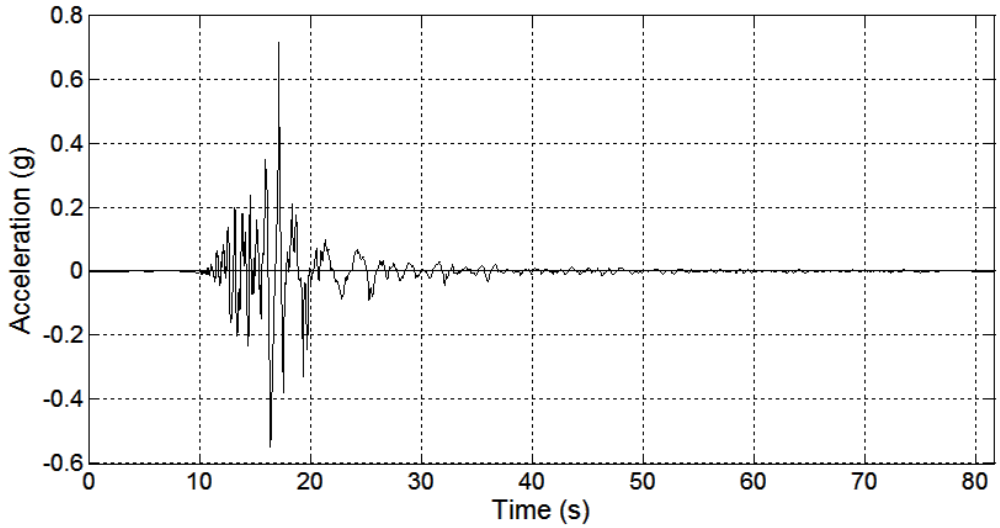

Figure 57: February acceleration time history (REHS east-west component)

Each ground motion's data has been processed by GeoNet (2013) and is simulated in OpenSees for the full duration, as shown in Figure 56 and Figure 57. Unidirectional analysis is performed on shear core A and shear core B configurations for both of the September and February ground motions. Each ground motion is run separately on the undamaged building.

7.1 **Results**

7.1.1 September

PGC did not collapse during the September earthquake yet cracks in the walls were evident based on post-earthquake observations as discussed in section 2.5 and occupant accounts summarized in the Royal Commission Final Report (2012a). The total response of the building during the September ground motion, for both configurations A and B is summarized in Figure 58, which displays a comparison of the roof drift time histories. The maximum roof drift measured from the center of mass for both configurations produced during the simulation is 0.46% from configuration B compared with 0.41% for configuration A. Since the drift is measured from the center of mass, configuration B displays a larger roof drift than configuration A due to the twisting action seen in configuration A. These drifts are below the expected roof drift at flexural capacity 0.95% and 0.94% for configuration A and B, respectively (Table 17) indicating that the core does not fail in flexure during the

September ground motion, however as seen in the pushover analysis, it is not flexure that governs the response of PGC, but shear in the critical web of CWN at level 1.

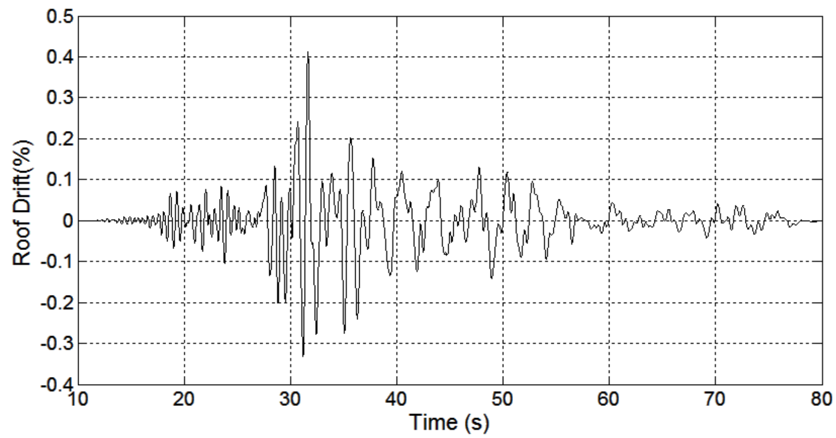

(a)

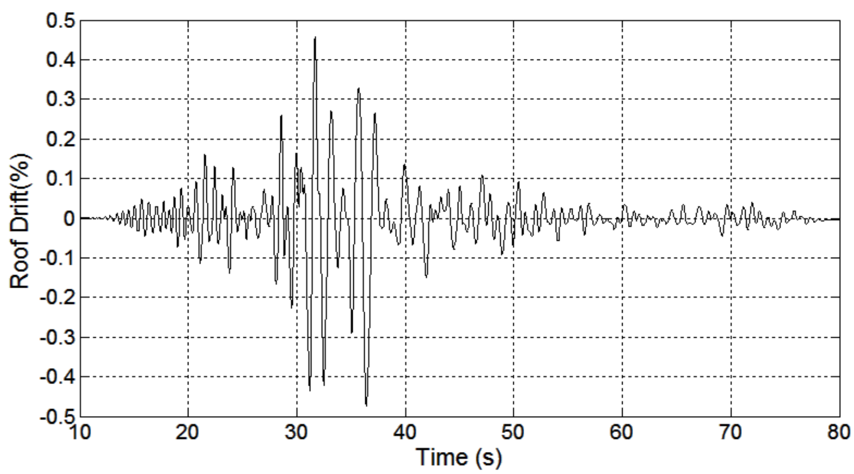

(b)

Figure 58: Roof drift time history for both configuration A (a) and configuration B (b)

The shear response for all three wall assemblages, CWN, CWC and CWS are displayed in Figure 59 and Figure 60 for configuration A and B, respectively. The magnitudes of both configurations A and B are similar, suggesting the eccentricity of the core contributed very little to the overall performance of the building (Figure 59 and Figure 60). The shear capacities displayed in the plots below, as determined in section 4.3.3.2 indicate that only the critical pier reaches capacity, as CWC and CWS do not. This is true for both configurations.

CWC nearly reaches its shear capacity at a few locations, but it is expected that the shear strength will not drop to zero instantly upon reaching capacity. CWS is below its capacity for the duration of the ground motion indicating shear failure does not occur.

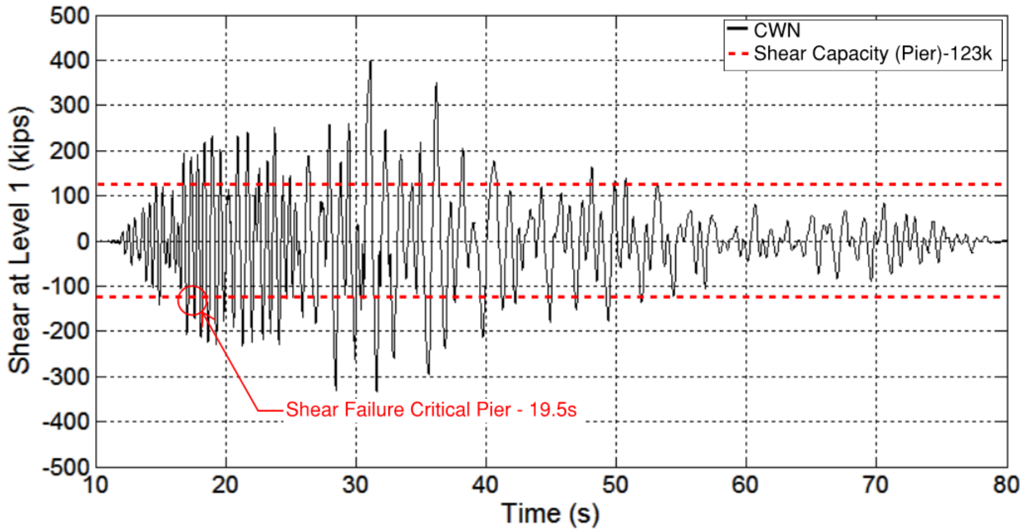

(a)

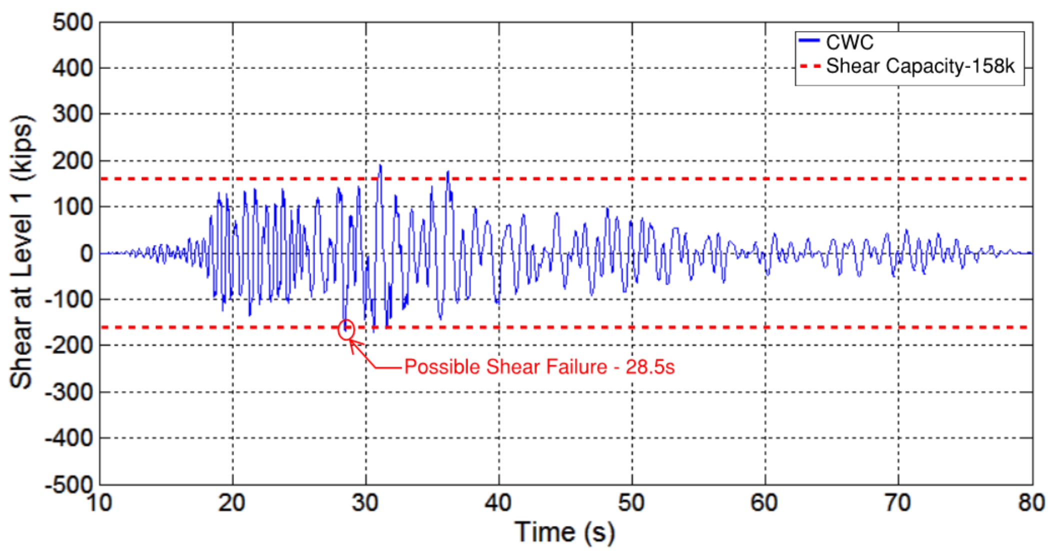

(b)

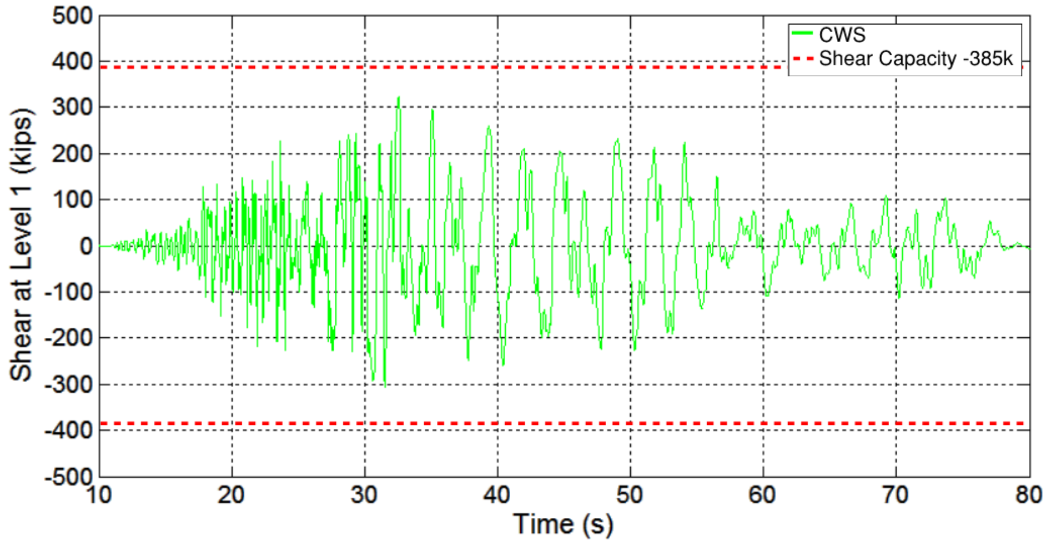

(c)

Figure 59: Configuration A - Shear time history for (a) CWN (b) CWC (c) CWS with the respective shear capacities indicated

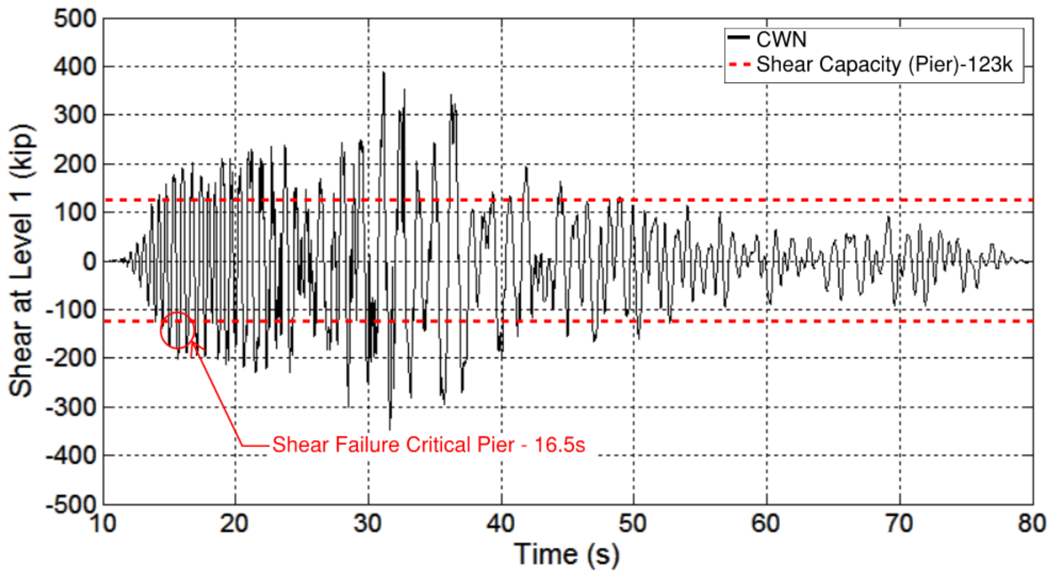

(a)

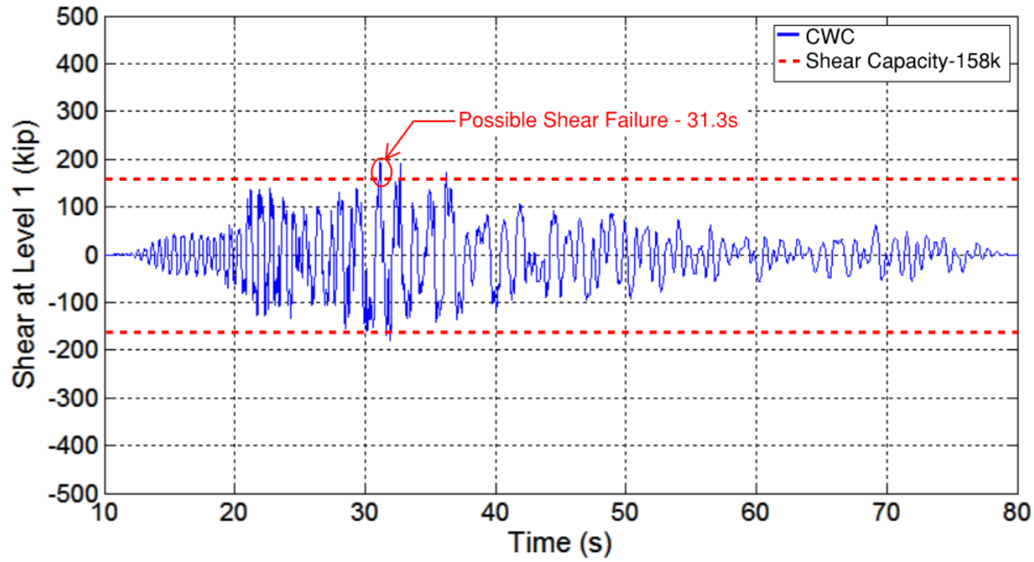

(b)

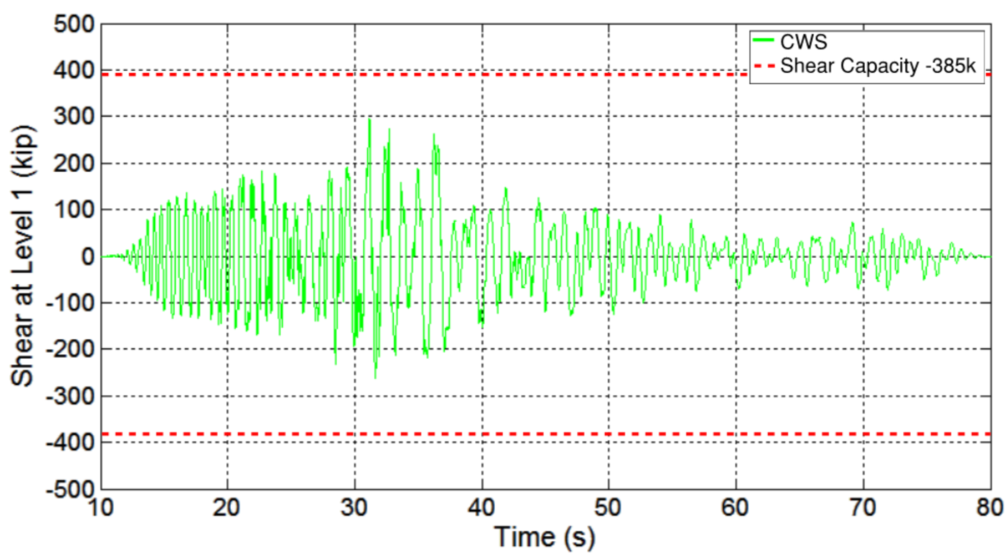

(c)

Figure 60: Configuration B - Shear time history for (a) CWN (b) CWC (c) CWS with the respective shear capacities indicated

Based on these findings, it is possible that upon failure of the pier within the web of CWN, CWC and CWS were able to resist the increased demand until the intense shaking ceased. CWN would still be resisting lateral load as well, as it is expected that the shear strength of CWN will not instantly drop to zero upon reaching capacity. Further investigation into the response of CWC and CWS would be necessary to confirm the redistribution of loads following failure of CWN.

Ignoring shear failure of CWN, and considering only the flexure response of the shear core, Figure 61 and Figure 62 below compare the moment-curvature response and curvature distributions up the height, for CWS and CWN at 31.2 seconds (timing of peak ground acceleration). Figure 61 (a) and (b) indicate that the flexural response of CWN and CWS are both below their curvature capacities. This is expected since there was no indication of flexural failure during the September earthquake. This is concurrent with the findings from the Beca technical report (2011a) as they determined that PGC did not fail in flexure during September. The relative flexural strength between CWN and CWS is as expected since CWN contains twice as much flange. CWN in Figure 61 (a) is at a curvature of roughly twice that of CWS indicating an eccentric loading, compared with Figure 61 (b) which shows CWN and CWS at roughly the same curvature indicating a more balanced response. The curvature distributions up the height of the building in Figure 62 reiterate the data shown in Figure 61, as CWN has the largest curvature at 31.2 sec. The concentration at level one is as expected since this is the location of the vertical strength discontinuity (refer to the observations section 2.5) and the expected failure location, this is more evident in the February earthquake described in the next section.

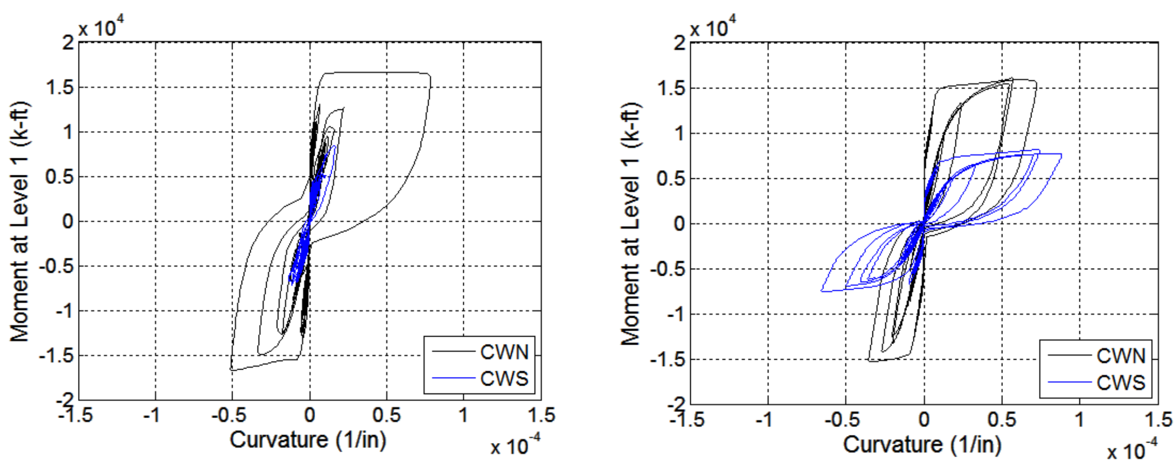

(a)

(b)

Figure 61: Moment curvature for CWN and CWS at level 1 during the September ground motion for (a) configuration A and (b) configuration B

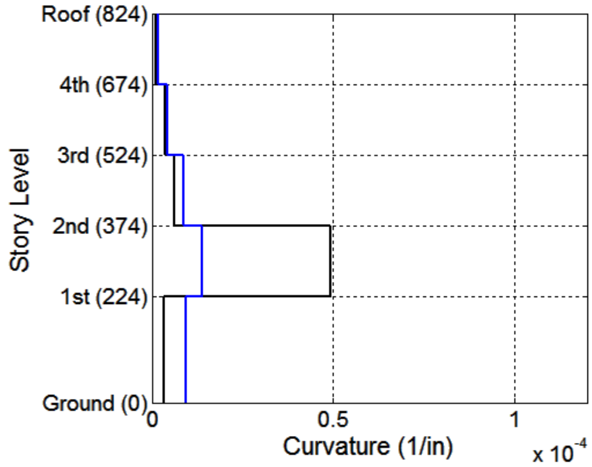

(a)

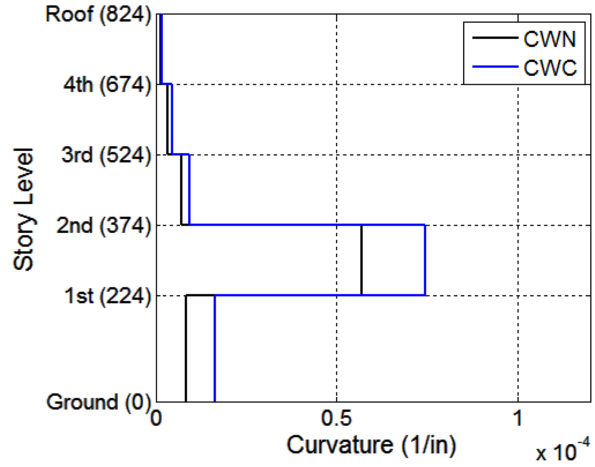

(b)

Figure 62: Curvature distribution up the height of CWN and CWS for (a) configuration A and (b) configuration B

7.1.2 February

Similar to the September earthquake, both configurations A and B for the February earthquake were governed by shear at level 1. The pier within the web of CWN reaches and surpasses its shear capacity at 11.5 seconds, this is only 0.5 seconds into the strong ground shaking (Figure 63 a). CWC and CWS also are expected to fail in shear prior to flexural failure for configuration A. At 11.5 seconds, when CWN is expected to fail in shear, CWC and CWS have not reached capacity and therefore it is possible that upon failure of CWN at such an early stage, CWC and CWS were able to withstand the increase in demand until further into the ground shaking when they are also expected to fail in shear. Their shear capacities are reached at 13 seconds and 13.8 seconds for CWC and CWS, respectively. The shear time history responses for CWN, CWC and CWS, with the expected shear failures indicated, are displayed below in Figure 63 and Figure 64, for configuration A and B, respectively. The responses for configurations A and B are very similar with the same trend as seen in the September motion. The demands increase for CWN from configuration A to B, but decrease for CWS. CWS does not reach its shear capacity prior to failing in flexure in configuration B. Following the failure of CWN and assuming full redistribution of lateral load from CWN, it is possible that CWS could have sustained the increase in load until flexural failure occurs at 16.9 seconds. This redistribution of shear after initial shear failure of CWN requires further study.

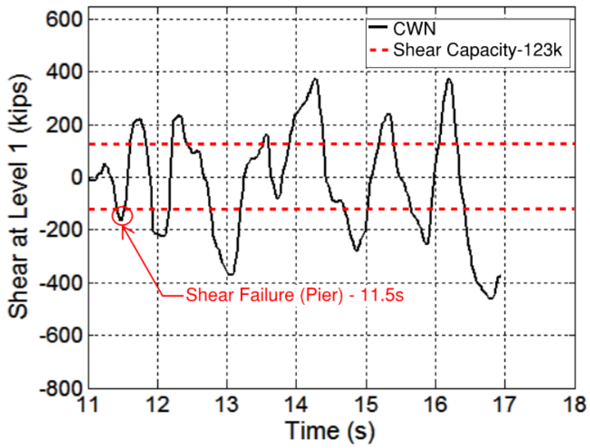

(a)

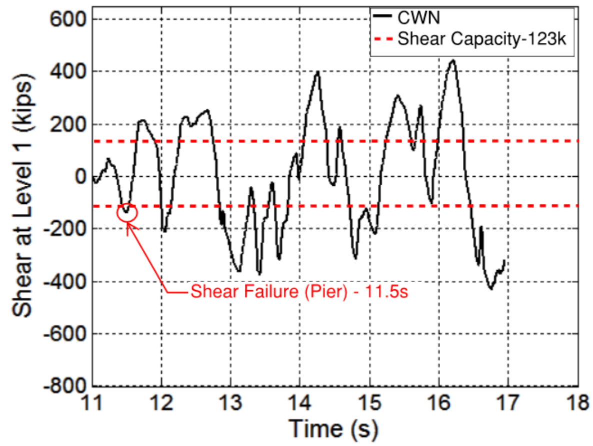

(a)

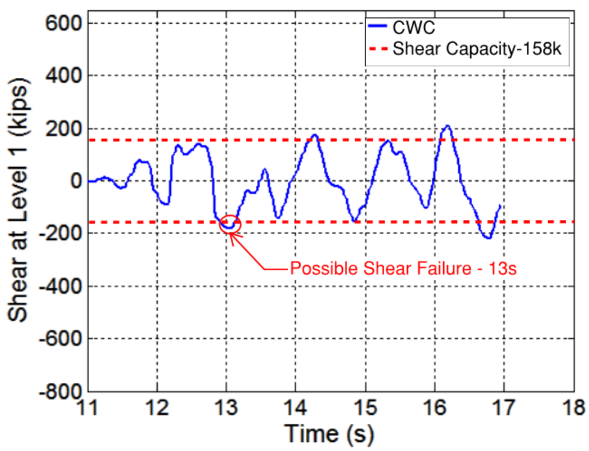

(b)

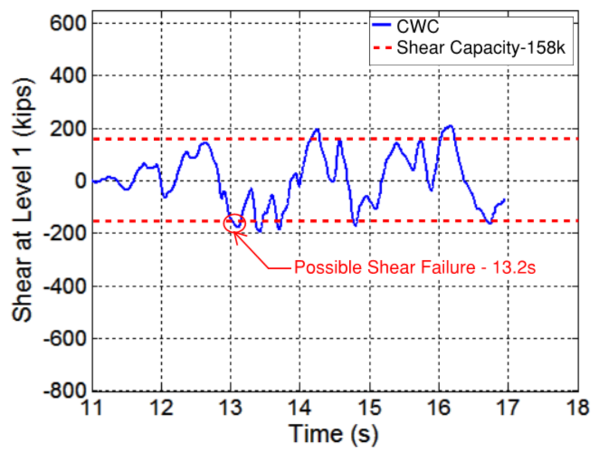

(b)

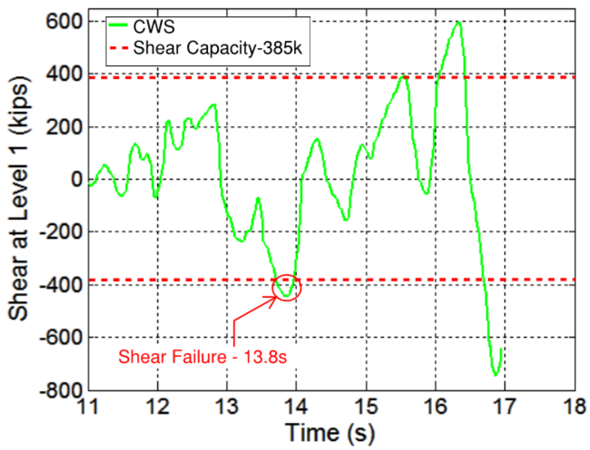

(c)

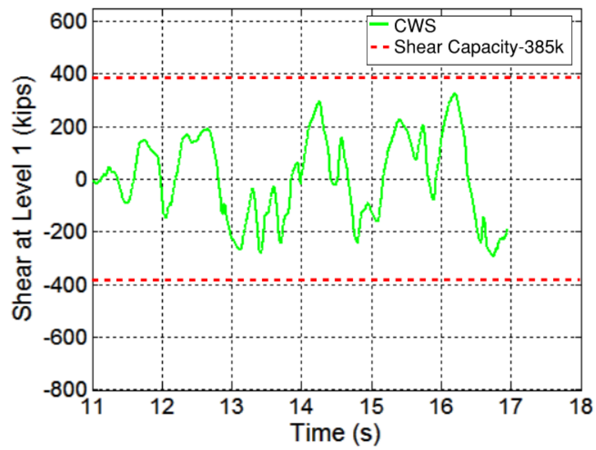

(c)

Figure 63: Configuration A - Shear time history of (a) CWN (b) CWC and (c) CWS with respective shear capacities indicated

Figure 64: Configuration B - Shear time history of (a) CWN (b) CWC and (c) CWS with respective shear capacities indicated

Considering the response as if shear failure does not govern, configuration A and configuration B indicate flexural failure at level 1 at 16.9 seconds, just prior to the PGA at 17.18 seconds. This is concurrent with the findings of Beca (2011a), which found that the governing failure mode was flexure within the shear core. Based on their investigation into an estimated timeline of collapse (section 3.1), the rupture of the tension reinforcement in the west wall flange occurred at a time of 17.15 seconds, a few hundredths of second before reaching the PGA and comparable to the 16.9 seconds determined from this analysis. Beca (2011a) did not indicate the location at which failure occurred first, other than that it was the west flange. Therefore it is unknown whether Beca determined that CWS or CWN would fail first and no comparison can be made with this analysis. Based on Figure 65, which displays the curvature distribution of CWN and CWS up the height of the building at the point of flexural failure, the west flange of CWS reaches failure before CWN. Flexural failure is determined by the use of the min-max material model utilizing strain limit states for both concrete in compression and steel in tension (as discussed in section 5.3.2). It is expected that bar rupture occurs at a curvature of 0.0004 (1/in) (based on sectional analysis shown in section 5.3.4), very comparable to the ultimate curvature for CWS at 0.0005 (1/in). Failure is occurring at level 1 which is evident from the large concentration of curvature at this level, similar to that seen in the September ground motion (Figure 62). This is as expected since the ground level is considerably stiffer than the stories above.

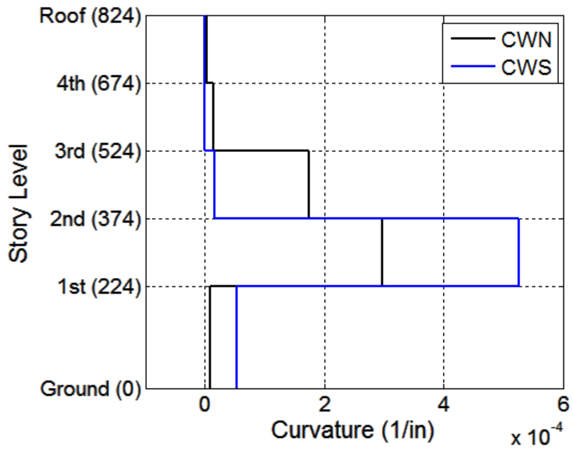

(a)

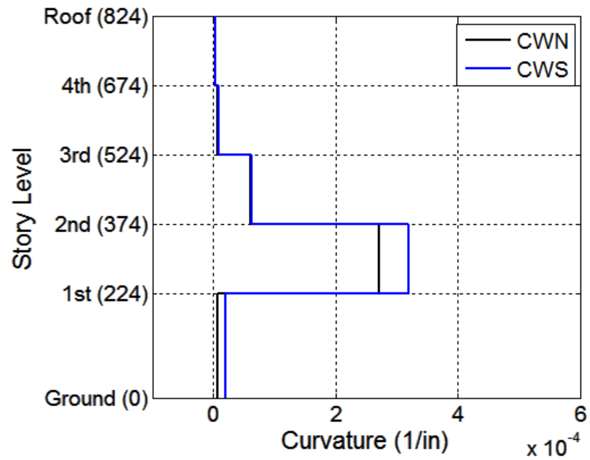

(b)

Figure 65: Curvature distribution up the height for CWN and CWS at the point at which flexural failure is indicated for (a) configuration A and (b) configuration B

Comparing Figure 62 with Figure 65, September curvatures and February curvatures, respectively, it is apparent that during the September ground motion the concentration of rotation at Level 1 did not occur to the same magnitude as during February. This would explain why flexural failure did not occur during September. Figure 66, shows the moment-curvature response of CWN and CWS. The flexural strength at curvature capacity for CWN and CWS compare well with the expected values from the sectional analysis in section 5.3.4.

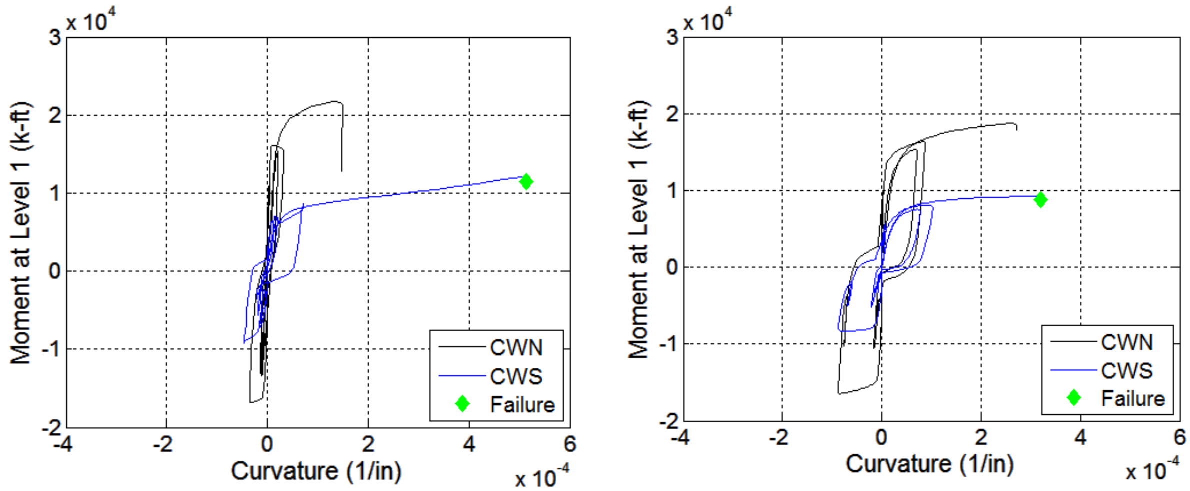

(a)

(b)

Figure 66: Moment-curvature of CWN and CWS up to failure for (a) configuration A and (b) configuration B

The roof drift recorded at flexural failure is 2% and 2.7% for configuration A and B, respectively as indicated in Figure 67. This is greater than the expected roof drift at flexural capacity, as recorded in the static pushover analysis of 0.94% (Table 17). The failure is occurring in the positive direction, which is towards the East. This supports the actual performance of PGC, as the building collapsed toward the East. Also indicated in Figure 67 is the estimated time of the governing failure mode, shear of the critical wall pier of CWN at 11.5 seconds. This corresponds to a roof drift of 0.2%. Although Figure 67 shows the predicted response of the core beyond initial shear failure up to the point of flexural failure at 16.9 sec, it should be emphasized that the analysis does not include redistribution of shear demands with degradation of shear resistance in the level 1 pier of CWN. Inclusion of such degradation will most certainly modify the predicted response.

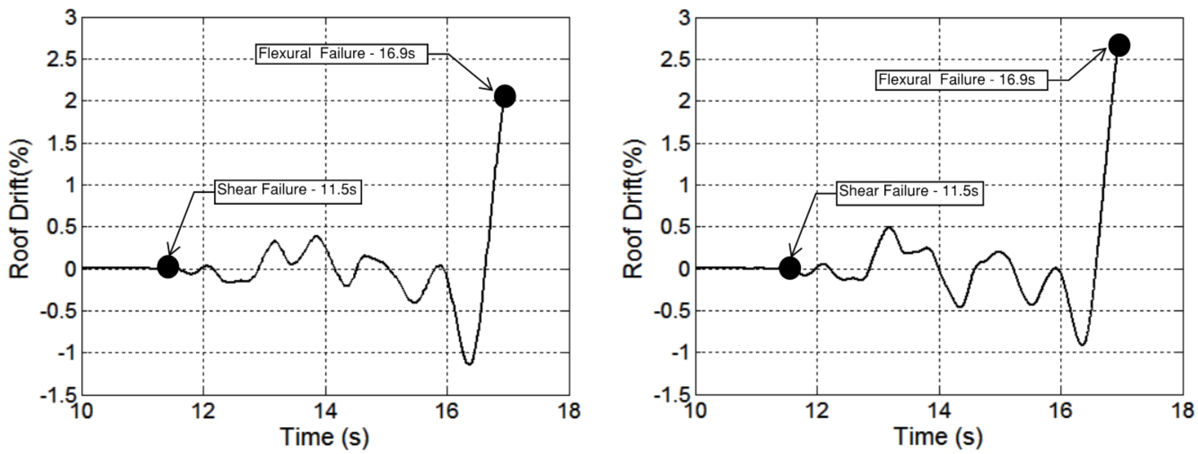

(a) (b)

Figure 67: Roof center of mass displacement time history indicating initial shear failure and flexural failure for (a) configuration A and (b) configuration B

7.2 Exterior Gravity Frame

The exterior gravity frame along gridline h (Figure 3) is susceptible to a joint shear failure mechanism, as indicated previously in section 4.3.2. Utilizing the rigid diaphragm assumption, the displacement demand from the February ground motion is determined at the exterior gravity frame for both configuration A and B models for the February and September ground motions. Based on the February ground motion, it appears from comparing Figure 68 (a) and (b) that there is minimal influence from the location of the core on the expected drift at the exterior gravity frame. The largest difference from the roof center of mass and the frame along gridline h is between 12 and 16 seconds, but as the model nears flexural failure (16.9 seconds) the difference between the center of mass and the frame nears zero. This is as expected for as the walls begin to soften, the center of rigidity will move closer to the center of mass diminishing the eccentricity. There is no difference between the roof drift at the center of mass and at the frame for configuration B (Figure 68 (b)), as expected.

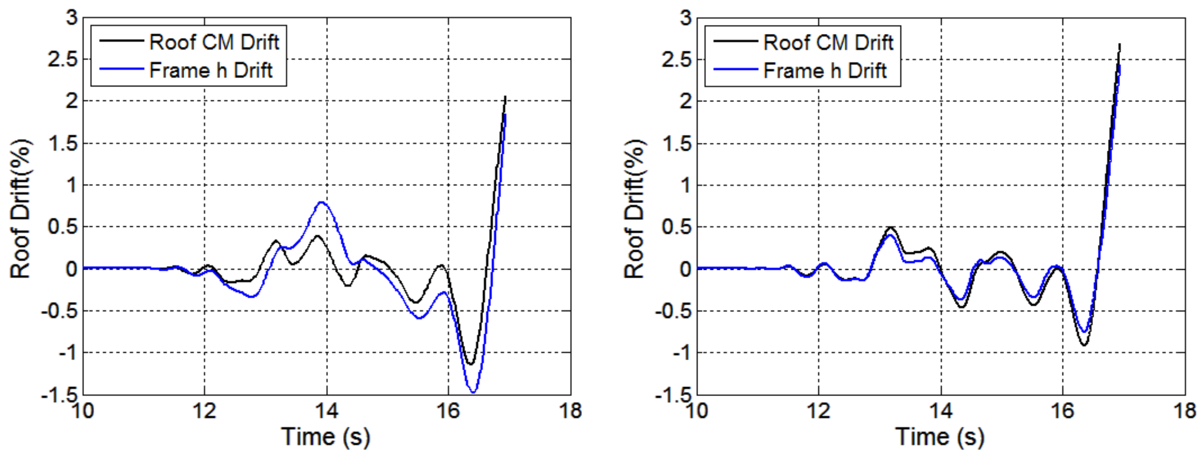

(a) (b)

Figure 68: Roof drift time history at the center of mass and the projected drift at the frame along gridline h for both (a) configuration A and (b) configuration B

From the sectional analysis of the beam-column joints in section 4.3.2, it is determined that the beam-column joints were the most critical element of the exterior gravity frame, since the beams and columns were not expected to reach yield prior to the joint failing in shear. According to Hassan (2011) this is considered joint failure in pure shear. The rotation capacity of the RC gravity frame has contributions from the columns, the beams, bar slip and the joint. From past research (Hassan 2011) the joint contributes majority of the rotation capacity, upwards of 50-60%, this is a large reason why it is important to model the joint rotation during analysis and not assume rigid joints. Using an approach described by Hassan (2011) a joint shear strain at the joint shear capacity is determined with contributions from the joint and columns only. Contribution from the beams is ignored considering they are nearly rigid. This is reflected by θ_b in equation 10 becoming zero. The column rotation is based on the shear demand at joint failure. By manipulating equation 3 to determine a column shear demand and using an effective stiffness, which includes bar slip based on the approach from Elwood and Eberhand (2006), the rotation contribution from the column was determined. The joint shear strain is determined from a linear relationship of the secant joint shear modulus, G_{03} (equation 11) and the maximum expected shear stress, τ_j (the process for determining the maximum shear stress is discussed in section 4.3.2). The other parameters in equation 11 areα_j, the joint aspect ratio (h_{beam}/h_{column}) and G_c, the elastic shear modulus.

$$\theta_{Tj} = \theta_j + \theta_c + \theta_{\boldsymbol{b}} \tag{10}$$

$$G_{03} = \left(0.14 - \frac{3}{80} * \alpha_j\right) * G_c \tag{11}$$

The expected drifts at shear failure of the joint, considering the rotation of the column and an upper and lower bound capacity of the joint (section 4.3.2) are shown in Figure 69 and Figure 70 for the February and September ground motions respectively.

All of the interstory drift ratios are beyond the upper bound drift capacity (section 4.3.2) for the February ground motion as indicated in Figure 69. Both configurations A and B are similar: configuration A exceeds the joint shear capacity at approximately 16.4 seconds during a cycle to the west whereas configuration B exceeds the limit at 16.7 seconds during the final cycle to the east. The timing of this failure, according to this analysis is prior to flexural failure in the flanges, but after the governing shear failure mechanism. Figure 70 shows the same response as in Figure 69, but for the September ground motion. As expected, joint shear failure does not occur, as the expected drift demand does not exceed the joint drift capacity limits at any point throughout the ground motion. Shear failure is still expected to occur in the critical pier during this ground motion as indicated previously.

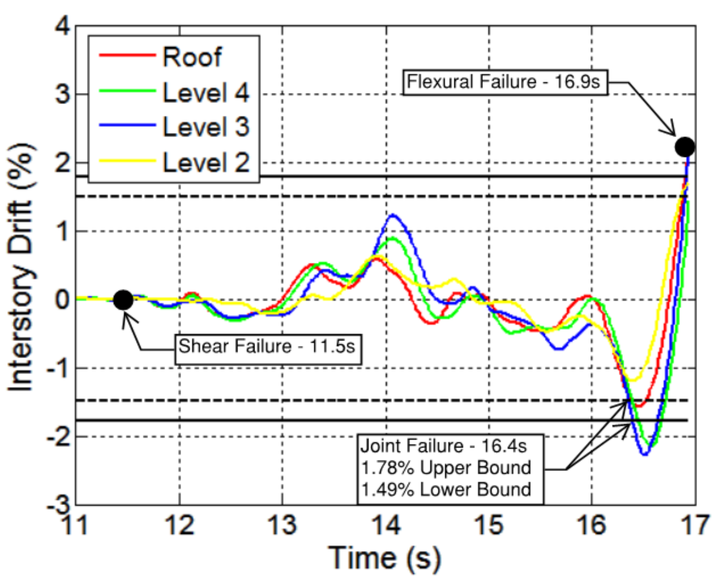

(a)

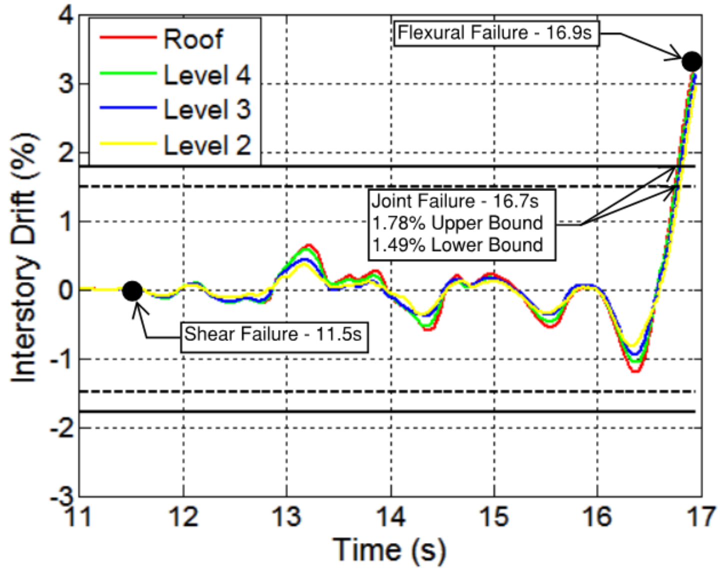

(b)

Figure 69: Interstory drift of the exterior gravity frame for each level under the February ground motion showing expected drift at joint shear failure for (a) configuration A and (b) configuration B. Initial Shear failure and flexural failure are also indicated.

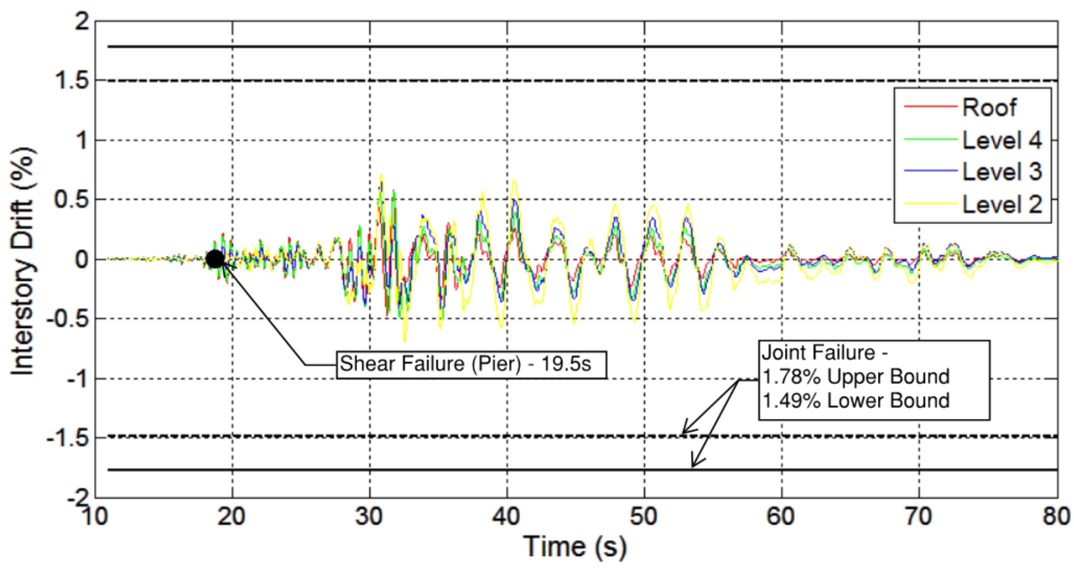

(a)

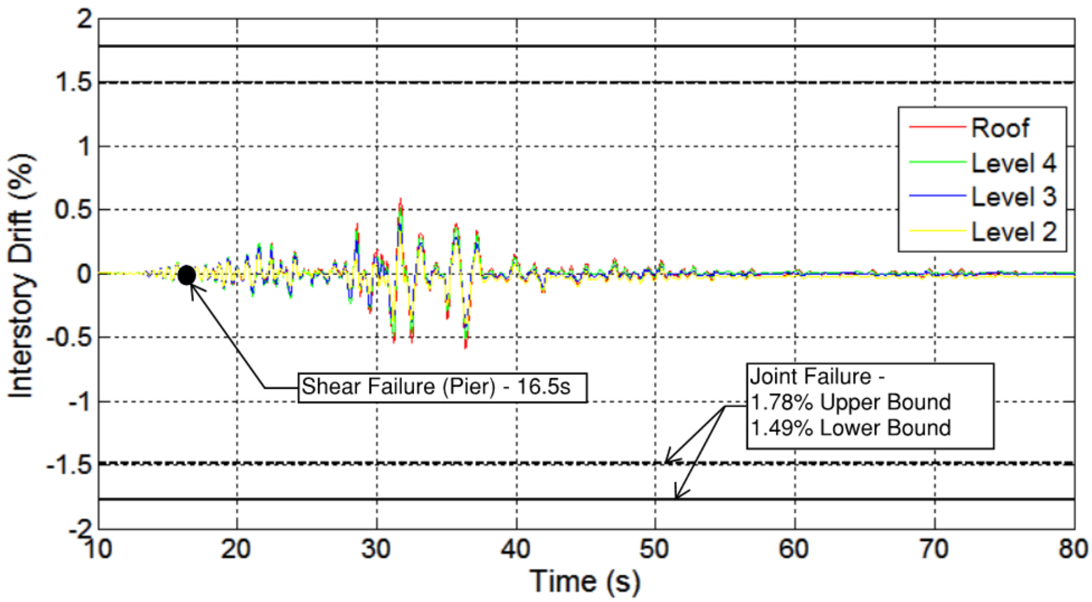

(b)

Figure 70: Interstory drift of the exterior gravity frame for each level under the September ground motion showing expected drift at joint shear failure for (a) configuration A and (b) configuration B. Initial shear failure of the critical pier as indicated.

Chapter 8 **Concluding Remarks**

Based on the post collapse photos, and strength estimates it was speculated that the web wall of CWN was shear critical, resulting in a brittle shear failure prior to reaching the flexural capacity of the walls. As discussed in section 2.5, the web segment of CWN at level 2 between the two window openings contained large diagonal cracks and the wall below (between level 1 and level 2) had catastrophically collapsed. This is assumed as the slab of level 2 is on top of level 1 (Figure 12 and Figure 14). The conclusions gathered from the static and dynamic analyses support all of these findings as the results indicate that shear failure of the critical wall pier in CWN governed over flexural failure.

During the September earthquake at a time of 19.5 seconds (Figure 59a), the critical pier of CWN is expected to have reached its calculated shear strength during the September earthquake at a time of 19.5 seconds Given the observed response of PGC during September and that only shear cracks were observed, it appears as though the predicted response of the analytical model is conservative in predicted shear failure.. Possible shear failure of the critical pier without total collapse could occur upon adequate strength to redistribute the load. Given it is expected that the shear strength of CWN will not drop to zero immediately upon reaching its capacity and that CWS does not reach capacity throughout the ground motion (Figure 59c), it is possible that CWS could resist more load, assuming the slab is adequate to redistribute load from CWN to CWS shear failure during September did not cause the building to collapse The actual sequence following shear failure of CWN is unclear as it is beyond the scope of these analyses to capture load redistribution within the core given the capability of the models used. Further investigation into the response of the other elements within the core is necessary to determine a more accurate sequence of failure after the initial shear failure occurs in CWN.

Shear failure of the pier is expected to occur where the demand in the wall assemblage CWN exceeds the shear capacity calculated in section 4.3.3.2. Three separate approaches were taken to determine shear capacity, ACI-318, CSA A23.3 and Response-2000, all of which were well below the expected demand. \The dynamic analysis for the February earthquake (section 7.2.2) supports the same findings, as the wall pier of CWN fails in shear prior to reaching the core wall flexural capacity. This is evident in Figure 69, which indicates the time where both shear failure is expected to occur at 11.5 seconds and where flexural rupture is expected to occur at 16.9 seconds. CWN fails in shear less than a second into the strong ground shaking, but it is expected that the shear strength will not drop to zero instantaneously and based on the response of the other walls, it is possible that CWS and CWC along with the remaining capacity of CWN were able to withstand the demand, prolonging the failure until CWC and CWS reach their shear capacities at 13 seconds and 13.8 seconds, respectively. This redistribution of shear after initial shear failure of CWN requires further study.

The exterior gravity frame is another critical piece of the structural system. Using the non-linear time history analysis and the rigid diaphragm assumption, the expected displacement demand on the exterior frame was determined. Utilizing past research by Hassan (2011) a drift capacity for the shear critical beam-column joints was determined and compared with the interstory drift time histories. Under the February loading the joints failed in shear at a drift capacity between 1.5% and 1.8%. The September ground motion resulted in lower displacement demand on the exterior gravity frame with all the drifts below the failure threshold.

Configuration A and B, with and without eccentricity, respectively, were both discussed and studied throughout the previous sections. The static pushover results compared the relative displacements of the exterior frame with the displacements at the center of mass, indicating a small difference in displacement for configuration A, but not significant enough to conclude any influence. In the dynamic analysis, both configurations showed similar responses, failing in similar ways indicating that regardless of the position of the core, the analysis would have predicted failure during the September and February earthquakes. It is evident that configuration B altered the performance of the building, as seen in the response histories shown in the dynamic analysis. It is also evident that by only altering the location of the core does not influence the building enough, to prevent collapse or prolong the collapse, as both shear failure and flexural failure occurred at the same time for both models, respectively. Therefore, concluding that the location of the core did not contribute in the collapse of PGC.

8.1 **Future Research**

The following topics of interest were beyond the scope of this thesis and will require further investigation:

- Parametric study of off center, lightly reinforced shear wall buildings, investigating the influence of the location of the core walls on the performance of the building. This was attempted by looking at both configuration A and configuration B, but the other vulnerabilities within the models outweighed the slight difference in response from one model to the other.
- The influence of torsional irregularity on drift demands for perimeter gravity frames of shear wall buildings.
- Further study of the shortcomings from modeling non-planar walls at their geometric centroid instead of their shear center or center of rotation.
- Investigating the sequence of failure after initial shear failure has occurred in a single wall of a core wall system.
- Biaxial demand on thin, lightly reinforced core walls.

References

ACI (2008). *Building Code Requirements for Structural Concrete (ACI 318-08) and Commentary,* Farmington Hills, MI.

ACI Working Document (2013). Unpublished.

Adebar, P. and Lorzadeh, A. (2012). "Compression Failure of Thin Concrete Walls," *15th World Conference on Earthquake Engineering,* Lisbon.

Applied Technology Council (ATC). (2010). "Program Plan for the Development of Collapse Assessment and Mitigation Strategies for Existing Reinforced Concrete Building." *ATC-76-5 Report*, prepared by the Applied Technology Council for the US Department of Commerce, Building and Fire Research Laboratory and National Institute of Standards and Technology (NIST), Redwood City, California.American Concrete Institute (ACI) (1963). *Building Code Requirements for Structural Concrete (ACI 318-63) and Commentary,* Farmington Hills, MI

American Society of Civil Engineers (ASCE). (2006). *Seismic Rehabilitation of Existing Buildings*, ASCE Standard ASCE/SEI 41-06, Reston, Virginia.

ASCE (2007). *ASCE/SEI 41 – Supplement 1*, American Society of Civil Engineers/ Structural Engineering Institute, Reston, Virginia.

Beca Carter Hollings and Ferner Ltd. (Beca). (2011a). *Investigation into the Collapse of the Pyne Gould Corporation Building on 22nd February 2011*, Christchurch, New Zealand. <http://www.dbh.govt.nz/UserFiles/File/Reports/quake-pyne-gould-corp-investigation-report.pdf>

Beca (2011b). *Investigation into the Collapse of the Pyne Gould Corporation Building on 22nd February 2011- Appendix*, Christchurch, New Zealand.

Bentz, E. C. (2000). “Section Analysis of Reinforced Concrete Members,” thesis, presented to the University of Toronto at Toronto, Ontario, in partial fulfillment of the requirements for the degree of Doctor of Philosophy.

Canadian Standards Association (CSA) (2004). *Design of Concrete Structures* (A23.3-04), Mississauga, ON.

Canterbury Earthquake Recovery Authority (CERA). (2013). “CBD Cordon Redection.” *CERA Canterbury Earthquake Recovery Authority*, <http://cera.govt.nz/maps/cordon-reduction> (January, 2013).

Celik, O.C., Ellingwood, B.R. (2008). “Modeling Beam-Column Joints in Fragility Assessment of Gravity Load Designed Reinforced Concrete Frames.” *Journal of Earthquake Engineering*, 12(3), 357-381.

Chopra, A. K. (2001). *Dynamics of Structures: Theory and Applications to Earthquake Engineering*, 2nd Ed., Prentice Hall, Upper Saddle River, NJ.

Coleman, J. and Spacone, E. (2001). “Localization Issues in Force-Based Frame Elements,” *Journal of Structural Engineering*, 127, 1257-1265.

Computer and Structures, Inc. (CSI) (2013). *Structural and Earthquake Engineering Software*, <http://www.csiamerica.com>

Department of Building and Housing Expert Panel. (2011). “Pyne Gould Corporation Building.” *Structural Performance of Christchurch CBD Buildings in the 22 February 2011 Aftershock – Stage 1 Expert Panel Report*, 42-31. <http://www.dbh.govt.nz/UserFiles/File/Reports/quake-stage1-expert-panel-report.pdf>

Department of Building and Housing Expert Panel. (2012). “Pyne Gould Corporation Building.” *Structural Performance of Christchurch CBD Buildings in the 22 February 2011 Aftershock –Expert Panel Report*, 54-62. <http://www.dbh.govt.nz/UserFiles/File/Reports/quake-final-expert-panel-report.pdf>

Department of Building and Housing (DBH). (2013). “Canterbury earthquake: Technical investigation.” *Ministry of Business, Innovation & Employment*, <http://www.dbh.govt.nz/canterbury-earthquake-technical-investigation> (November, 2011).

Earthquake Engineering Research Institute (EERI). (2011). “Learning from Earthquakes.” *EERI Special Earthquake Report*, Oakland, California.

Elwood, K. J., Eberhard, M. O., (2006). “Effective Stiffness of Reinforced Concrete Columns.” *PEER Research Digest*, 2006-1, 1-5.

Federal Emergency Management Agency (FEMA). (2006). *Techniques for Seismic Rehabilitation of Existing Buildings (FEMA 547)*, Washington, D.C.

Fischinger, M., Vidic, T., Selih, J., Fajfar, P., Zhang, H.Y., and Damjanic, F.B. (1990). “Validation of a Macroscopic Model for Cyclic Response Prediction of RC Walls,” *Computer-Aided Analysis and Design of Concrete Structures.”* Pineridge Press, Swansea, Wales, 1131-1142.

Fischinger, M., Vidic, T., and Fajfar, P. (1992). “Nonlinear Seismic Analysis of Structural Walls Using Multiple-Vertical-Line-Element Model.” *Nonlinear Seismic Analysis of RC Buildings,* Elsevier Science Publishers Ltd., London and New York, 191-202.

GeoNet. (2013). “Historical Earthquakes.” *GeoNet,* <http://info.geonet.org.nz/display/quake/Historical+Earthquakes> (December, 2012).

Ghosh, S.K., Markevicius, V.P. (1991). “Design of Earthquake Resistant Shearwalls to Prevent Shear Failure.” Proceeding of International Workshop on Concrete Shear in Earthquakes, (1991), Houston, TX.

Hassan, W. M., (2011). “Analytical and Experimental Assessment of Seismic Vulnerability of Beam-Column Joints without Transverse Reinforcement in Concrete Buildings,” thesis, presented to the University of California at Berkeley, CA, in partial fulfillment of the requirements for the degree of Doctor of Philosophy.

Heo, Y., Zhang, G., Kunnath, S., Xiao, Y. (2009). “Modeling Cyclic Behavior of Reinforcing Steel: Relevance in Seismic Response Analysis of Reinforced Concrete Structures.” *Key Engineering Materials*, 400-402, 301-309.

Hyland Consultants. (2011). *Pyne Gould Corporation Building Site Examination and Materials Tests*, Auckland, New Zealand. <http://www.dbh.govt.nz/UserFiles/File/Reports/quake-pgc-site-and-materials-report.pdf>

Layssi, H., Cook, W. D. andMitchell, D. (2012). “Seismic Response and CFRP Retrofit of Poorly Detailed Shear Walls,” *Journal of Composites for Construction*, 16, 332-339.

Liel, A. B., (2008) “Assessing the Collapse Risk of California’s Existing Reinforced Concrete Frame Structures: Metrics for Seismic Safety Decisions,” thesis, presented to Stanford University, CA, in partial fulfillment of the requirements for the degree of Doctor of Philosophy.

Lowes, L.N., Lehman, D., Birely, A.C., Kuchma, D., Marley and K. Hart, C.R. (2011). “Behavior, Analysis, and Desing of Complex Wall Systems: Planar Wall Test Program Summary Document, “http://nees.org/resources/3677 (September 2013).

Mander, J. B., Panthaki, F. D., and Kasalanati, A. (1994). “Low-Cycle Fatigue Behavior of Reinforcing Steel.” *Journal of Materials in Civil Engineering*, 6(4), 453-468.

Moehle, J. P., Ghodsi, T., Hooper, J. D., Fields, D. C. and Gedhada, R. (2011). “Seismic Design of Cast-in-Place Concrete Special Structural Walls and Coupling Beams: A Guide for Practicing Engineers.” *National Earthquake Hazard Reduction Program (NEHRP) Seismic Design Technical Brief No. 6.*

Nicholls, P. (2013). *Christchurch Quake Map*, <http://www.christchurchquakemap.co.nz/> (September, 2012).

NIST GCR 10-917-8, (2010) “Evaluation of the FEMA P-695 Methodology for Quantification of Building Seismic Performance Factors,” National Institute of Standards and Technology, Gaithersburg, MD, November 2011.

Oesterle, R. G., Fiorato, A. E., Johal, L. S., Carpenter, J. E., Russell, H. G. and Corely, W. G. (1976). “Earthquake Resistant Structural Walls – Tests of Isolated Walls.” *National Science Foundation*.

Orakcal, K., Massone, L.M., and Wallace, J.W. (2007). “Analytical Modeling of Reinforced Concrete Walls for Predicting Flexural and Coupled-Shear-Flexural Responses.” *Pacific Earthquake Engineering Research Center*.

Orakcal, K., Wallace, J.W. and Conte, J.P. (2004). “Flexural Modeling of Reinforced Concrete Walls – Model Attributes.” *ACI Structural Journal*, 688-698.

Pacific Earthquake Engineering Research (PEER). (2013). Open System for Earthquake Engineering Simulation (*OpensSees)*. <http//opensees.berkeley.edu>

Paulay, T., and Priestley, M.J.N. (1992). *Seismic Design of Reinforced Concrete and Masonry Buildings*, John Wiley and Sons Inc., New York.

Pegon, P., Plumier, C., Pinto, A., Molina, J., Gonzalez, P., Tognoli, P., and Hubert, O. (2000). “U-Shaped Walls: Quasi-Static Test in the X-direction – Test Report.” *JRC Special Publication*.

Peng, X., and Wong, Y. (2011). “Behavior of Reinforced Concrete Walls Subjected to Monotonic Pure Torsion – An Experimental Study,” *Engineering Structures*, 33(2011), 2495-2508.

Pristley, M.J.N., Calvi, G.M., and Kowalsky, M.J. (2007). *Displacement-Based Seismic Design of Structures*. Istituto Universitario di Studi Superiori di Pavai (IUSS Press), Pavia, Italy.

Pugh, J. S. (2012). Numerical simulation of walls and seismic design recommendations for walled buildings. (Order No. 3552847, University of Washington). ProQuest Dissertations and Theses, , 449. Retrieved from http://search.proquest.com.ezproxy.library.ubc.ca/docview/1312511080?accountid=14656. (1312511080).

“Photos: Before and After the Christchurch Earthquake.” (2012). http://www.stuff.co.nz/the-press/news/christchurch-earthquake-2011/12-51/photos/6422210/Photos-Before-and-after-the-Christchurch-earthquake

Royal Commission. (2011). “Royal Commission of Inquiry into Building Failure Caused by Canterbury Earthquakes.” *Terms of Reference*, <http://canterbury.royalcommission.govt.nz> (August, 2013).

Royal Commission. (2012a). *The Canterbury Earthquakes Royal Commission - Final Report*. <http://canterbury.royalcommission.govt.nz> (December, 2012).

Royal Commission. (2012b). “The Performance of Christchurch CBD Buildings.” *The Canterbury Earthquakes Royal Commission - Final Report Volume 2*, Christchurch, NZ., 12-49.

Sezen, H. (2000). “Seismic Behavior and Modeling of Reinforced Concrete Building Columns,” thesis, presented to the University of California Berkeley, CA, in partial fulfillment of the requirements for the degree of Doctor of Philosophy.

Terzic, V. (2011). “Force-based Element vs. Displacement-based Element.” *OpenSees Webinar*, December 2011.

Vulcano, A., Bertero, V.V. and Colotti, V. (1988). “Analytical Modeling of RC Structural Walls.” *Proceedings, 9th World Conference on Earthquake Engineering*, Tokyo-Kyoto, Japan, 6, 41-46.

Wallace, J. (2013). “ RC Structural Wall Modeling for Collapse Assessment Utilizing Monte Carlo Simulations,” *Collapse Workshop*.

Zhu, L., Elwood, K. J. and Haukaas, T. (2007). “Classification and Seismic Safety Evaluation of Existing Reinforced Concrete Columns.” *Journal of Structural Engineering*, 1316-1330.

Appendices

Appendix A

A.1 Structural Drawings

Original 1964 structural drawings (Courtesy of the Beca Technical Report (Beca 2011b))

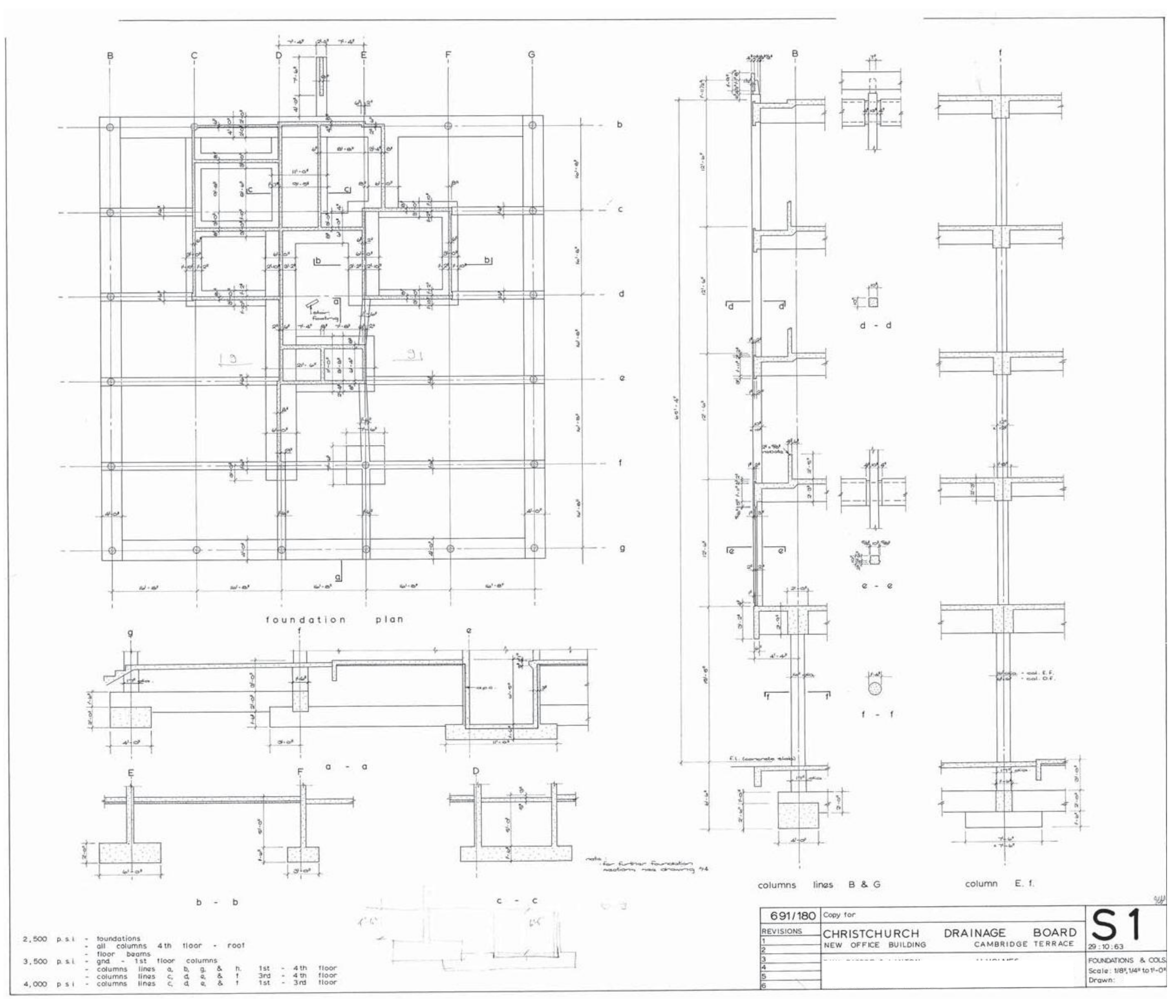

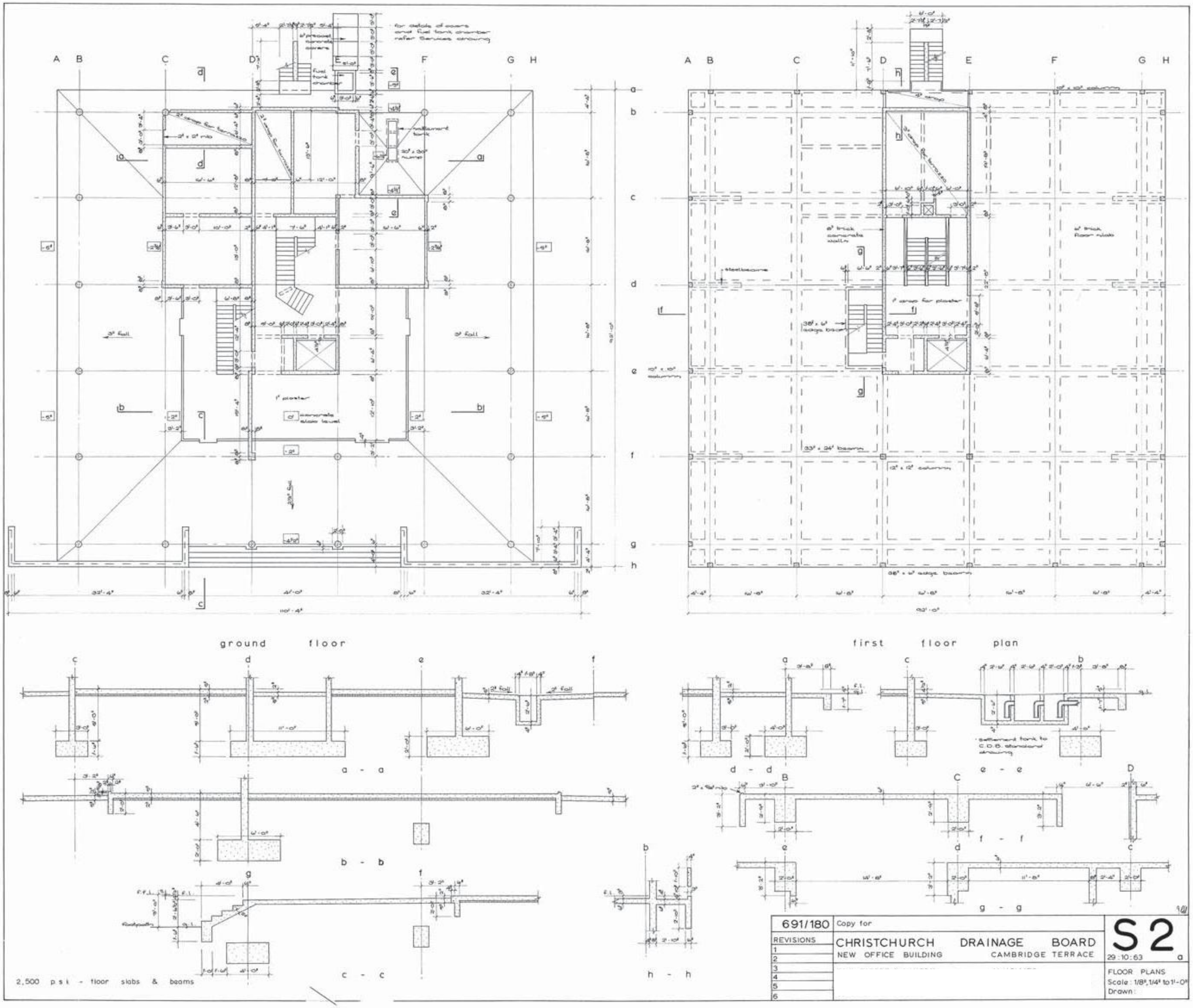
ground floor
first floor plan
a - a
d - d
e - e
b - b
f - f
c - c
h - h
g - g
2,500 p.s.i. - floor slabs & beams
691/180
Copy for
REVISIONS
CHRISTCHURCH DRAINAGE BOARD
NEW OFFICE BUILDING
CAMBRIDGE TERRACE
S2
29:10:63
a
FLOOR PLANS
Scale: 1/8", 1/4" to 1'-0"
Drawn:

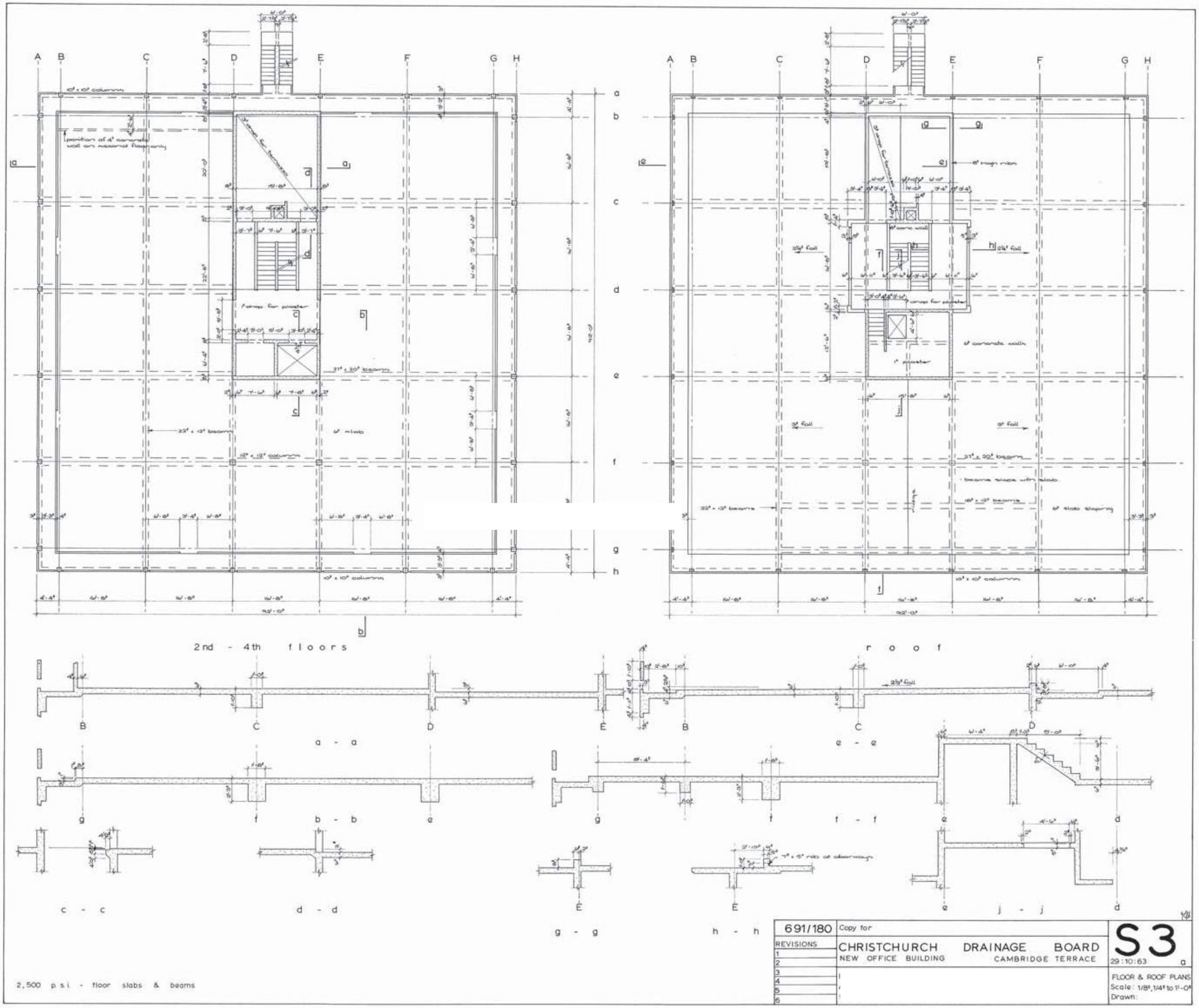
2nd - 4th floors
roof
a - a
e - e
b - b
f - f
c - c
d - d
g - g
h - h
j - j
10" x 10" column
22" x 12" beam
6" slab
12" x 12" column
27" x 20" beam
ramp for plaster
6" concrete walls
8" high nib
3" fall
2½" fall
beams slope with slab
18" x 12" beams
6" slab sloping
92'-0"
691/180
Copy for
REVISIONS
CHRISTCHURCH DRAINAGE BOARD
NEW OFFICE BUILDING
CAMBRIDGE TERRACE
S3
29:10:63
FLOOR & ROOF PLANS
Scale: 1/8", 1/4" to 1'-0"
Drawn:
2,500 p.s.i. - floor slabs & beams

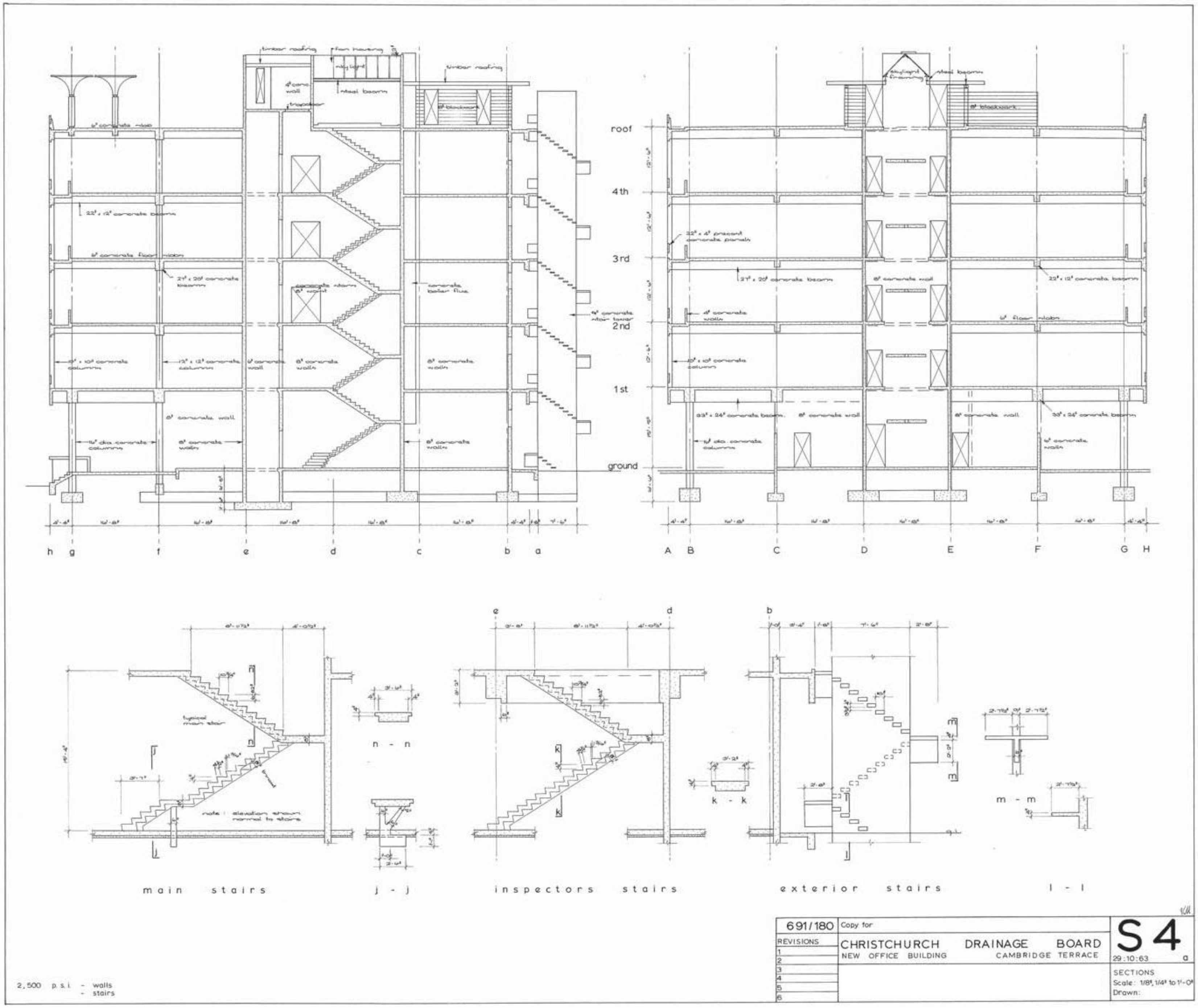
roof
4th
3rd
2nd
1st
ground
h g f e d c b a
A B C D E F G H
main stairs
j - j
inspectors stairs
exterior stairs
l - l
n - n
k - k
m - m
691/180
Copy for
REVISIONS
CHRISTCHURCH DRAINAGE BOARD
NEW OFFICE BUILDING
CAMBRIDGE TERRACE
S4
29:10:63
a
SECTIONS
Scale: 1/8", 1/4" to 1'-0"
Drawn:
2,500 p.s.i. - walls
- stairs

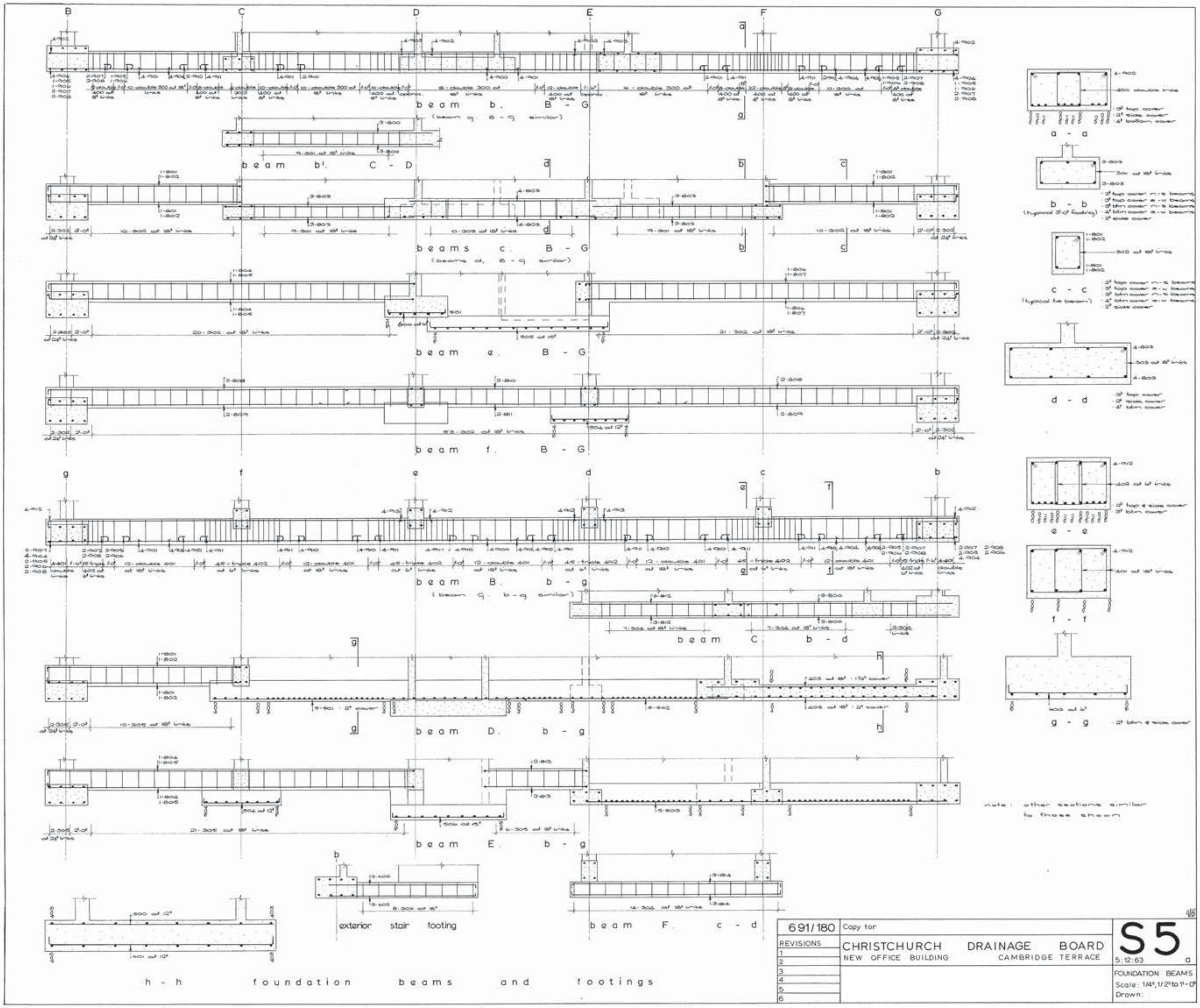
beam b. B - G
(beam g. B - G similar)
beam b'. C - D
beams c. B - G
(beams d, B - G similar)
beam e. B - G
beam f. B - G
beam B. b - g
(beam G. b - g similar)
beam C. b - d
beam D. b - g
beam E. b - g
beam F. c - d
exterior stair footing
a - a
b - b
c - c
d - d
e - e
f - f
g - g
h - h
note: other sections similar to those shown
foundation beams and footings
691/180
Copy for
REVISIONS
CHRISTCHURCH DRAINAGE BOARD
NEW OFFICE BUILDING
CAMBRIDGE TERRACE
S5
5:12:63
a
FOUNDATION BEAMS
Drawn:

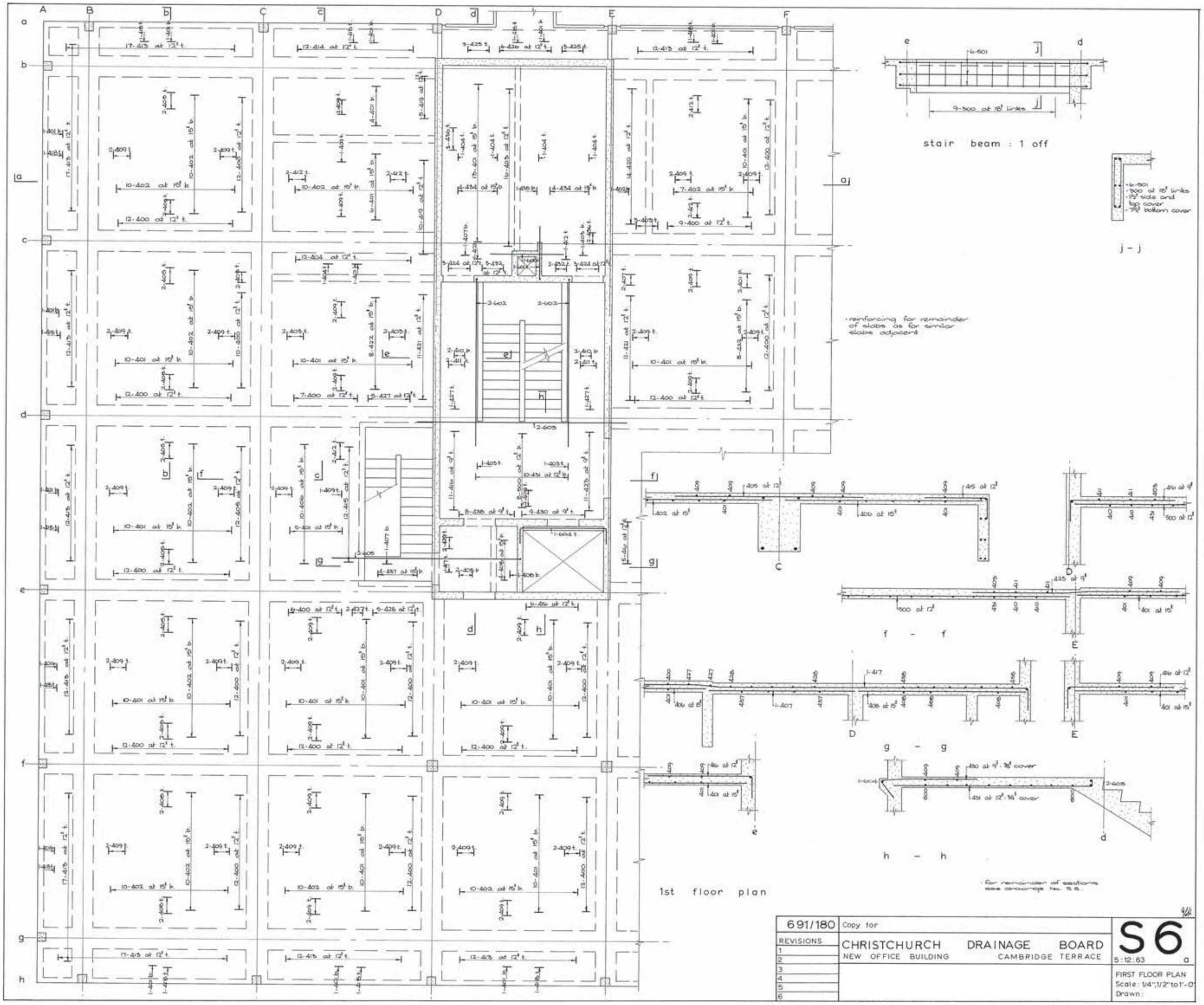
stair beam : 1 off
j - j
reinforcing for remainder of slabs as for similar slabs adjacent
f - f
g - g
h - h
1st floor plan
for remainder of sections see drawings No. S 8.
691/180
Copy for
REVISIONS
CHRISTCHURCH DRAINAGE BOARD
NEW OFFICE BUILDING
CAMBRIDGE TERRACE
S6
5:12:63
a
FIRST FLOOR PLAN
Scale: 1/4",1/2"to1'-0"
Drawn:

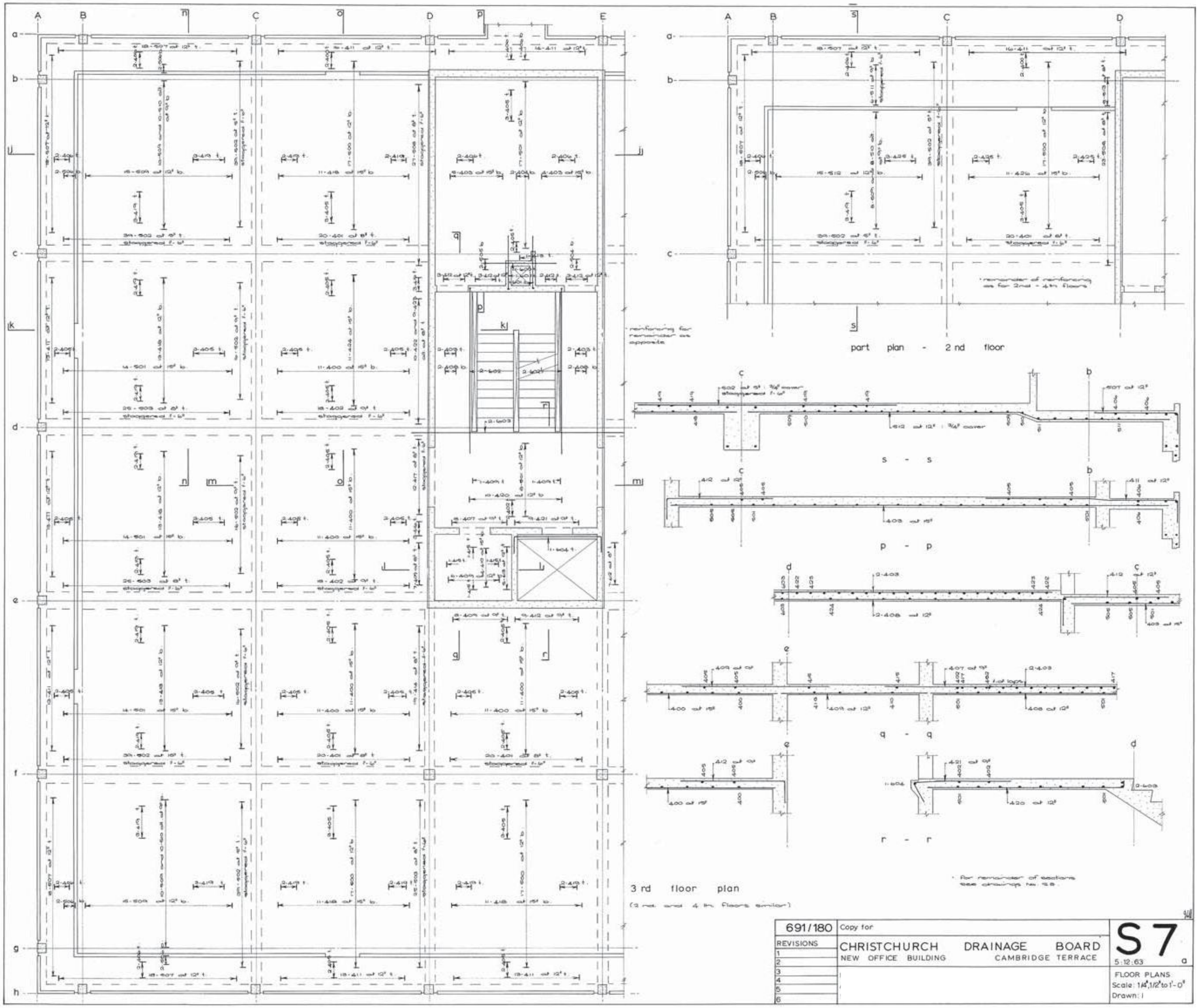
3 rd floor plan
(2 nd and 4 th floors similar)
part plan - 2 nd floor
remainder of reinforcing as for 2nd - 4th floors
reinforcing for remainder as opposite
s - s
p - p
q - q
r - r
for remainder of sections see drawings No. S8.
691/180
Copy for
REVISIONS
CHRISTCHURCH DRAINAGE BOARD
NEW OFFICE BUILDING
CAMBRIDGE TERRACE
S 7
5.12.63
a
FLOOR PLANS
Scale: 1/4", 1/2" to 1'-0"
Drawn: I

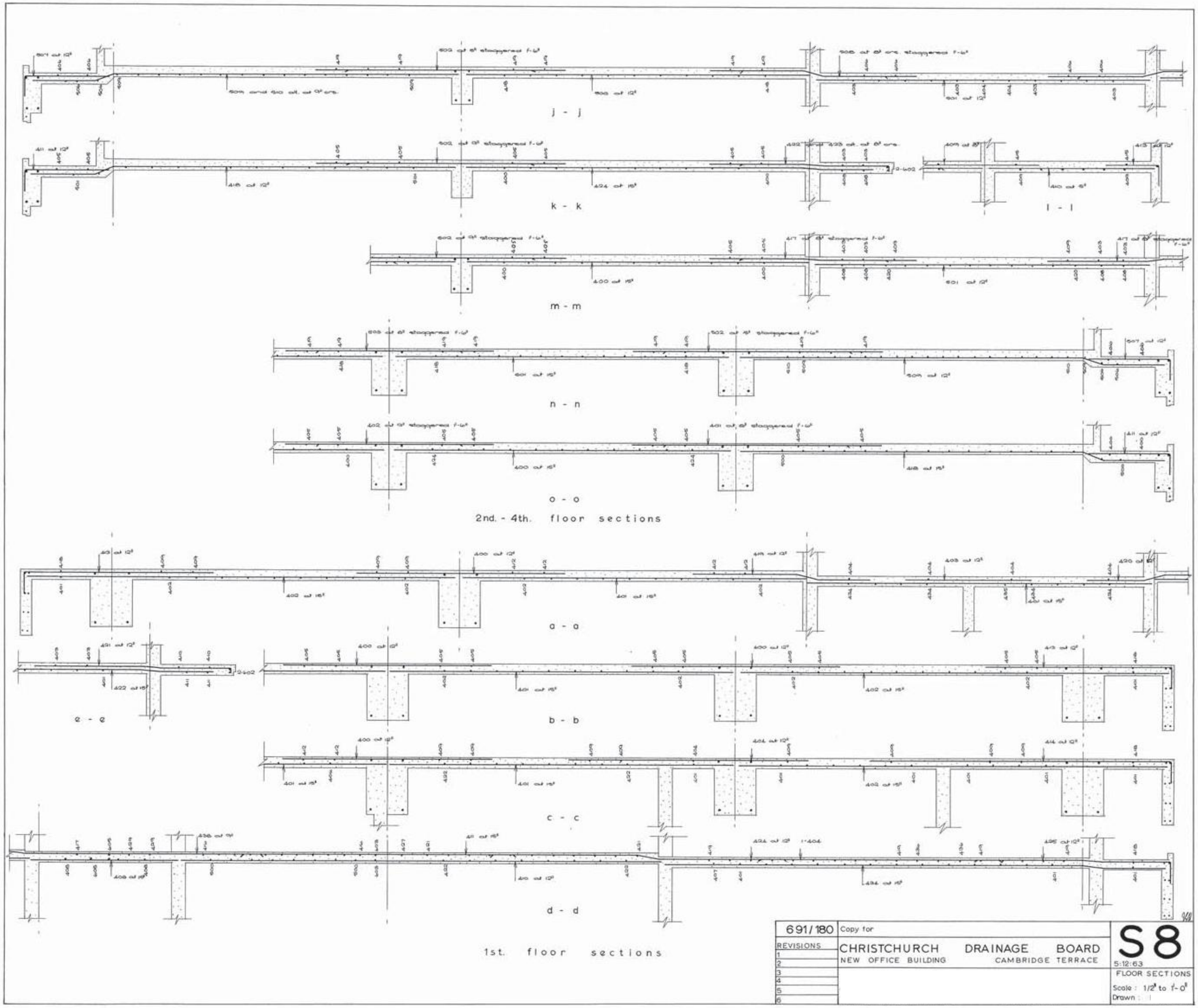
j - j
k - k
l - l
m - m
n - n
o - o
2nd. - 4th. floor sections
a - a
e - e
b - b
c - c
d - d
1st. floor sections
691/180
Copy for
REVISIONS
1
2
3
4
5
6
CHRISTCHURCH DRAINAGE BOARD
NEW OFFICE BUILDING
CAMBRIDGE TERRACE
S8
5:12:63
FLOOR SECTIONS
Scale : 1/2" to 1'-0"
Drawn :

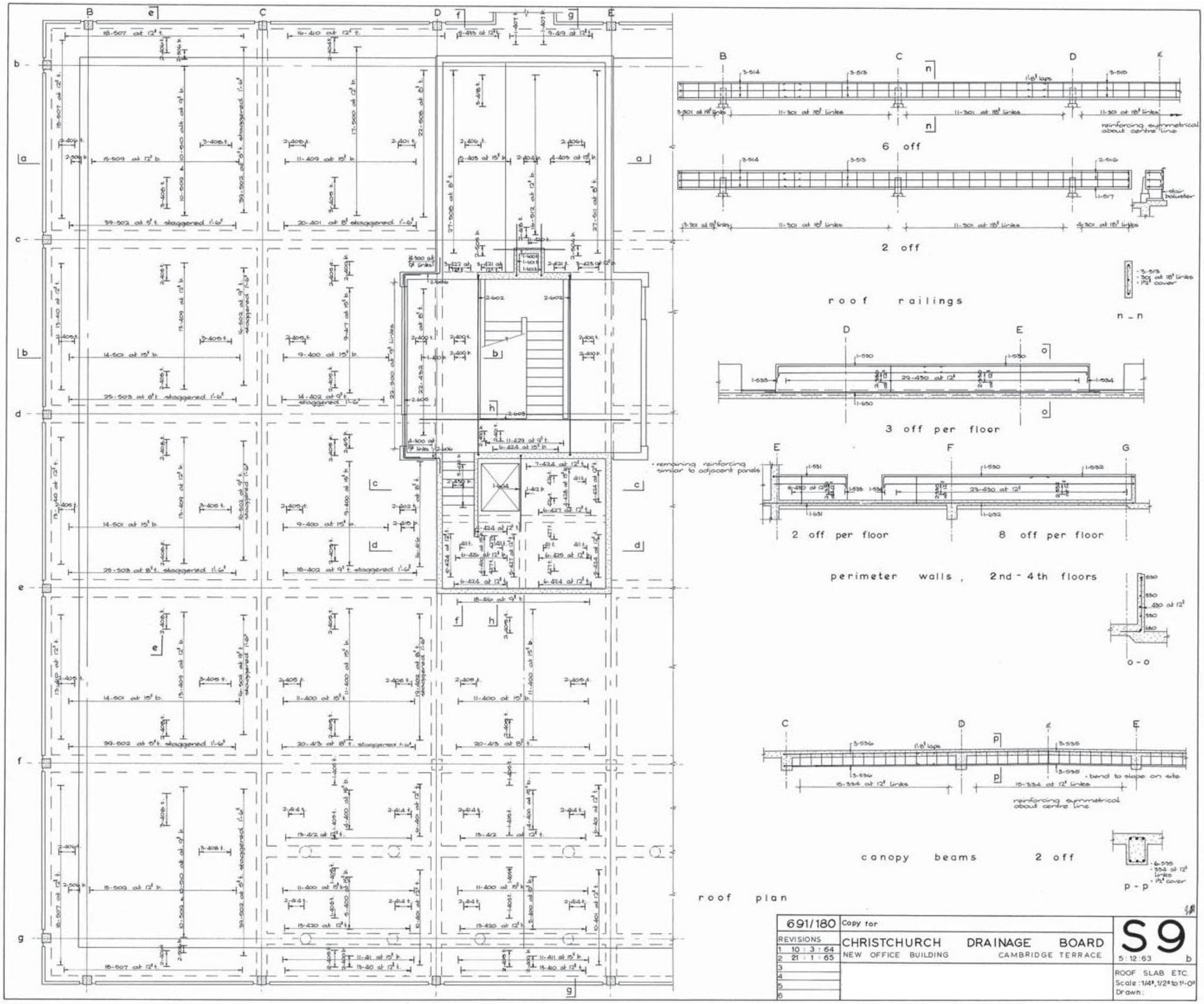
roof railings
6 off
2 off
n _ n
3 off per floor
2 off per floor
8 off per floor
perimeter walls , 2nd - 4th floors
o - o
canopy beams 2 off
p - p
roof plan
691/180
Copy for
REVISIONS
1 10 : 3 : 64
2 21 : 1 : 65
CHRISTCHURCH DRAINAGE BOARD
NEW OFFICE BUILDING
CAMBRIDGE TERRACE
S9
5 : 12 : 63
b
ROOF SLAB ETC.
Drawn:

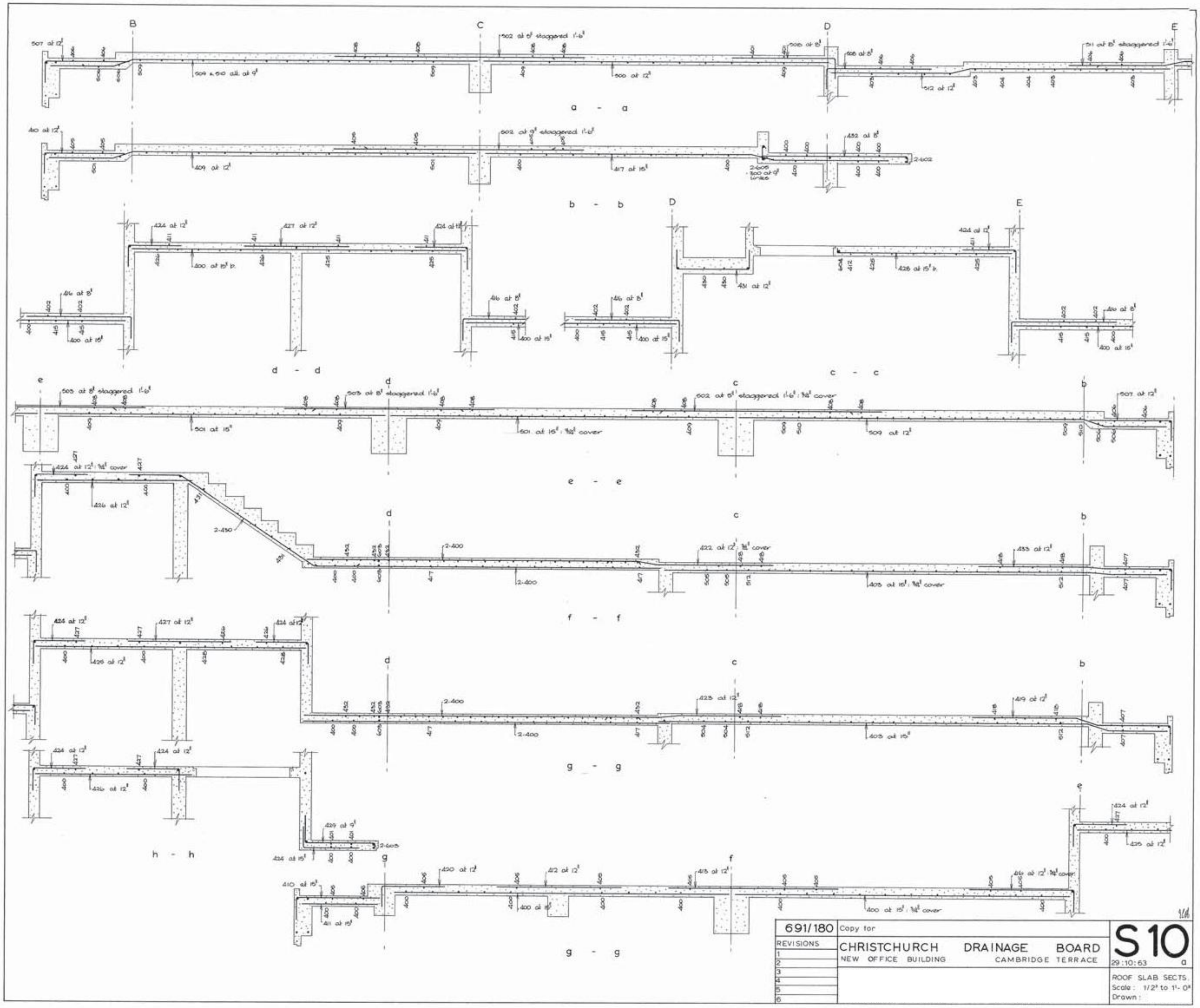
a - a
b - b
d - d
c - c
e - e
f - f
g - g
h - h
g - g
691/180
Copy for
REVISIONS
CHRISTCHURCH DRAINAGE BOARD
NEW OFFICE BUILDING
CAMBRIDGE TERRACE
S10
29:10:63
a
ROOF SLAB SECTS.
Scale: 1/2" to 1'- 0"
Drawn:

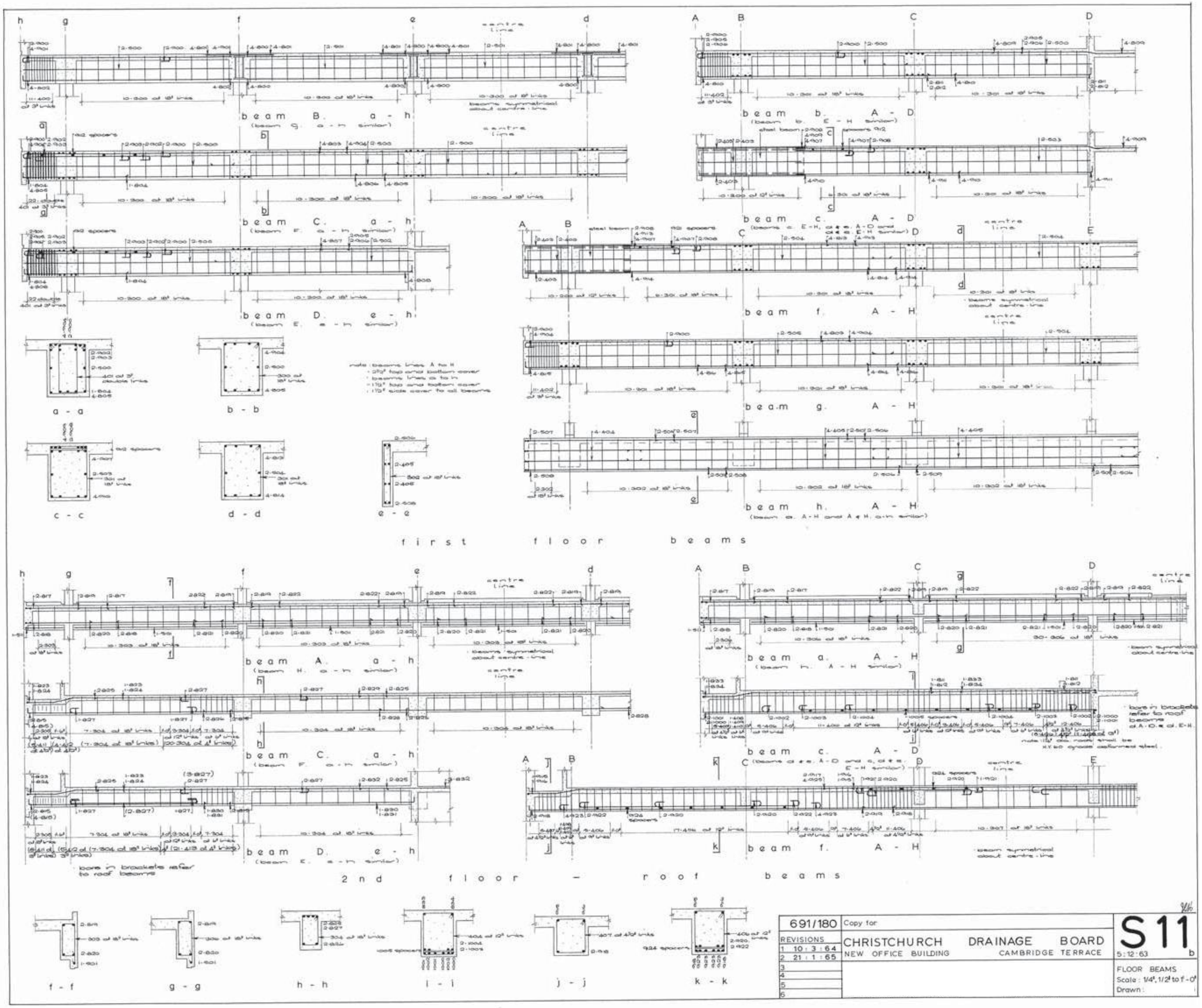
beam B. a - h
(beam g. a - h similar)
beam C. a - h
(beam F. a - h similar)
beam D. e - h
(beam E. e - h similar)
beam b. A - D
beam c. A - D
beam f. A - H
beam g. A - H
beam h. A - H
a - a
b - b
c - c
d - d
e - e
first floor beams
beam A. a - h
(beam H. a - h similar)
beam a. A - H
(beam h. A - H similar)
beam c. A - D
beam f. A - H
2nd floor - roof beams
f - f
g - g
h - h
i - i
j - j
k - k
691/180
Copy for
REVISIONS
1 10:3:64
2 21:1:65
CHRISTCHURCH DRAINAGE BOARD
NEW OFFICE BUILDING
CAMBRIDGE TERRACE
S11
5:12:63
b
FLOOR BEAMS
Drawn:

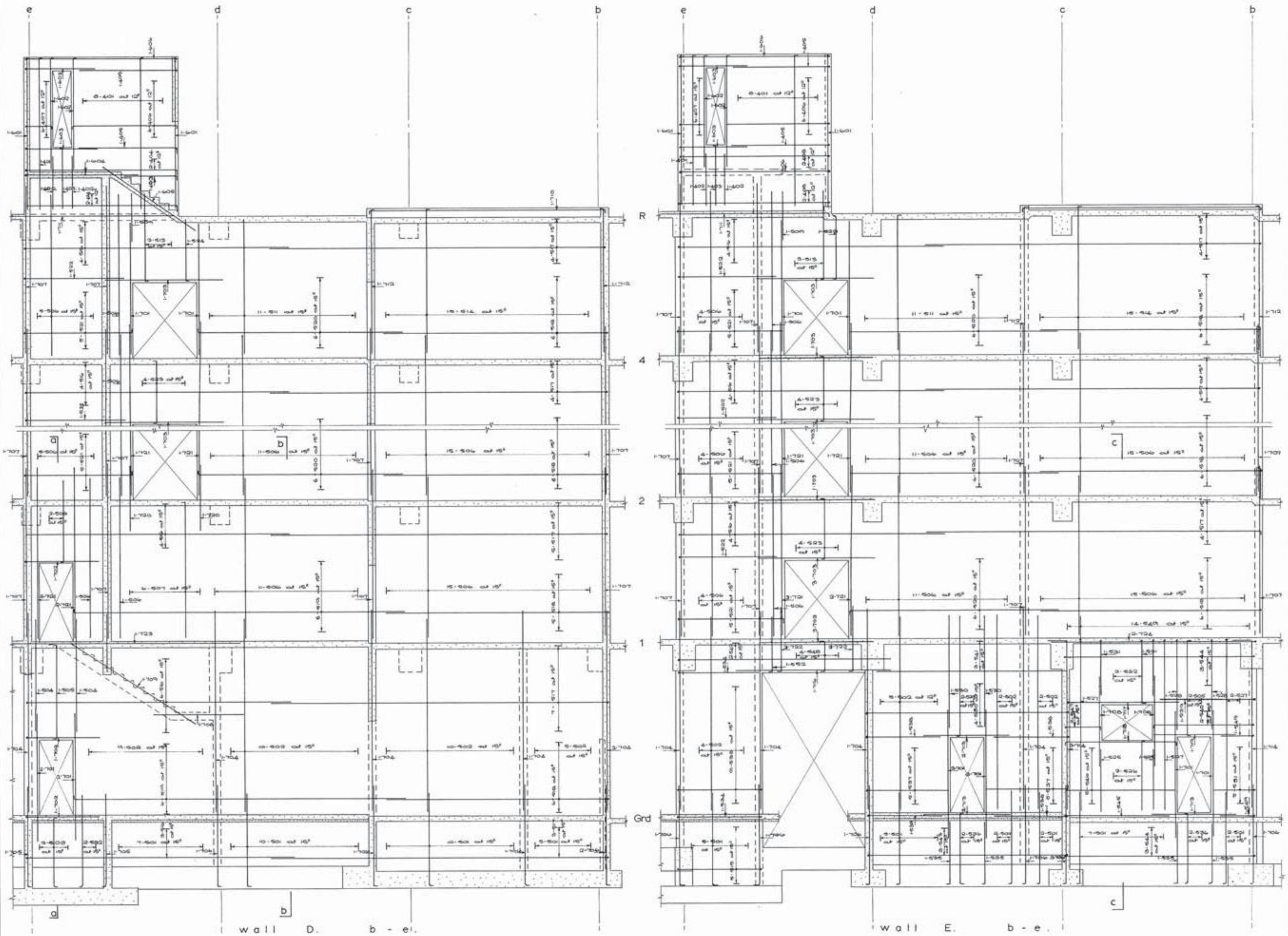

691/180	Copy for	S12
REVISIONS	CHRISTCHURCH DRAINAGE BOARD	5:12:63 a
1	NEW OFFICE BUILDING CAMBRIDGE TERRACE	WALLS
2		Scale: 1/4" to 1'-0"
3		Drawn:
4		
5		
6		

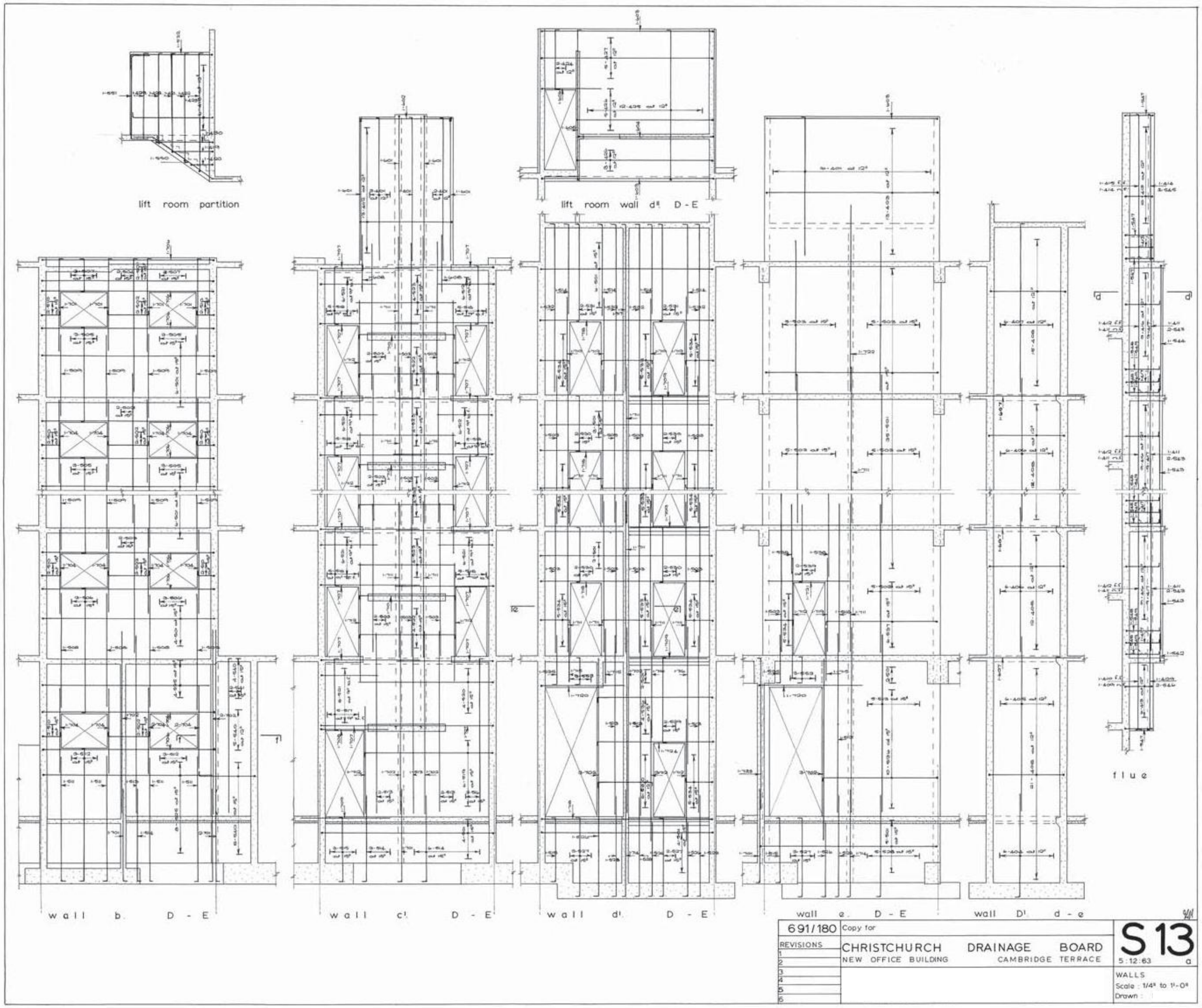
lift room partition
lift room wall d². D - E
wall b. D - E
wall c¹. D - E
wall d¹. D - E
wall e. D - E
wall D¹. d - e
flue
691/180 Copy for
REVISIONS
CHRISTCHURCH DRAINAGE BOARD
NEW OFFICE BUILDING CAMBRIDGE TERRACE
S 13
5 : 12 : 63 a
WALLS
Scale : 1/4" to 1'-0"
Drawn :

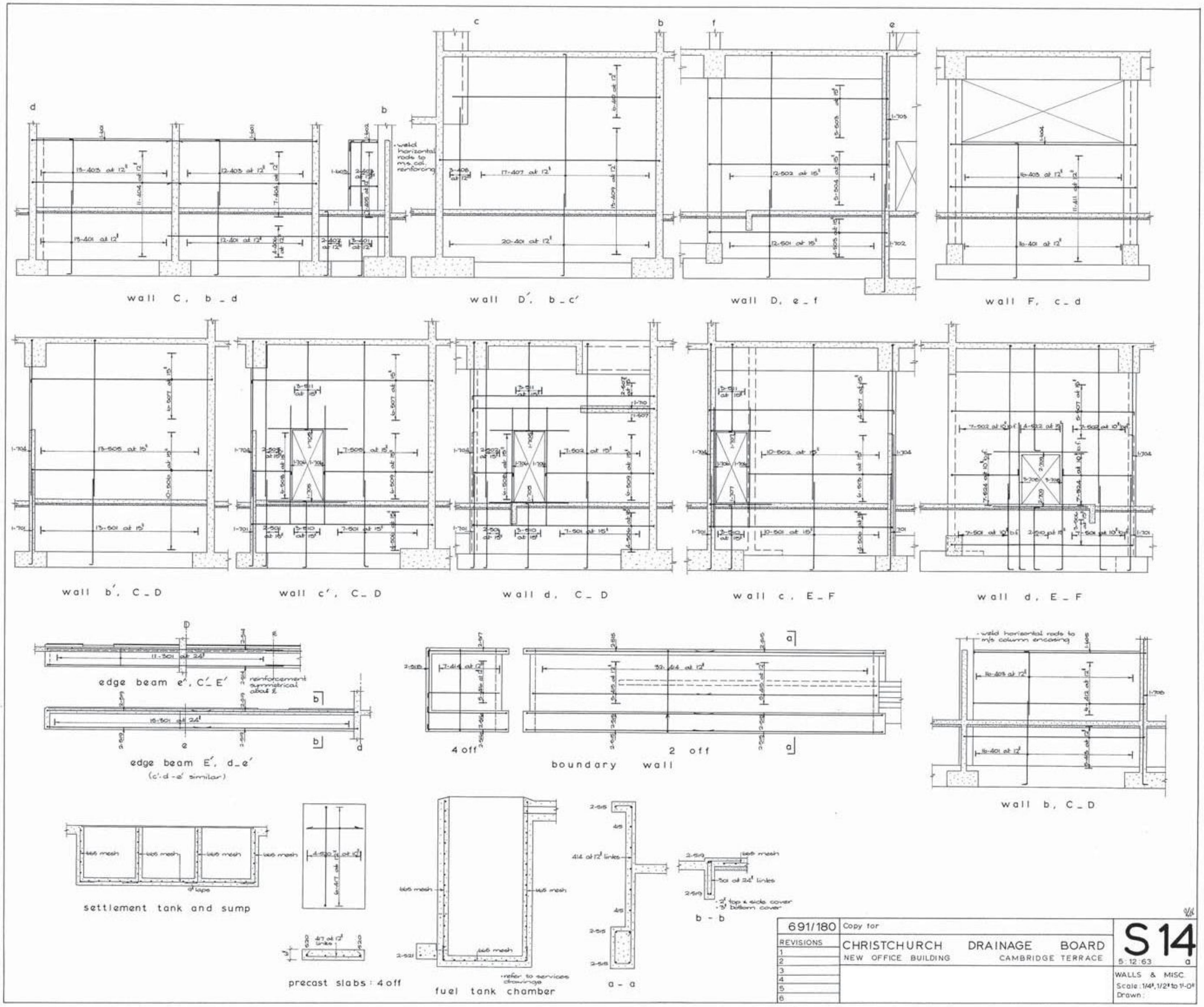
wall C, b_d
wall D′, b_c′
wall D, e_f
wall F, c_d
wall b′, C_D
wall c′, C_D
wall d, C_D
wall c, E_F
wall d, E_F
edge beam e′, C′_E′
reinforcement symmetrical about ℄
edge beam E′, d_e′
(c′-d-e′ similar)
4 off
boundary wall
2 off
wall b, C_D
settlement tank and sump
precast slabs : 4 off
fuel tank chamber
a – a
b – b
691/180
Copy for
REVISIONS
CHRISTCHURCH DRAINAGE BOARD
NEW OFFICE BUILDING
CAMBRIDGE TERRACE
S14
5:12:63
a
WALLS & MISC.
Drawn:

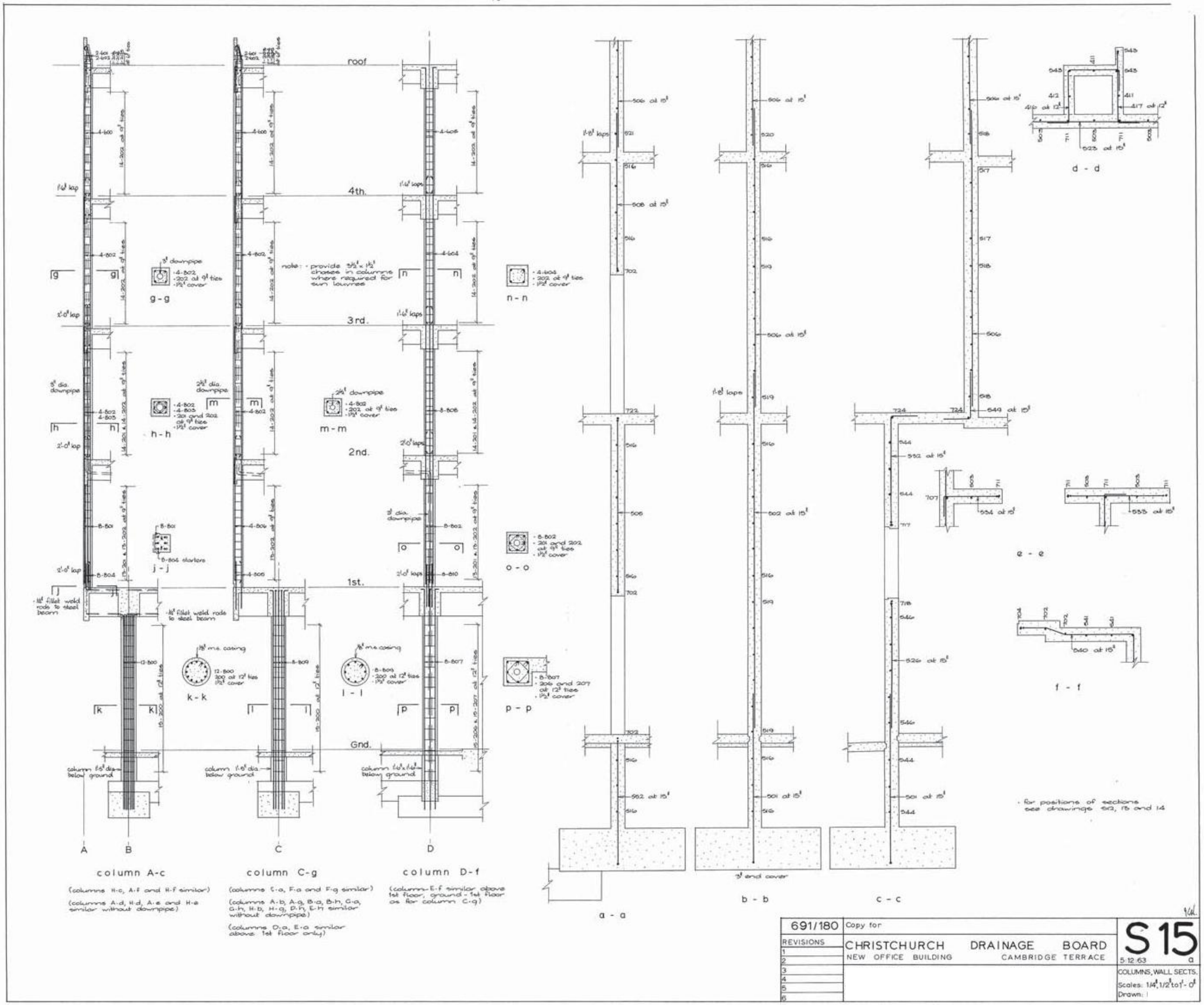
roof
4th.
3rd.
2nd.
1st.
Gnd.
note: - provide 3½" x 1½" chases in columns where required for sun louvres
g - g
h - h
j - j
k - k
l - l
m - m
n - n
o - o
p - p
a - a
b - b
c - c
d - d
e - e
f - f
column A-c
(columns H-c, A-F and H-F similar)
(columns A-d, H-d, A-e and H-e similar without downpipe)
column C-g
(columns C-a, F-a and F-g similar)
(columns A-b, A-g, B-a, B-h, C-a, G-h, H-b, H-g, D-h, E-H similar without downpipe)
(columns D-a, E-a similar above 1st floor only)
column D-f
(column E-f similar above 1st floor, ground - 1st floor as for column C-g)
· for positions of sections see drawings S12, 13 and 14
691/180
Copy for
REVISIONS
CHRISTCHURCH DRAINAGE BOARD
NEW OFFICE BUILDING
CAMBRIDGE TERRACE
S15
5-12-63
a
COLUMNS, WALL SECTS.
Scales: 1/4", 1/2" to 1'- 0"
Drawn:

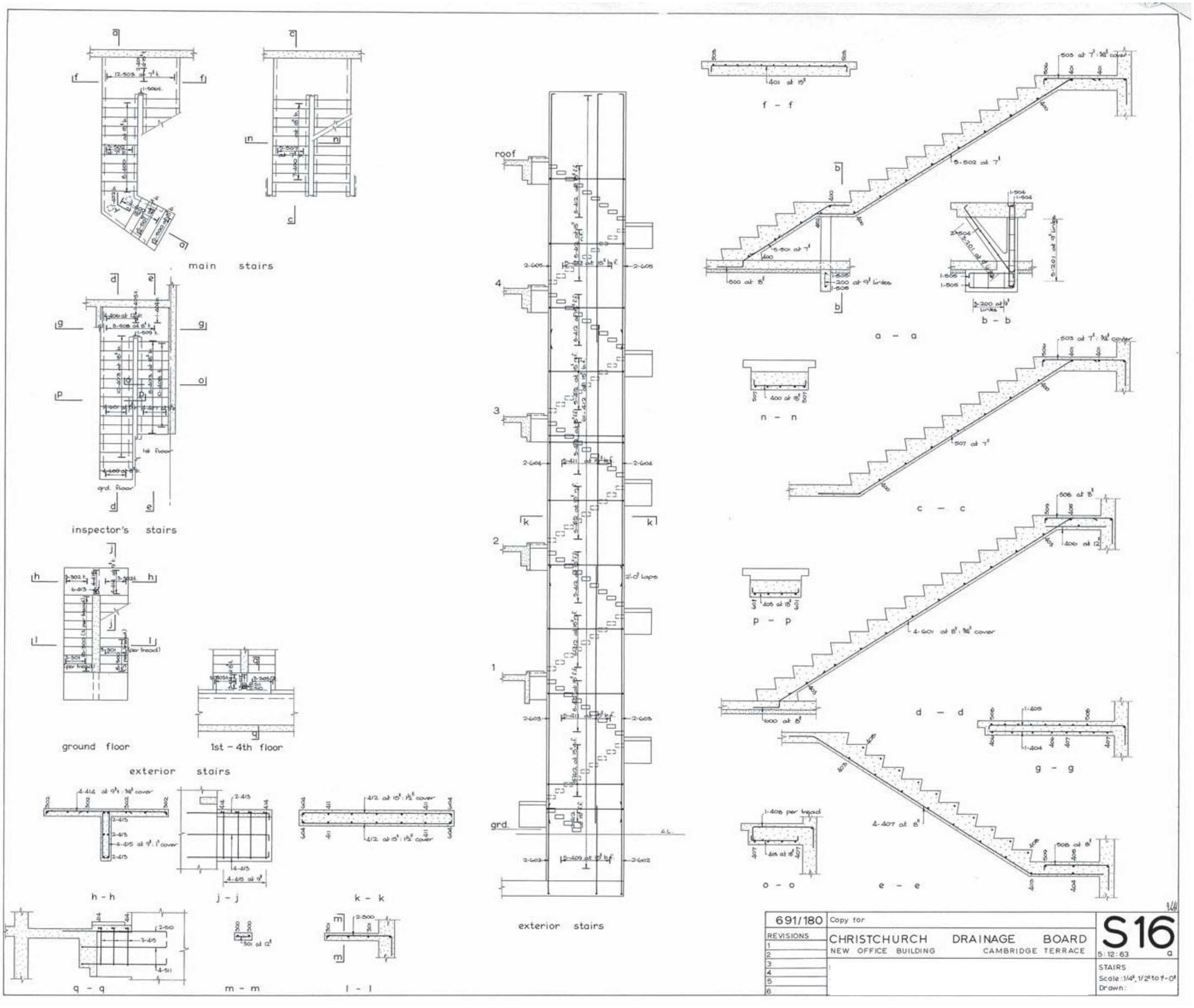
main stairs
inspector's stairs
grd. floor
1st floor
exterior stairs
ground floor
1st - 4th floor
exterior stairs
roof
grd.
a - a
b - b
c - c
d - d
e - e
f - f
g - g
n - n
p - p
o - o
h - h
j - j
k - k
q - q
m - m
l - l
691/180
Copy for
REVISIONS
CHRISTCHURCH DRAINAGE BOARD
NEW OFFICE BUILDING
CAMBRIDGE TERRACE
S16
5: 12: 63
a
STAIRS
Scale: 1/4", 1/2" to 1'-0"
Drawn:

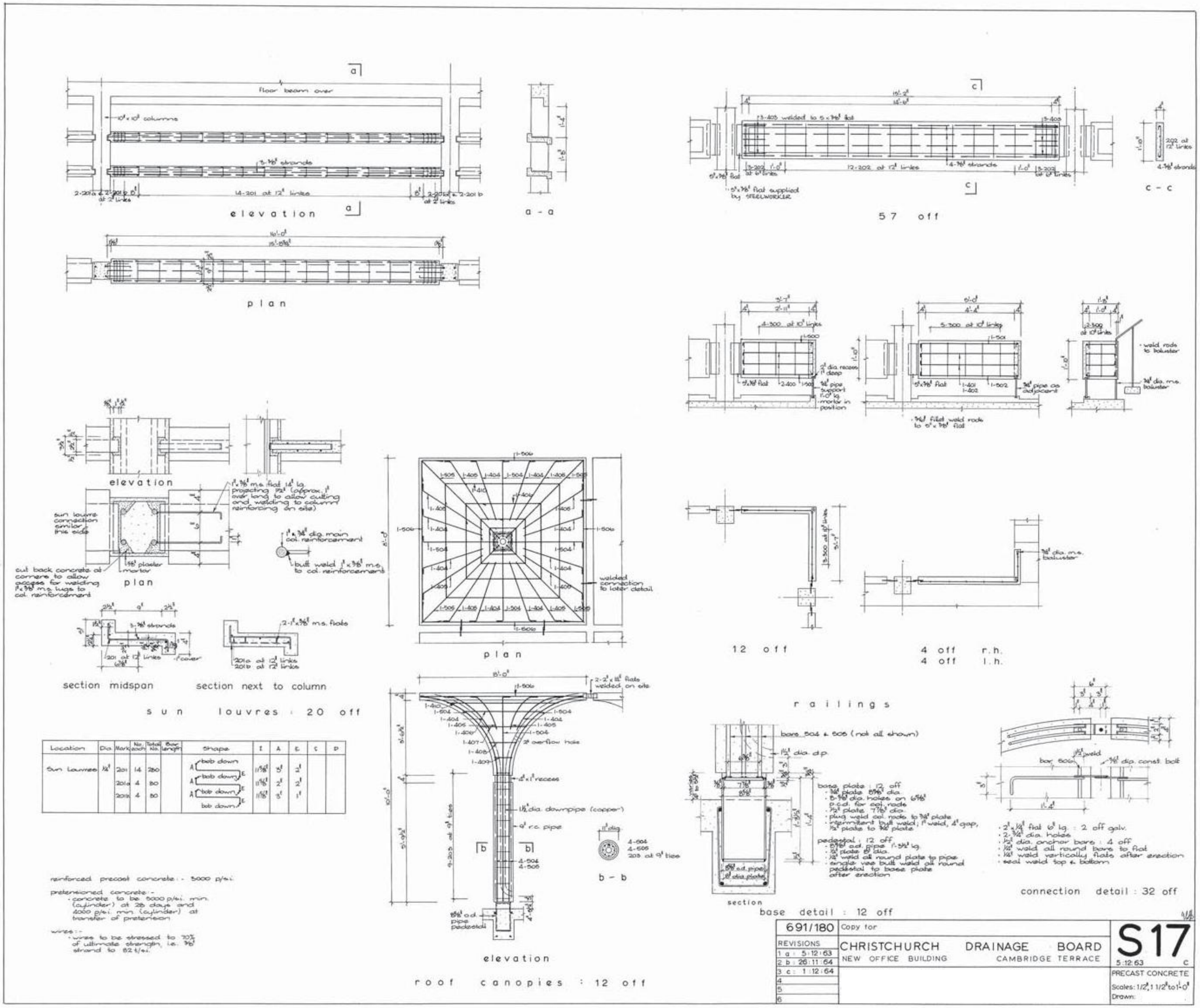
elevation
a – a
plan
57 off
c – c
elevation
plan
section midspan
section next to column
sun louvres : 20 off
plan
elevation
roof canopies : 12 off
b – b
12 off
4 off r.h.
4 off l.h.
railings
section
base detail : 12 off
connection detail : 32 off
reinforced precast concrete :- 5000 p/s.i.
691/180
Copy for
REVISIONS
1 a : 5:12:63
2 b : 26:11:64
3 c : 1:12:64
CHRISTCHURCH DRAINAGE BOARD
NEW OFFICE BUILDING
CAMBRIDGE TERRACE
S17
5:12:63
c
PRECAST CONCRETE
Scales: 1/2", 1 1/2" to 1'-0"
Drawn:

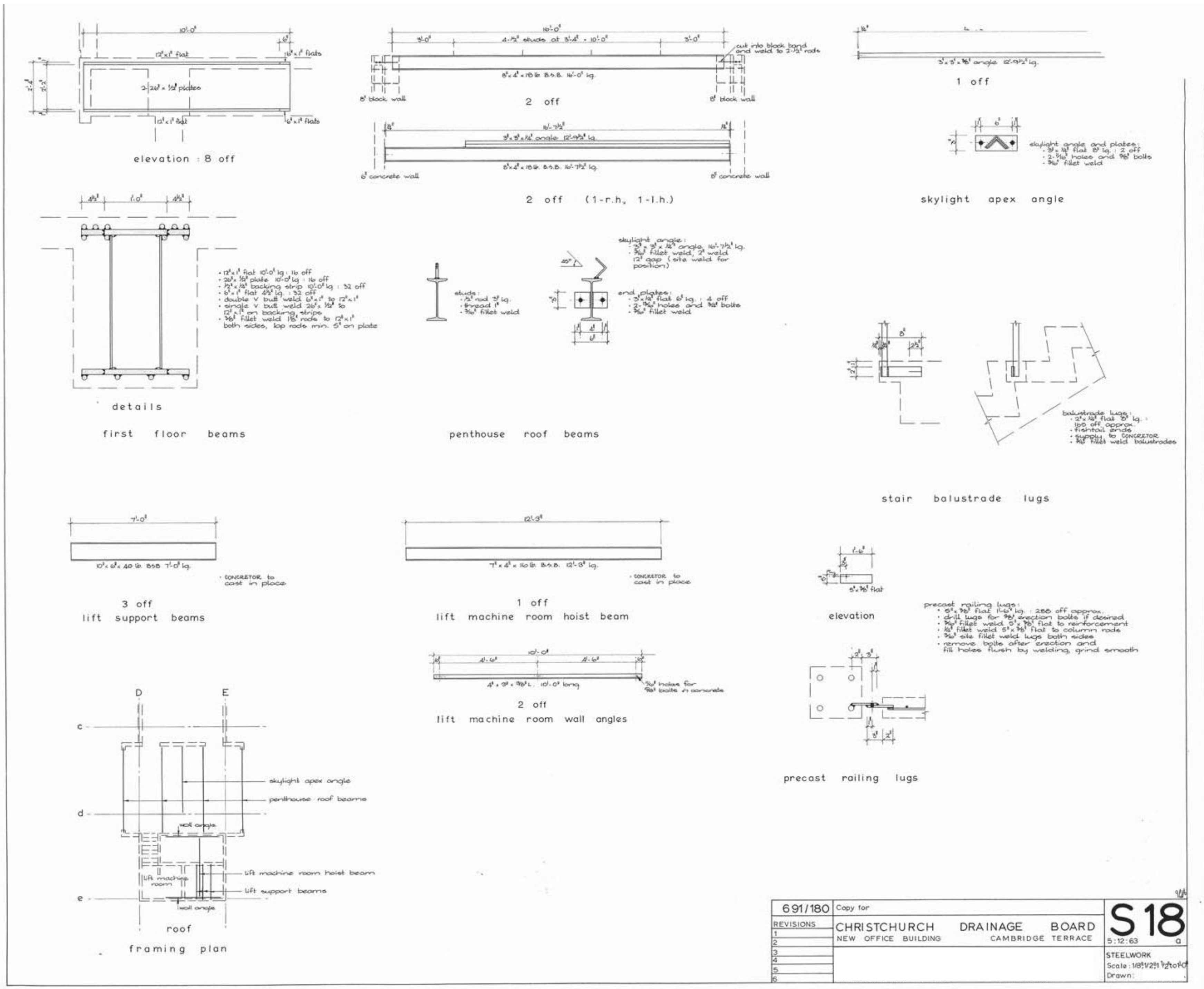

elevation : 8 off
details
first floor beams
2 off
2 off (1-r.h., 1-l.h.)
8" block wall
6" concrete wall
penthouse roof beams
1 off
skylight apex angle
stair balustrade lugs
3 off
lift support beams
1 off
lift machine room hoist beam
2 off
lift machine room wall angles
CONCRETOR to cast in place
elevation
precast railing lugs
D
E
c
d
e
skylight apex angle
penthouse roof beams
wall angle
lift machine room hoist beam
lift support beams
lift machine room
roof
framing plan
691/180
Copy for
REVISIONS
CHRISTCHURCH DRAINAGE BOARD
NEW OFFICE BUILDING
CAMBRIDGE TERRACE
S18
5:12:63
a
STEELWORK
Scale:
Drawn:

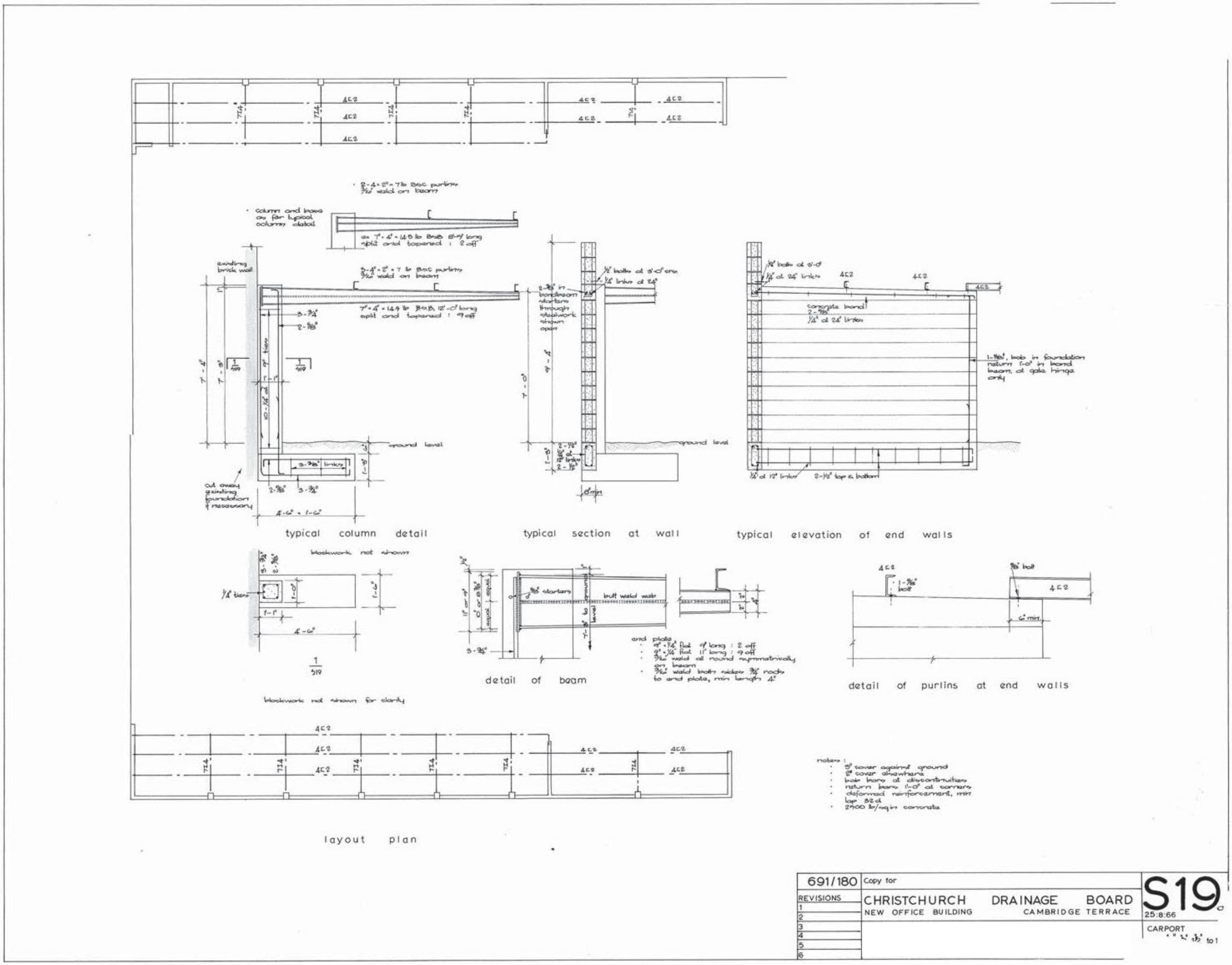
typical column detail
typical section at wall
typical elevation of end walls
detail of beam
detail of purlins at end walls
layout plan
existing brick wall
ground level
blockwork not shown
blockwork not shown for clarity
691/180
Copy for
REVISIONS
CHRISTCHURCH DRAINAGE BOARD
NEW OFFICE BUILDING
CAMBRIDGE TERRACE
S19
25:8:66
CARPORT

A.2 New Zealand Design Code History for Concrete Structures

The great Hawke's Bay earthquake of 1931which caused the most loss of life and most destruction of any NZ earthquake to date changed how buildings were designed. Prior to 1931 no government standard, as to the design of concrete structures was present in New Zealand. By 1935 a bylaw document coined NZSS no. 95 was produced in reaction to the great devastation of the Hawke's Bay event. This document was not nationwide; each subsidiary had a choice whether or not to follow these guidelines. NZSS no. 95 gave recommendations for the design of timber, RC frames and steel structures. This document was altered and revised over the next 30 years, most notably in 1955 where the inverted triangular load distribution over the height of the building was introduced. Due to wars and depression from 1935 to 1955 very few buildings were constructed resulting in little change to the design code. In 1964-1965 the first concrete code was produced, NZSS 1900 chapter 8. This was a very basic design manual, mostly referencing the US concrete code at the time ACI 318-63. John Hollings, a Beca engineer was the first to talk about capacity design for concrete structures in 1969, describing the hinging and the correct location for the greatest response (i.e. beam hinging instead of column hinging and a hinge at the base of the wall) By 1970 a booklet, PW 81/10/1970 directly related to ductility design was produced as part of the code of practice. Throughout the 70s and into the 80s numerous research projects were conducted regarding seismic design of reinforced concrete structures by notable engineers, Paulay, Park and Priestly. These experiments laid the track for the 1982 code and current standard for concrete NZS 3101. This particular code is nationwide in NZ and is required to follow in all subsidiaries. As the NZS 3101 has been updated, revised and amended throughout the years, the current installment is NZS 3101-2006 amendment 1 and 2. It is likely that the NZS 3101 will be again revised in the near future directly related to the recent events in Christchurch.

A.3 Wall to Beam Connection: Bond Strength

TYPICAL SET-UP:

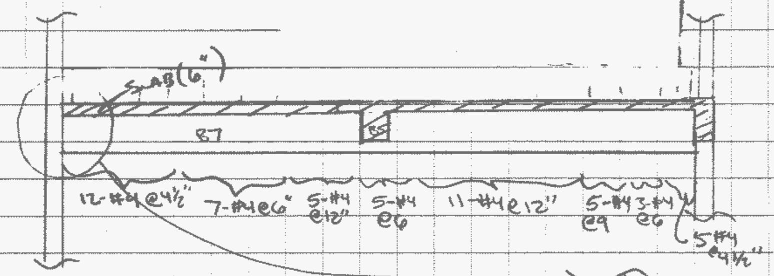

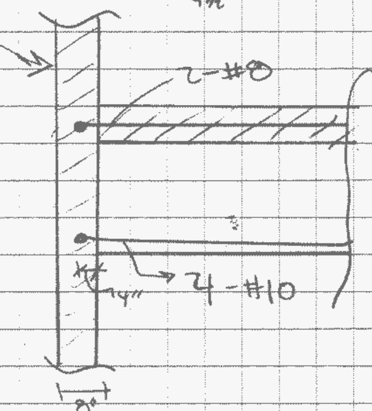

B5: 22"x12"

B7: 27"x20"

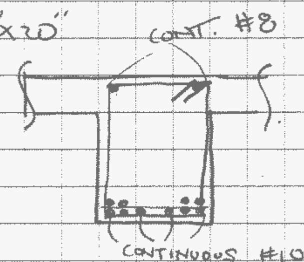

PULL-OUT

CAPACITY OF 4#10 ; 2#8 FROM A 8" WALL w/ 4" EMBEDMENT

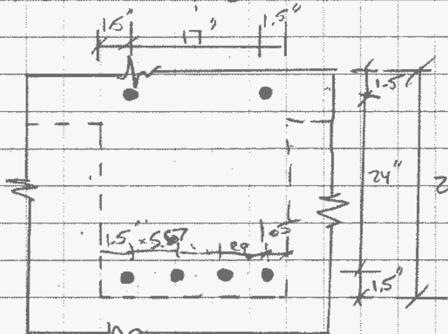

BOND SLIP OF #8 @ TOP (TENSION)

$$f_b = \frac{F_s}{\pi \phi l_e}$$

f_{bu} = ULTIMATE BOND CAPACITY BASED ON BOOK "RC: DESIGN & THEORY"

$$f_{bu} = \beta \sqrt{f'_c}$$

DEFORMED BAR IN T = $\beta = .5$

$$F_s = f_{bu} \pi \phi l_e$$

(ϕ → equivalent diameter for 2 bars; l_e → 4")

$$= .5 \sqrt{17\,MPa}\; \pi (35.8)(101.6)$$

$$\boxed{= 23603\,N = 5.3^k}$$

$$\phi \quad 2 \times \frac{\pi \left(\frac{8}{8}\right)^2}{4} = 1.57 = \frac{\pi (\phi)^2}{4}$$

$$\phi = 1.42" = 35.8\,mm$$

BOND SLIP 4-#10 BOT IN TENSION

$$F_s = .5 \left(\sqrt{17}\right) \pi (64.6\,mm)(101.6)$$

$$F_s = 47507.99\,N = \underline{9.6^k}$$

$$\phi = 2.54" = 64.6\,mm$$

A.4 Modeling Assumptions Overview

- General Modeling
  - Rigid Diaphragm assumption
    - all the mass is lumped at the center of mass of each level
    - Validated by a distributed mass model using ETABS.
    - To account for the mass inertia forces that would be considered in a distributed mass model, rotational mass is added by means of mr^2, where $\mathbf{r} = (b^2 + d^2)/12$, where b and d are the plan dimensions of the full building. This is based on findings from Chopra (2001).
  - The distributed mass in the ETABS model is based on the tributary area for each component
  - The mass consists of :
    - Self-weight of the components
      - 150 pcf for normal weight concrete
    - Additional 20 psf dead load considered to account for partitions, MEP and miscellaneous items.
- The rooftop structure, CMU, wood structure is not modeled, but the mass is distributed over the roof slab in the appropriate area.
- All walls are assumed full height, no discontinuities were modeled, the typical wall section for all levels is that of level 2- 4.
- The plans show a 5-ft crawl space below the ground level before reaching the grade beams and strip footings, this is not modeled for simplicity.
- The foundation is assumed to be fully fixed.
- The openings for doors and windows were not taken into account in the model but were considered when determining capacity limits.
- The exterior and interior stairs are ignored.
- Coupling beams
  - Only coupling beams along gridlines D and E between west flanges and east flanges of CWN and CWS and the connections of CWC and CWN
  - Coupling beams are modeled using Elastic Beam Column elements with a cracked stiffness of 0.1EI. It is assumed that the coupling beams contribute

very little to overall response. This is only slightly less than desired in new building modeling of 0.15EIg.

- Loading
  - Spectral Analysis –the REHS spectrum created from the actual recorded ground motion
  - Pushover- inverted Triangular load, based on a weighted scale of relative heights.
    - It is not recommended to use the code procedures for buildings with torsional irregularity and also no mode 1 shape used because mode 1 is torsional mode. The ratios for the triangular load are very similar to that of the code based approach and thus are considered acceptable.
  - Dynamic load – the processed REHS recorded ground motion S88E, which is 2 degrees off of being a directly E-W motion therefore assumed the motion was E-W.
  - Vertical accelerations were ignored.
  - Gravity – used for all models, assumed to be based on tributary area to all components, since only the core walls are being modeled, they take majority of the gravity load.
- Dynamic Damping
  - 2% damping is used for this structure
  - Raleigh damping is assumed using the first and 4th periods. This assumed that the first and 4th modes are at 2%, where the second and third modes will be slightly smaller than 2% and anything larger than the 4th mode period will be slightly larger than 2% damping as seen in Figure 71. This will give credible results assuming very little contribution from higher modes.
  - It should be noted as the structure yields the frequencies will shift possible causing an unwanted amount of damping. This should not be an issue in this case since it is assumed that shortly after yielding during the February event failure occurs. This is applied to all elements and nodes for the fiber element model. The MVLEM nodes and elements were not damped due to

convergence issues but since the MVLEM is not used in the dynamic analysis this is not an issue.

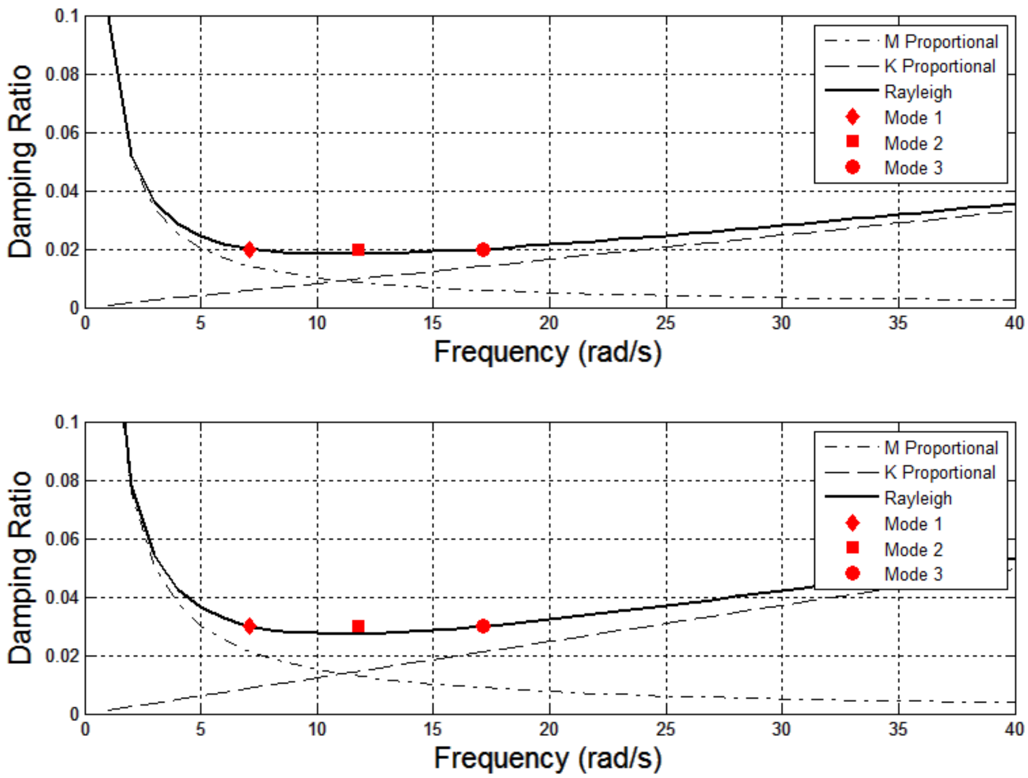

Figure 71: Raleigh damping curves

A.5 PGC Wall Models

The actual hysteretic model using the parameters determined from material properties of the PGC walls is shown below. This includes the hysteretic responses from the vertical springs referred to as verticalspring2 in the MVLEM, the steel02 and concrete02 materials from the fiber element model. Both compression and tension responses are shown.

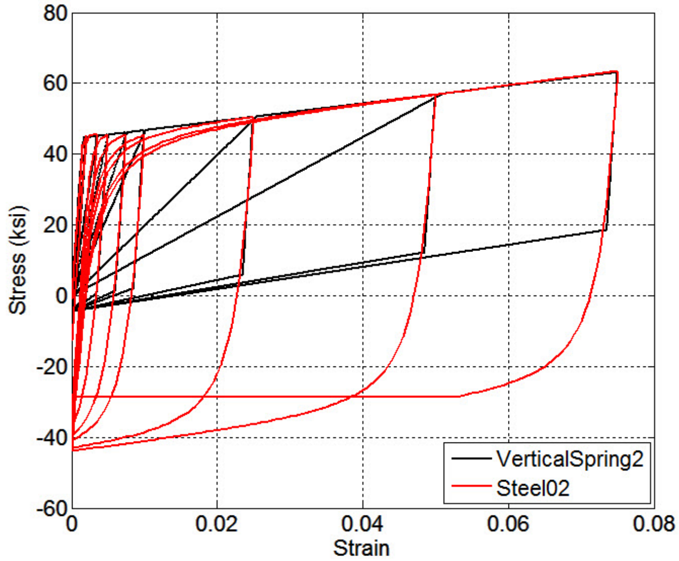

Figure 72: Tension hysteretic response for materials verticalspring2 from the MVLEM and steel02 from the fiber element model

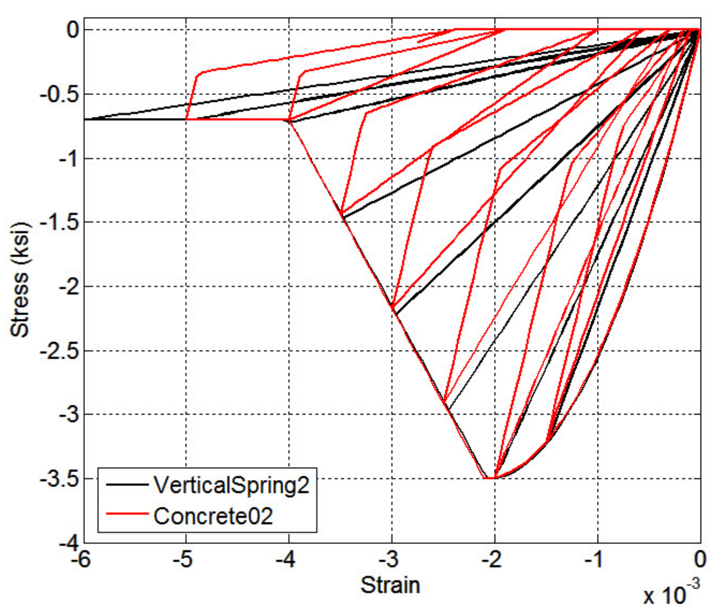

Figure 73: Compression hysteretic response for materials verticalspring2 from the MVLEM and concrete02 from the fiber element model

A.6 Torsion Study

In order to accurately model the entire configuration 1 as a single element, as in configuration 2, certain properties could not simply be added, such as J, the torsional constant. Using a similar approach to the parallel axis theorem, J_3 the torsional constant for element 3 was determined using equation 12.

$$J_3 = J_1 + A_{v1}d_1^2 + J_2 + A_{v2}d_2^2 \quad \textbf{12}$$

J_1 and J_2 are the torsional constants of elements 1 and 2, A_{v1} and A_{v2} is the shear area of elements 1 and 2 and d_1 and d_2 are the respective distances of the geometric centers of elements 1 and 2 from the center of rigidity. Also as important as correctly representing the torsional stiffness was determining the torque within configuration 1 from the shear couple, as this was not output by OpenSees.

$$\Delta_{\boldsymbol{1}} = \Delta_{\boldsymbol{2}} = \Delta_{\boldsymbol{T}} \quad \textbf{13}$$

$$\Delta_{\boldsymbol{f1}} + \Delta_{\boldsymbol{s1}} = \Delta_{\boldsymbol{1}} \quad \textbf{14}$$

$$\Delta_{\boldsymbol{s}} = \frac{3VL}{EA_v} \quad \textbf{15}$$

$$\Delta_f = \frac{VL^3}{12EI} \quad \textbf{16}$$

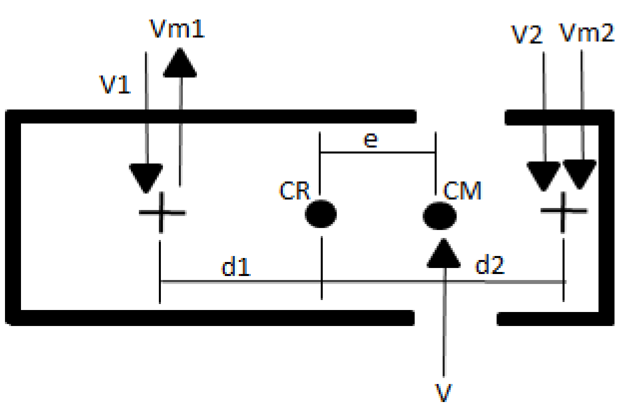

Figure 74: Free body diagram of configuration 1

The shear output within the element recorder is the total shear acting within that element, which is the sum of the shear from translation (V_1) and rotation (V_{m1}), see Figure 74 (a) and

(b) for clarity. Using the compatibility of deformations (equation 13) based on the rigid diaphragm assumption and substituting the contributions from flexure and shear deformations (equations 15 and 16) a term β can be determined. Beta is the ratio of total shear, V to the translational shear, V_2, as shown in equation 17. This relationship is not general as it pertains specifically to the conditions of configuration 2 as well as the conditions of PGC. Beta would be equal to 1 if element 1 and element 2 had the exact same rigidities and were equal distance from the CR, since this is not the case β must be estimated using the previously described procedure.

$$V_2\beta = V \tag{17}$$

$$V_1 = V_2(\beta - 1) \tag{18}$$

Once beta has been determined both translational shears, $V_1$and V_2can be established by using equations 17 and 18Since the recorded element shear force from OpenSees is the superimposed translational and rotational shear V_2 and V_{2m}, the coupled shear force V_{2m} can be determined. This force multiplied by the distance between its couple, V_{1m}which is the sum of $d_1$and d_2 from Figure 74 is the additional torsional moment that was added to the recorded moments of elements 1 and 2 to produce the total torsional moment versus diaphragm rotation plots for configuration 1.

A.7 Global Models

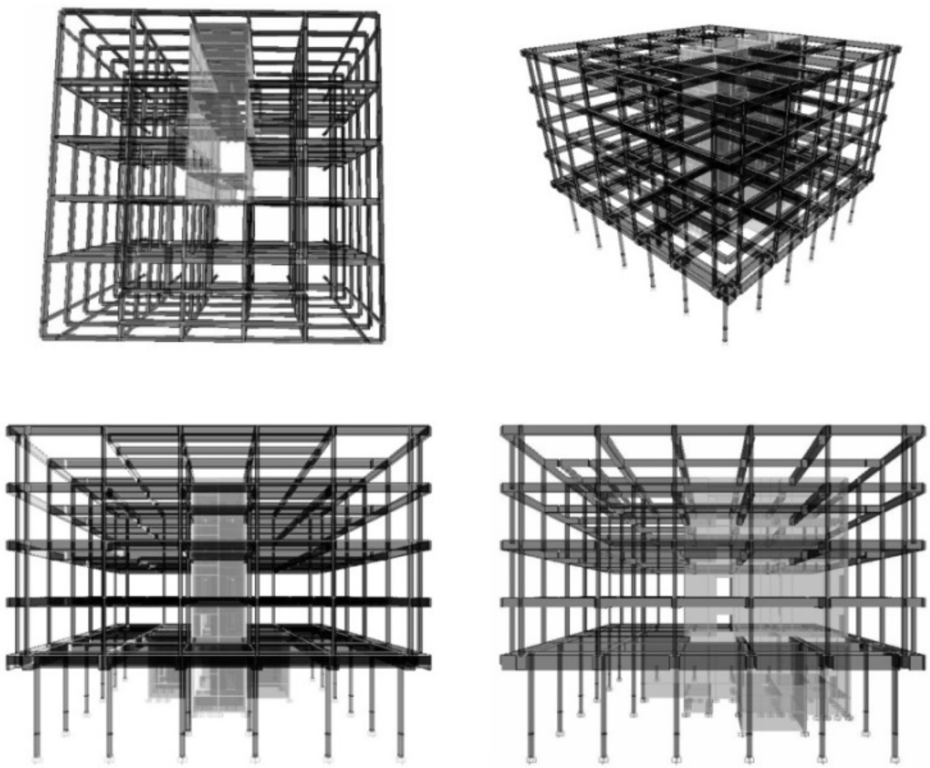

Figure 75: ETABS model, plan (top left) isometric (top right), south elevation (bottom left), east elevation (bottom right) (CSI 2013)

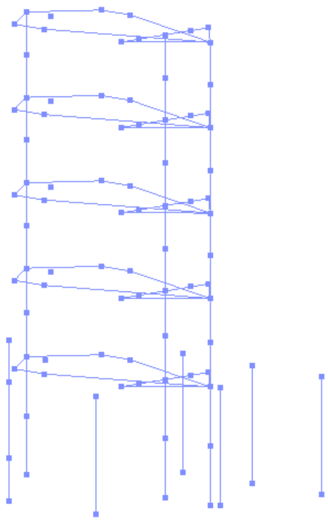

Figure 76: OpenSees Model - isometric view of line elements (PEER 2013)

A.8 Mode Shapes

Below shows the comparison in the first three mode shapes from MVLEM, fiber element model and ETABS.

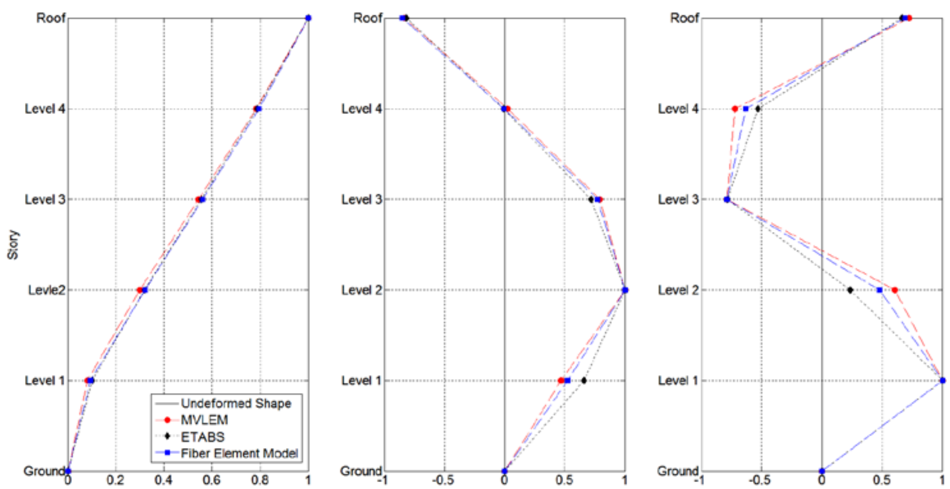

Figure 77: The first three east to west mode shapes from ETABS, MVLEM and fiber element models